Cranfield University

AMIR EBRAHIM CHAHARDEHI

Fatigue Crack Growth in Complex Stress Fields

SCHOOL OF ENGINEERING

PhD THESIS

Cranfield University

SCHOOL OF ENGINEERING

PhD THESIS

Academic Year 2007-2008

AMIR EBRAHIM CHAHARDEHI

Fatigue Crack Growth in Complex Stress Fields

Supervisor: Prof Feargal Brennan

August 2008

Abstract

Fatigue crack growth has been traditionally modelled using LEFM through the use of the Paris law. This requires an accurate method for stress intensity factor (K) calculation. Weight functions have been developed for one-dimensional cracks (e.g. edge and through cracks); these are functions that enable separation of the loading and geometry and considering the effect of each one of these two factors on the stress intensity factor (SIF) separately. They have been proven to be useful for arbitrary stress distributions where an accurate empirical formula for the stress intensity factor does not exist. Such cases include residual stress fields due to surface treatments or welds.

However, in the case of surface cracks, or part-through cracks, the problem of modelling the growth of these cracks poses two main questions, namely, how should the Paris law be generalised to suit the two-dimensional scenario, and under arbitrary loadings, how can the SIFs be calculated for these cracks. Current solutions involve tedious mathematical calculations and are complicated functions.

In this thesis, the concept of root mean square (RMS) SIF is examined and by drawing mathematical analogy with the one-dimensional case, a novel weight function is derived which enables calculation of RMS SIF values for a range of semi-elliptical surface cracks under arbitrary loadings. The accuracy of the weight function is verified through comparisons with finite elements results for a variety of loadings/geometries. The simplicity of the weight function construction method makes it a useful tool for fatigue life predictions where incremental recalculations of SIF is required as the crack grows.

Surface treatments such as shot peening and laser peening are used for crack growth retardation. It is generally believed that it is through the introduction of what is termed 'beneficiary compressive residual stresses' that crack retardation occurs. The compressive residual stresses are superimposed on the 'detrimental tensile stresses' due to loading and hence lead to a lower SIF level. By having such a strong tool as weight functions, this general belief can be put to test. To this end, a set of experiments were carried out to study the behaviour of cracks in residual stress fields arising from laser peening. Edge cracks were grown in partially-peened specimens. Neutron diffraction stress measurements were taken and stress profiles were obtained for these specimens. Measurements of strain fields near the crack show the interaction between the crack and the stress field induced by the peening process. The effect of laser peening on crack growth is discussed and recommendations for future work are proposed.

Overall the thesis proposes a weight function for surface cracks the uniqueness of which is in its simplicity, and develops an understanding of the nature of induced and transient stresses in laser-peened components. The concept of 'effective fatigue stress' is introduced and its calculation is described, and conclusions are drawn from the nature of this stress distribution.

Acknowledgements

A work of this magnitude is the result of the support of many individuals, and it is not possible to thank all the people who have helped me during the last three years.

First of all I would like to thank Prof Feargal Brennan for his excellent supervision and valuable guidance throughout this research. His support has been a source of comfort and inspiration and has made this research possible.

I would like to thank Prof Bill Dover and Dr Raymond Karé for their support during the early stages of this research.

I would specially like to thank my colleagues at the UCL NDE Centre and Cranfield University: Abdul, Andy, Athanasios, Bello, Bijan, Song and Tanya. You have made my time during this PhD research a wonderful experience. Andy, Bijan and Song, your constructive support has made an enormous impact on my work.

To my friends Miltiadis and Bijan, you have certainly made a difference and I will never forget your invaluable friendship and support.

I wish to express my gratitude to Barry Walker and Tanya for all their assistance during the experiments.

I also need to express my gratefulness to Metal Improvement Company for their advice and for laser peening the specimens.

To Dr Jon James of the Open University for providing me with the SScanSS software and his instructions, and to Dr Axel Steuwer and Dr Ed Oliver for their support in the neutron diffraction measurements at ISIS go my sincere gratitudes.

This research was funded by an Additional Dorothy Hodgkin Postgraduate Award. I would like to thank the EPSRC and NDT Technology Ltd for making this research possible by providing this source of funding.

Most importantly, I would like to thank my family for all their love and support.

Dedicated to Farnaz, Ali and Rana

List of Contents

Glossary

a	Crack length, surface crack depth
a_0	Initial crack length, initial surface crack depth
Δa	Crack growth increment
C	Paris law coefficient
c_0	Surface crack half-width
Δc	Surface crack half-width increment
E	Young's modulus
ΔF	Applied force range
h(a,x)	Weight function
K	Stress intensity factor
K_{crit}	Critical stress intensity factor
$K_{\exp}$	Experimental stress intensity factor
M	Paris law exponent
N	Total number of load cycles
ΔN	Number of load cycles
r	Cylindrical coordinate
T	Plate thickness
u, u	Crack face displacement
W	Plate width
Y	Geometry factor

LEFM	Linear Elastic Fracture Mechanics
MRS	Multiple Reference States
RMS	Root Mean Square
SIF	Stress Intensity Factor
WF	Weight Function

ε	Elastic strain
φ, ϕ	Surface crack parametric angle
ρ	Cylindrical coordinate
σ	Applied stress
σ_0	Initial stress
σ_{xx}	Longitudinal stress
$\Delta\sigma$	Stress range

CHAPTER 1

1.0) Introduction and Background

1.1) Fatigue

Linear Elastic Fracture Mechanics is a mature subject, and the study of fatigue is an important part of this science. The occurrence of cracks in structures and components poses a real threat to the well-being of these structures. These cracks may grow and result in loss of integrity and at times, total structural failure. This research is focused on the study of fatigue crack growth in components under non-uniform stress distributions.

Fatigue is considered an unfavourable phenomenon because of the economic damages it incurs to structures. Indeed most of the material failures are directly or indirectly due to fatigue [1.1]. Therefore the study of mechanical failures has been mainly focused on fatigue of metals.

Materials contain intrinsic flaws due to manufacturing techniques. Some processes during production, such as welding, rolling, surface preparation etc. also create small imperfections and defects. Under cyclic loading, these defects may start to grow into cracks, which if not stopped, would eventually grow to a critical size whence fracture occurs. However, this relatively slow fatigue crack growth phase gives the opportunity of preventive action while the critical crack size has not been reached.

Systematic study of fatigue was initiated by Wöhler [1.2], who examined the effect of cyclic loading on materials. Wöhler proposed the concept of the fatigue curve, or S-N curve, where the number of cycles to failure for a material is plotted against the value of stress. However, fatigue in a broad sense is a complicated phenomenon and many conditions affect this number of cycles to failure, or the life of the specimen. For

example, steels at elevated temperatures tend to exhibit creep, therefore under a cyclic load, creep fatigue takes place. On the other hand, at lower temperatures plasticity of metals decreases and brittle fracture becomes more probable. Corrosion fatigue is the combination of fatigue and corrosion, whereas delayed fracture under the combination of active environment and non-cyclic load is termed stress corrosion cracking, or static fatigue. When fatigue is mentioned hereafter in this text and no comment is made, cyclic fatigue is meant.

The resistance of a material against fatigue depends on a number of factors such as: surface roughness, residual stress fields, environmental conditions such as temperature and corrosion, loading history etc., each demanding a separate study. The fact that most fatigue cracks start on the surface of the materials is also worth noting. It is believed that because the surface elements of the material experience less constraint from the surrounding material, they tend to have less fatigue resistance. A more mathematical description for this condition is that the state of stress at the surface of the material is different from that of the subsurface since the surface, when not loaded directly, is essentially traction-free (plane stress). The surface area is also more vulnerable to damage and defects, which could act as stress raisers and suitable sites of fatigue crack initiation.

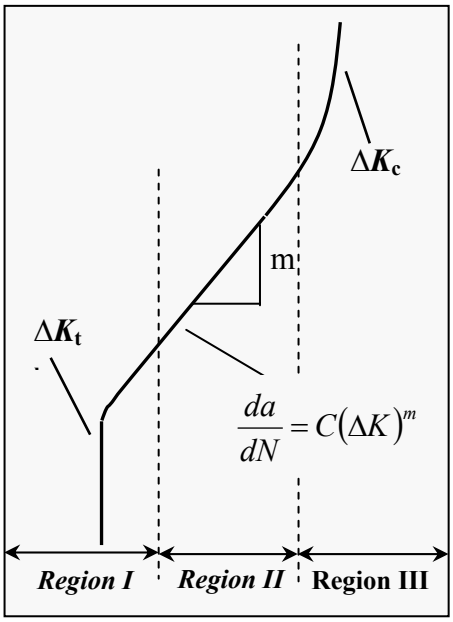

Figure 1.1- Fatigue crack growth rate versus ΔK

Fatigue crack growth is usually divided to three stages as shown in the sigmoidal curve of figure 1.1. Stage I is when the stable crack growth rate has not reached the threshold value. Stage II is the stable crack growth phase, and stage III is the region of unstable fracture. However, if the initial defect is a sizeable crack, the first stage may be very short in duration or even non-existent, and the crack may grow as the second stage of figure 1.1. Stage II has been the subject of numerous studies [1.3-1.7], since it is only at this stage that the growth of the crack can be easily observed and measured.

Paris et al. [1.8] argue that since the stresses and strains near the tip of the crack are "completely specified" by the stress intensity factor (K) and the ratio of the maximum to minimum load during cyclic loading, it is reasonable to assume that any phenomena occurring in this region, e.g. crack extension, are controlled by these parameters, therefore relating fatigue to fracture mechanics. Later Paris and Erdogan [1.9] compared different existing crack growth models and established an empirical relation based on the experimental data available, known as the Paris Law, thus solidifying the link between fatigue and fracture mechanics.

This chapter covers a review of only those areas of LEFM that are directly relevant to fatigue. The main purpose of this study is to develop a better understanding of fatigue through tools such as stress intensity factors (SIF). A background to the phenomenon of fatigue is given here, and then different methods of stress intensity factor evaluation are reviewed. The versatility of weight functions makes them an invaluable tool in the determination of SIF values.

1.2) Stress Intensity Factor and its Evaluation

It has been observed that certain components fracture upon reaching a certain value of the stress intensity factor, known as K_{crit}, thus requiring the engineer to determine the stress intensity factor under likely structural loading cases. Additionally, as seen in the previous section, stress intensity factors can assist in the task of *fatigue crack growth calculation*, therefore making their evaluation more important.

Broadly speaking, methods of stress intensity factor determination, like any other stress-field related parameter in solids, fall within one of the following categories:

1) *Analytical Methods*
2) *Experimental Methods*
3) *Numerical Methods*

Some examples of these different techniques are mentioned herein. For details on these methods and their limitations refer to the cited references. For an excellent account of the different methods of stress intensity factor determination see the book by Sanford [1.10].

1.2.1) Analytical Methods

1) Conformal mapping (Conformal Transformation), where a body is mathematically transformed into another geometry, for which the solution to the stress field is easier to obtain. For details on the conformal mapping technique see the classic comprehensive book of Muskhelishvili [1.11]. For an application of this technique in fracture mechanics and a discussion on the limitations see the work of Hasebe and Iida [1.12].

2) Body force method, proposed by Nisitani [1.13]. In this method, the problem is formulated as a system of singular integral equations, where the unknown functions are the densities of body forces distributed in an infinite body. However, this technique can only be employed for problems with a simple geometry and loading.

1.2.2) Experimental Methods

Some of the experimental techniques are named here:

1) Photoelastic determination of mode I stress intensity factor. For a good review, please refer to the work of Etheridge and Dally [1.14]. This method can not be

used for two-dimensional surface cracks as the measurement of SIF is done at the surface.

2) The method of caustics [1.15, 1.16]. This method is an optical way of visualising the stress distribution close to the crack tip. Also called the shadow-spot method, it relies upon deflection of light rays due to stress-field gradients. Since the in-plane stresses near the crack tip are both tensile, the Poisson effect causes a local contraction (or thinning) of the material in the out-of-plane direction, which itself acts as a divergent lens and deflects the light. It is instantly recognised that this technique can only be used for edge or through one-dimensional cracks, with small-scale yielding at the crack tip.

3) Strain gauges [1.17]. Strain gauges can be used to give local values of strain, from which the stress field is then inferred.

4) Moire patterns [1.18].

5) Thermo-elasticity [1.19], in which the small change in temperature due to the deformation of the material at the crack tip region can be measured and used to evaluate the stress levels.

6) Compliance methods [1.20]. Here the change in the compliance of the specimen is used to obtain the stress intensity factor. This method is based on the work-energy theorem.

1.2.3) Numerical Techniques

These methods are briefly described here:

1) The Alternating method, proven to be particularly useful for three-dimensional problems [1.21] in which the exact solutions to two problems related to the problem of interest are available, each of which satisfying some of the boundary

conditions for the new problem. Beginning from a known solution, by adding an appropriate solution which corrects for a specific set of boundary conditions, the result will contain some errors on other boundaries, which in turn can be eliminated by addition of a new known solution correcting for this condition, and thus hopefully reducing the overall error. This 'alternation' between the solutions is continued until the overall error falls within an acceptable range.

2) The Compounding method, proposed by Cartwright and Rooke [1.22], where the stress intensity factor for a complex geometry is obtained as the sum of a series of ancillary problems. Here, the K value due to each of the geometrical features is determined independently, and the results are 'compounded', with the addition of an extra stress intensity value which denotes the interaction of the different boundaries in terms of the stress intensity factor [1.22, 1.23]. This method is not based on the principle of superposition, where the geometry is unchanged, and the effects of different independent loadings are added to obtain the combined effect, hence the addition of the 'interaction' correction term.

3) The transform method of Sneddon and Lowengrub [1.24].

4) The Laurent series expansion [1.25, 1.26].

5) The Boundary Collocation method is used when a solution that satisfies the governing equations everywhere in the interior and along the crack plane is known. In the Boundary Collocation method, in contrast with analytical solutions in which the boundary conditions are satisfied at every point, the boundary conditions at a discrete number of points are made to be met. However, its use is limited to a specific group of problems. By its nature, the boundary collocation method determines the SIF from the boundary stresses. Therefore, if the stress-field disturbance due to a crack is confined to a small region away from the boundaries, its effect on the stresses at the boundaries would be negligible, and therefore undetectable by the boundary collocation method.

6) The Finite Element method is usually the preferred method for stress intensity factor evaluation for practical purposes. It has two main advantages over the boundary collocation technique: (a) an a priori knowledge of the stress series solution is not needed for the interior of the body and, (b) contrary to the boundary collocation method there are numerous finite element software packages in existence with many capabilities.

7) The Weight Function technique. Strictly speaking, this method should be categorised as an analytical method, but because of the approximations that are usually introduced for convenience, it could also be taken as a numerical method. The following sections provide a detailed study of the application of weight functions for stress intensity factor determination.

1.3) Weight Functions

1.3.1) One-dimensional Crack Problems

In calculating the stress intensity factor for a crack, the complex nature of the problem is instantly recognised: stress intensity factors not only depend on the geometrical characteristics of the cracked body, but they also depend on the loading, i.e. surface tractions and body forces, which may result in a complicated stress distribution near the crack tip.

The idea of the weight function approach for calculation of the stress intensity factor arises from the fact that "it is generally much simpler to compute the stress field in the un-notched specimen" [1.27]. In his paper published in 1970, Bueckner showed that for a one-dimensional crack problem, in which the crack is loaded symmetrically, the stress intensity factor can be expressed using a 'weight function', as follows:

$$K = \int_0^a \sigma(x) h(a,x) dx \qquad (1.1)$$

where a is the crack length, and σ is the stress on the crack face plane in the un-cracked body under the action of the same boundary and body forces. Therefore this approach simplifies the task of stress intensity factor calculation by replacing the complex stress analysis for the cracked body with the much simpler job of stress analysis of the un-cracked body [1.27]. *h(a,x)* is called the Weight Function.

It has also been shown that this weight function is unique for the specific crack-specimen geometry configuration and is not a function of the load [1.27, 1.28]. But Bueckner did not provide any practical means of numerical determination of the weight function.

Rice [1.28] showed that for any symmetrical load system leading to stress intensity factor K and displacement field $\mathbf{u}$, the weight function in (1.1) can be expressed as:

$$h(a,x) = \frac{H}{2K}\frac{\partial \mathbf{u}}{\partial a} \tag{1.2}$$

Here, H is an appropriate elastic modulus: for an isotropic material it is $\frac{E}{1-\nu^2}$ for plane strain and E for plane stress; for anisotropic materials see the work of Sih et al. [1.29].

Equation (1.2) has a very significant meaning and that is that if the stress intensity factor value and the corresponding crack displacement are known under any arbitrary stress distribution (i), then by use of the weight function, the stress intensity factor for any other stress system (ii) acting on the same specimen can be calculated as:

$$K^{ii} = \int_0^a \sigma^{ii}(x)\frac{H}{2K^{i}}\frac{\partial \mathbf{u}^{i}}{\partial a}dx \tag{1.3}$$

Though the stress intensity factor values for a large variety of crack-loadings are known [1.30-1.32], they are rarely accompanied by data on the crack-face displacement field.

A major breakthrough was achieved by the work of Petroski and Achenbach [1.33]. In their paper first published in 1978, it is suggested that equation (1.3) can be used to self-substitute for K^i, i.e.

$$K^i = \frac{H}{K^i}\int_0^a \sigma^i(x)\frac{\partial \mathbf{u}^i}{\partial a}dx \tag{1.4}$$

Equation (1.4) is an integral equation for the **u** field, which can only be analytically solved for a limited number of cases [1.33].

For this reason, based on the limiting behaviour of the displacement field in the vicinity of the crack tip [1.34], Petroski and Achenbach further assumed a functional dependence of **u** on *x* as the following approximate formula:

$$\mathbf{u}(a,x) = \frac{\sigma_0}{H\sqrt{2}}\left\{4F\left(\frac{a}{L}\right)a^{1/2}(a-x)^{1/2} + G\left(\frac{a}{L}\right)a^{-1/2}(a-x)^{3/2}\right\} \tag{1.5}$$

where σ_0 and L are characteristic stress and length parameters. Here F is known, while G is to be determined from equation (1.4). This form has the advantage of ease of integration when substituted in equation (1.4).

For an edge crack in a half plane, Petroski and Achenbach have shown that by taking uniform remote tension as the reference, this assumption yields a maximum error of 3% in the calculation of the stress intensity factor for the case of concentrated normal loads [1.34].

By applying the same technique to various other scenarios, they have concluded that their method is a robust way for the determination of the weight function except for "extremely deep cracks in a particular application" [1.33]. However, in their paper, they do not deal with cases where the stress differs greatly from the uniform case, i.e. *σ=const.*

Gorner et al. [1.35] have exemplified the inaccurate nature of the above method for the cases in which a highly non-uniform stress is taken as the reference. Although they do not give a comprehensive analysis of the limitations of the Petroski-Achenbach approximation, they rightly conclude that the method should be used with extra care, especially since the choice of the reference problem is arbitrary, the uniformly distributed stress reference case should be taken to minimise the errors in the determination of **u**.

Niu and Glinka [1.36] argue that the discrepancy between the Finite Element results of Gorner et al. and Petroski-Achenbach's method is due to numerical errors in integration. They use two different references of linear stress distribution on the plane of the crack face and conclude that the Petroski-Achenbach approximation for the displacement field leads to accurate results. Nevertheless Gorner's argument is that the Petroski-Achenbach approximation should be used with some cautiousness for inhomogeneous reference stress distribution. Fett [1.37] concludes that in the case of linear varying load along the complete length of the crack the errors of Petroski-Achenbach's method are negligible for practical use. In the case of partially loaded cracks or very steep reference stress profiles, however, their approximation may fail.

Due to the abovementioned disputes, using the same concept of self-substitution of equation (1.3), Fett [1.37] suggests another functional form for the crack-face displacement field as:

$$u/u_N = 1 + \sum_{\nu=1}^{\infty} C_\nu \left(1 - \frac{x}{a}\right)^\nu \tag{1.6}$$

in which u_N is the near tip field of the crack opening displacement:

$$u_N = \sqrt{8/\pi}\,\frac{K}{H}\sqrt{a-x} \tag{1.7}$$

The coefficients C_1 and C_2 in equation (1.6) are determined by, in addition to the principle of self-consistency, using $\partial u/\partial x = 0$ at x=0 for the Griffith crack, and $\partial^2 u/\partial x^2 = 0$ at x=0 for the edge crack, as proven by Fett et al. [1.37, 1.38].

By comparison with some reference solutions, Fett has shown that these additional conditions result in more accurate approximate solutions; Petroski and Achenbach's approximation represents the first two terms in the series (1.6).

However, the Petroski-Achenbach technique and the improved displacement field of Fett require the numerical differentiation of the crack-face displacement field. Therefore, in order to reduce the number of computations needed to obtain weight functions, and thence stress intensity factors, Ojdrovic and Petroski [1.39] assumed the *derivative of the crack profile* to be in the form of a series:

$$\frac{\partial u(a,x)}{\partial a} = \frac{2\sigma}{H}\sqrt{2}\sum_{j=0}^{M} c_j \left(1-\frac{x}{a}\right)^{j-1/2}; c_0 = \frac{F\left(a/d\right)}{2} \tag{1.8}$$

And then, in order to evaluate a number of the unknown coefficients, they have introduced the method of Multiple Reference States, which makes it possible to calculate as many unknown coefficients as there are known reference stress intensity factors.

In other words, assuming that M stress intensity factors are known for a particular geometry under M symmetric loading states, then equation (1.3) can be re-written as:

$$\int_0^a H\sigma_i(x)\frac{\partial u_1(a,x)}{\partial a}dx = K_i(a)K_1(a) \tag{1.9}$$

Where subscript i denotes the ith reference case. This is a system of M equations which yields M unknown coefficients. By having these values, the weight function can be constructed by substituting (1.8) into equation (1.2). Brennan [1.40] has given a more

portable form of the Multiple Reference States method in the form of a matrix equation, along with a comparison of the methods through an examination of their self-consistency, which is essentially a numerical accuracy test. It is, however, a trivial fact that by increasing the number of reference solutions, more accurate weight functions can be derived.

Because the existing 'exact' solutions for the stress intensity factor for a certain geometry are usually those of remote tensile and bending modes [1.32], the number of terms that can be evaluated in equation (1.9) are three, which is the same as that of Fett's approximation [1.37]. No comparison has been made between Fett's approximation and the multiple reference states technique.

1.3.2) Surface Cracks

1.3.2.1) Significance of Surface Cracks

As mentioned before, cracks usually initiate from small surface defects, which then develop into what is called the 'part through crack'. "In the examination of fracture failures one rarely finds that the initial starting crack extends completely through the thickness or that the starting-crack development, say by fatigue, occurs along a line extending completely through a cross section of a component" [1.41]. Figure 1.2 shows an idealised semi-elliptical surface crack.

Here, the stress intensity factor varies along the crack front. Because of the frequent occurrence of the surface crack in components, many attempts have been made to evaluate the stress intensity factor variation along a surface crack front for different load modes [1.42].

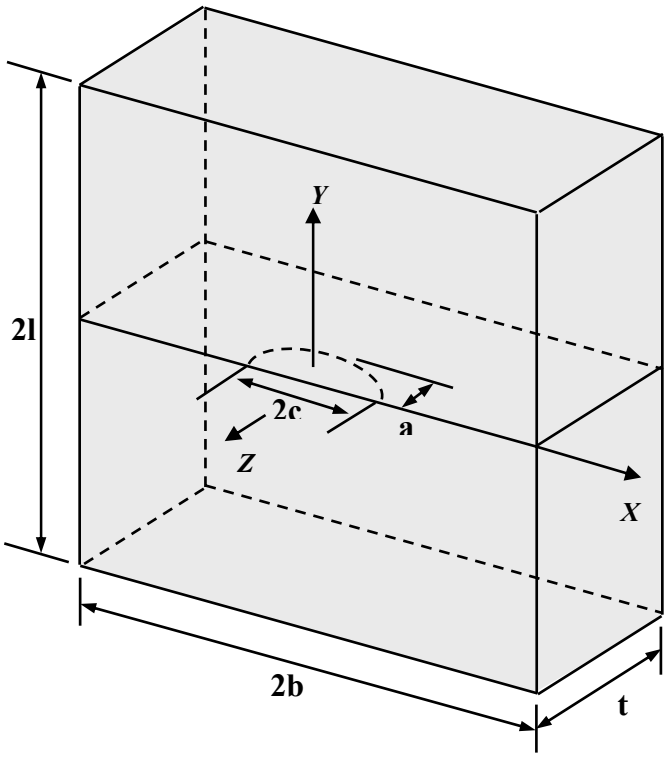

(a)

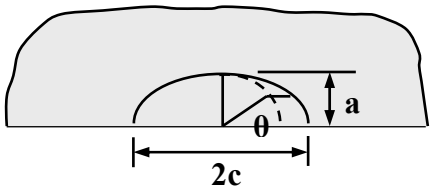

(b)

Figure 1.2- Surface crack

It is generally assumed, for the sake of mathematical simplicity, that surface cracks are of a semi-elliptical shape. Observation of many instances of surface cracks confirms the suitability of this approximate assumption. Nevertheless, the effect of a disturbance in the shape of the crack- such that whence the crack does not retain the semi-elliptical form- on the stress intensity factor has not been rigorously studied [1.43- 1.45].

However, it has been observed that even when the starting-crack is not semi-elliptical, surface cracks do tend to grow into a semi-elliptical shape [1.46].

1.3.2.2) Stress Intensity Factor Evaluation in Surface Cracks

The first classic work on the study of the semi-elliptical surface crack, under the action of remote tension, was presented by Irwin [1.41]. Knowing the stress intensity factor distribution of an embedded elliptical crack [1.47], Irwin assumed that for a real crack similar to that shown in figure 1.2, the solution consists of that of the embedded crack with the addition of some corrections to account for the free surfaces. However, the introduced correction terms were somewhat arbitrary and unsubstantiated, and at the time there was no other reference solution available for comparison purposes.

A major breakthrough was the work of Newman and Raju [1.48], where they introduced the following parametric equation of stress intensity factor distribution for semi-elliptical surface cracks on a plate subject to tension and bending:

$$K_I = \left(S_t + HS_b\right)\sqrt{\pi \frac{a}{Q}} F\left(\frac{a}{t}, \frac{a}{c}, \frac{c}{b}, \phi\right) \tag{1.10}$$

The parameters are shown in figure 1.2. Newman and Raju derived their empirical equations for F from a large set of three-dimensional finite element analyses. For all configurations for which the ratios of crack depth to plate thickness (a/t) do not exceed 0.8, the equation is within ±5% of the finite element results [1.48].

Hosseini and Mahmoud [1.49] give an excellent examination of the Newman and Raju formula for tensile plates, comparing the K values against the recommended tabulated values given by Society of Experimental Stress Analysis (SESA) [1.43] and also against photoelastic data [1.50]. They also used the Newman-Raju solution to predict growth patterns of surface defects in tensile plates, assuming that fatigue cracks grow in a semi-elliptical shape, and that the Paris growth correlation is valid, i.e.

$$\frac{da}{dN} = C_a\left(\Delta K_a\right)^m \quad \text{and} \quad \frac{dc}{dN} = C_c\left(\Delta K_c\right)^m \tag{1.11}$$

The crack shape evolution curves are then compared with the data from literature, and they conclude that the Newman-Raju formulae give the most accurate value for stress intensity factor among the available empirical formulae [1.49].

Based on experiments reported by Corn showing that small semi-circular surface cracks propagate as semi-circles [1.51] for low *a/t*, Newman and Raju [1.48] suggest that $C_c = (0.9)^m C_a$. This assumption has been used by other workers in the field [1.52], but Corn's observation does not include medium-sized or large semi-circular cracks, which at the very least is good grounds to question the validity of this assumption. Newman and Raju [1.48] also argue that one reason for the inequality between C_a and C_c may be the change in the correlation between the growth rate and stress intensity factor as the stress state changes from plane strain at the deepest point to plane stress on the surface. If this inequality does really exist, then their argument simply re-states its existence and does not impart any new knowledge.

It is, however, sometimes the case that surface cracks should propagate in stress fields that are not uniform or linear. Such instances include crack growth in residual stress fields [1.53]. Again, like the one-dimensional crack, it seems that the concept of a weight function approach could be beneficial. The first work on the surface crack weight function was published as an appendix in Rice's classic paper [1.28], in which it was proven that for a given crack geometry in a given three-dimensional body, the weight function is unique and independent of the loading. Rice also points out, that there are cases for which knowledge of an integrated average of the intensity factor is sufficient for the calculation of the weight function.

Shen and Glinka [1.54] proposed the use of local weight functions for the surface and deepest points of a semi-elliptical crack. Their weight function is derived from an approximate displacement field and contains three unknown coefficients as follows:

$$m_A(x,a) = \frac{2}{\sqrt{2\pi(a-x)}}\left[1 + M_{1A}\left(1-\frac{x}{a}\right)^{1/2} + M_{2A}\left(1-\frac{x}{a}\right) + M_{3A}\left(1-\frac{x}{a}\right)^{3/2}\right] \qquad (1.12)$$

for the deepest point, and

$$m_B(x,a)=\frac{2}{\sqrt{\pi x}}\left[1+M_{1B}\left(\frac{x}{a}\right)^{1/2}+M_{2B}\left(\frac{x}{a}\right)+M_{3B}\left(\frac{x}{a}\right)^{3/2}\right] \tag{1.13}$$

for the surface point. Here, the unknown parameters M_{1A}, M_{2A} and M_{3A} can be obtained from two reference stress intensity factor solutions at the deepest point and an additional condition $\frac{\partial^2 m_A(x,a)}{\partial x^2}=0$ for x=0, and M_{1B}, M_{2B} and M_{3B} can be obtained from two reference stress intensity factor solutions at the surface point and an additional condition $m_B(x,a)=0$ for x=a.

Apart from the approximate nature of the weight functions proposed by Shen and Glinka, there are a few points worth mentioning here. The additional condition for determination of the unknown parameters for $m_A(x,a)$ assumes that at the plate surface (x=0), the curvature of the crack surface in the x-y plane is zero. This is indeed true for edge cracks as proven by Fett et al. [1.55] but it can not be easily generalised to all surface cracks. It is worth noting that unlike the one-dimensional crack, e.g. the Griffith crack, no analytical solution is available for the simple case of a semi-elliptical surface crack face displacement under any load.

Moreover, the proposed weight functions of (1.12) and (1.13) can only account for a loading which varies in the x direction, i.e. in the depth direction. However, there are occasions in which the loading may vary in the y direction (i.e. surface direction). A good example of this type of stress field is the residual stress field induced in specimens with partially shot-peened surfaces. Here, the residual stress field varies both in the depth and in the surface direction.

Another problem in their methodology is that the weight functions can only evaluate values of stress intensity factors at the surface and deepest points, and then assuming a

semi-elliptical crack shape, the growth is dealt with as a two-degree of freedom problem. It may however be possible that a certain stress field results in a stress intensity factor distribution which is maximal at a point somewhere between the surface and the deepest point, and therefore the crack growth rate would be higher at that point. Shen and Glinka's approach does not allow for such an eventuality.

In order to evaluate stress intensity factors at any point along the crack front, Wang and Lambert [1.56] have proposed a local weight function, which is close in form to Shen and Glinka's formulae. It is a piece-wise function of ϕ and contains four unknown parameters:

For $0 \le x \le a\sin\phi$,

$$m_P(x,a) = \frac{\sqrt{\sin\phi + 1}}{\sqrt{\pi(a\sin\phi - x)}}\left[1 + M_{1P}\left(1 - \frac{x}{a\sin\phi}\right) + M_{2P}\left(1 - \frac{x}{a\sin\phi}\right)^2\right] \tag{1.14}$$

And for $a\sin\phi \le x \le a$,

$$m_P(x,a) = \frac{\sqrt{1 - \sin\phi}}{\sqrt{\pi(x - a\sin\phi)}}\left[1 + M_{3P}\left(\frac{x}{a\sin\phi} - 1\right)^{1/2} + M_{4P}\left(\frac{x}{a\sin\phi} - 1\right)\right] \tag{1.15}$$

where the four unknown parameters M_{1P}, M_{2P}, M_{3P} and M_{4P} are determined from two stress intensity factor solutions and the same additional conditions as for Shen and Glinka's method, i.e.. $\frac{\partial^2 m_P(x,a)}{\partial x^2} = 0$ for x=0 and $m_P(x,a) = 0$ for x=a. Again it is assumed that the curvature of the crack surface at x=0 is zero. However, as mentioned before, no analytical solution for the crack displacement is available for surface cracks to support this assumption.

Orynyak et al. have taken a new approach in developing an approximate point weight function for the semi-elliptical surface crack [1.57]. First, they have derived an

approximate weight function for an embedded elliptical crack based on the existing weight function [1.58] available for the embedded penny-shaped crack, and the semi-infinite crack with a straight front. They argue that this weight function for the embedded elliptical crack is no less accurate than the existing solution of Oore and Burns [1.59], but at the same time much easier to use. For the surface crack weight function, they introduce a 'free surface correction term', which should introduce the effect of the free surface on the stress intensity factor in semi-elliptical surface cracks. The resulting stress intensity factors from this weight function show relatively small errors (usually within ±5%) when compared to the Newman and Raju solution for tensile and bending loadings. However, they show a greater deviation when dealing with other loading (e.g. partial loading) on the crack face. Although their approximate weight function for the embedded crack may be easier to apply than other existing approximate weight functions, for the surface crack it is quite complicated to determine and apply [1.60].

1.3.2.3) The Averaged Stress Intensity Factor or RMS SIF Weight Function

In his classical paper [1.28], Rice points out that there are cases for which knowledge of an integrated average of the intensity factor is sufficient for the calculation of the weight function. Besuner and Cruse [1.61] were the first to utilise this concept in what is now known as the Root Mean Square (RMS) stress intensity factor, in two different directions of crack growth, with the formal definition of $\overline{K}_i$ given by Besuner [1.62] as:

$$\overline{K}_x{}^2 = \frac{1}{\delta A_x}\iint_{\delta A_x} K^2(s)dA \text{ and } \overline{K}_y{}^2 = \frac{1}{\delta A_y}\iint_{\delta Ay} K^2(s)dA \tag{1.16}$$

where

$$\delta A_x = \pi a_y \delta a_x \text{ and } \delta A_y = \pi a_x \delta a_y \tag{1.17}$$

Their method involves definition of a number of characteristic dimensions (usually two) for a crack; the crack propagation being described by keeping track of these dimensions.

For the crack shown in figure 1.3, these parameters are a_x and a_y, which denote crack lengths in the two perpendicular dimensions as shown. They have assumed that the coefficients of Paris Law for this type of analysis are the same as for when normal stress intensity factor values are used.

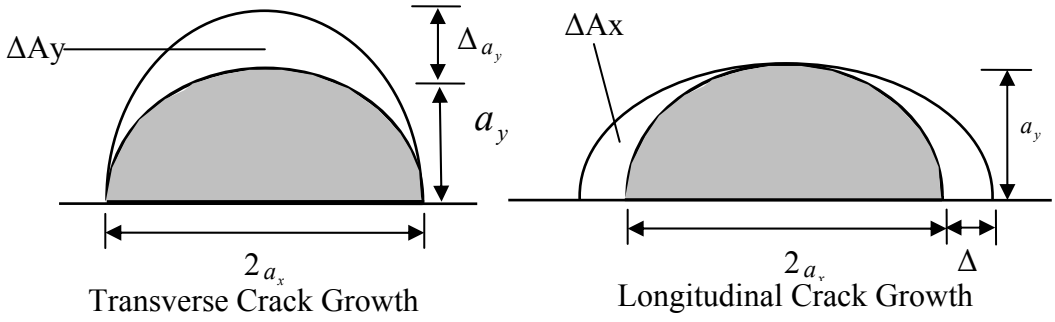

Figure 1.3- Two characteristic growth dimensions

However, if the stress intensity factor variation for a crack under arbitrary loading is not known, the RMS stress intensity factor calculation is extremely complicated. Besuner [1.62] used the energy balance principle for an increment of crack growth, and with analogy to Rice's work [1.28], has derived the following expression for the average stress intensity factor weight function, where q^* is the crack face displacement for the reference crack face loading of σ_{zz}^* and *i* and *j* are the characteristic dimension indices:

$$h_{ij} = \left(\frac{2\partial\left(Q_m^* q_m^*\right)}{H\partial A_i} \right)^{-\frac{1}{2}} \frac{\partial q_j^*}{\partial A_i} \tag{1.18}$$

Here, the repeated index *m* denotes summation. Q is the normal load, defined such that for a case where the forces on the crack face can be expressed as a bivariate normal stress $\sigma_{zz}(x, y)$, the following simple equation holds:

$$dQ(x, y) = \sigma_{zz}(x, y) dA \tag{1.19}$$

Therefore the averaged stress intensity factor for an arbitrary loading can be expressed in terms of the stress and a reference displacement field as [1.62]:

$$\overline{K}_i = \left(\frac{2\partial \left[\iint A \sigma_{zz}{}^{*} q^{*} dA \right]}{H \partial A_i} \right)^{-\frac{1}{2}} \iint_A \sigma_{zz} \frac{\partial q^{*}}{\partial A_i} dA \tag{1.20}$$

It is obvious that this equation has little practical significance as no reference crack displacement is known for surface cracks.

The concept of the RMS stress intensity factor certainly simplifies the analysis of crack growth -like the deepest and surface points approach- by reducing the problem to a two degrees of freedom analysis, while unlike the local weight function method, an integrated average of the stress intensity factor is evaluated. Any anomaly in the stress intensity factor distribution somehow shows its effect in the resulting RMS stress intensity factor. Mahmoud conducted a series of analyses on surface crack growth and aspect ratio variation under tension [1.63] and bending [1.64] and concludes that use of average K rather than local K improves the accuracy of growth pattern prediction for tensile plates, but for plates under bending, using average stress intensity factor does not add to the accuracy of the shape prediction.

Mattheck et al. [1.65] have derived an approximate average weight function for the semi-elliptical crack by approximating the crack displacement field of the deepest point of the crack as that of an edge crack, with the stress intensity factor taken at the deepest point. They have also assumed the surface profile of the crack (x=0 plane) to be similar to a Griffith crack. Using the Newman and Raju [1.48] formula for the stress intensity factor reference, they have derived the following approximate displacement field for the surface crack [1.65]:

$$u_r(x,y) = \frac{\sigma_0}{H\sqrt{2}} \left\{ 4F_0(a^{*}) \sqrt{a^{*}} \sqrt{a^{*} - x} + G_0(a^{*}) \frac{(a^{*} - x)^{3/2}}{\sqrt{a^{*}}} \right\} \tag{1.21}$$

Comparison between the results obtained from the weight function based on the approximate displacement field and the solution of Newman and Raju shows that this method, though showing an agreement in the trend of variations, predicts lower stress intensity factor values [1.65], leading to unsafe predictions. Considering the fact that Newman and Raju's solution has been used for the reference solution for the displacement field derivation, this exercise does not lead to a decisive and systematic verification of the methodology as the results are again compared with the Newman and Raju's values.

Appreciating the influence of the displacement field on the accuracy of the weight function, Fett [1.66] adopted a more rigorous approach to the crack displacement determination. Fett assumed that the crack-face displacement for the reference loading case of $\sigma_r = const$ can be expressed in the form of a series as:

$$u_r(\rho,\phi) = \sum_{\nu=0}^{\infty} C_\nu(\phi)\left(1 - \rho/r\right)^{\nu+1/2} \tag{1.22}$$

The parameters ρ and ϕ for the semi-elliptical surface crack denote the cylindrical coordinates of any point inside the semi-ellipse. Here the coefficients are assumed to be functions of a/c and a/t and the parametric angle ϕ. Similar to Wang and Lambert's conditions [1.56], the coefficients are determined from a number of geometrical assumptions and self-consistency of the energy balance equation. This method leads to a more accurate determination of the average stress intensity factor compared to Mattheck et al.'s approach [1.65]. However, similar to Wang and Lambert's method [1.56], the assumptions are based on observation and are not substantiated analytically. Similar to their weight function, it is expected that the error in the results would increase for non-uniform stress fields. The fact that sometimes the results are lower than those given by the Newman and Raju's formulae renders the predictions unsafe.

Based on the above displacement field, Fett [1.67] later suggested a new method for the determination of the weight function by adjustment to existing reference solutions. This technique has some similarity to the multiple reference states technique of Ojdrovic and

Petroski [1.39], where the first coefficient is determined from a knowledge of the near-tip behaviour of the displacement field and the other coefficients are determined from adjustment to reference stress intensity factor values. However, in order to derive the coefficients, integral equations have to be solved for each case; moreover, as the number of references increases, the equations become more and more complicated which makes the task of the practical engineer increasingly cumbersome, if not impossible. Therefore this method lacks the main advantage of simplicity that the one-dimensional MRS techniques posses [1.40]. There is also another downside to this weight function, namely that the weight function using one reference solution (two-term weight function) differs considerably from the three-term weight function, i.e. the weight function derived from three reference solutions.

1.4) Residual Stresses

Residual stresses are those stresses which remain in a body under static equilibrium when all external forces (surface tractions and body forces) are removed. Depending on their nature and the loading of a specimen, these stresses can be detrimental or beneficial. For example, tensile residual stresses are detrimental when a specimen undergoes cyclic tensile loading, because the effective or overall stress at each instant, being the resultant of the algebraic addition of residual and applied stresses, is higher than the applied stress level. An example of such a stress state is found in welds [1.68].

However, compressive residual stresses induced in reinforced concretes increase the resistance of the structure to tension. Another example of beneficial residual stresses is the compressive surface stress induced by mechanical surface treatments such as shot-peeing in metals. Under cyclic tensile or bending loads, the existence of the compressive stresses at the surface reduces the effective stress and therefore, can increase the duration of crack initiation or fatigue life of components [1.69, 1.70].

1.4.1) Types of Residual Stress

Residual stresses may be categorised by cause (such as thermal or elastic mismatch), by the scale over which they self-equilibrate, or according to their measurement technique [1.71]. These stresses could vary continuously over relatively large distances, which is the type of residual stresses that will be the main focus of this thesis. Alternatively, they may vary over the grain scale (inter-granular stresses) or the atomic scale [1.71]. In this thesis, wherever the term residual stress in mentioned, it is meant to refer to the first type, i.e. stresses that act over relatively large distances.

1.4.2) Origins of Residual Stress

Residual stresses are caused by misfits, be it in the same component or between different parts [1.72]. Macro residual stresses can occur through the mis-fitting parts

within an assembly (e.g. in reinforced concrete), or through the generation of chemical, thermal, and plastically induced misfits within one part [1.72].

Residual stresses can be produced in components during manufacture from many processes such as plastic deformation or forming, including rolling, bending; or from surface treatments techniques such as shot peening and laser shock peening. Also during manufacturing processes such as welding and machining, residual stresses usually arise [1.73].

Welding usually results in a tensile residual stress area [1.68]. Here, the expansion of the material is inhibited by the surrounding material, and when cold, the tendency to contract results in a tensile residual stress in the weld. In some cases this stress may be at the level of yield magnitude [1.68].

1.4.2.1) Shot Peening

Another important group of sources of engineering residual stresses, i.e. those methods that deliberately introduce residual stresses in components, is surface treatment, generally called peening. These include hammer peening, shot-peening, laser shock peening and ultrasonic peening. Shot peening involves bombardment of the metallic surface with shots, which produces compressive residual stresses very close to the surface of the material [1.74]. A high velocity stream of hard particles is directed at a materials surface producing a compressive residual stress at and below the surface. It has been shown that shot peening under pre-stress can produce an even higher level of compressive stress. [1.75]. Leverant et al. [1.76] showed substantial delays in crack initiation and also higher numbers of cycles required for failure in shot-peened titanium specimens in both low and high cycle fatigue. Farrahi et al. [1.70] studied the effect of shot peening on fatigue life of steel components and concluded that the increase in yield stress of the shot peened material due to strain hardening of the surface, the compressive residual stresses induced in the superficial layers, and the quality of the surface texture of the shot-peened part are the three main factors affecting mechanical properties of the shot peened part. Figure 1.4 [1.77] shows the surface texture of a steel specimen after

the shot peening process and figure 1.5 (taken from [1.77]) shows the residual stress distribution through the thickness of this specimen.

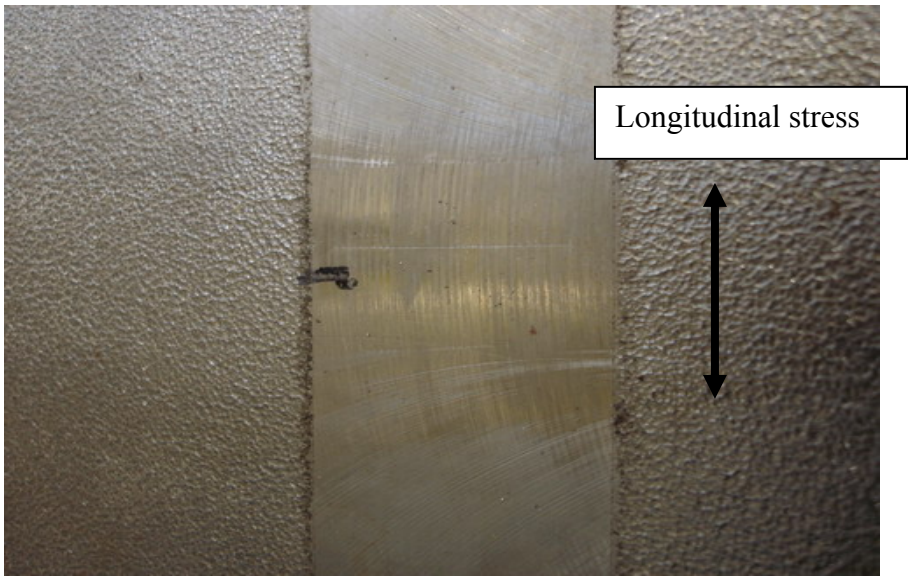

Figure 1.4- Surface texture of shot-peened steel [1.77]

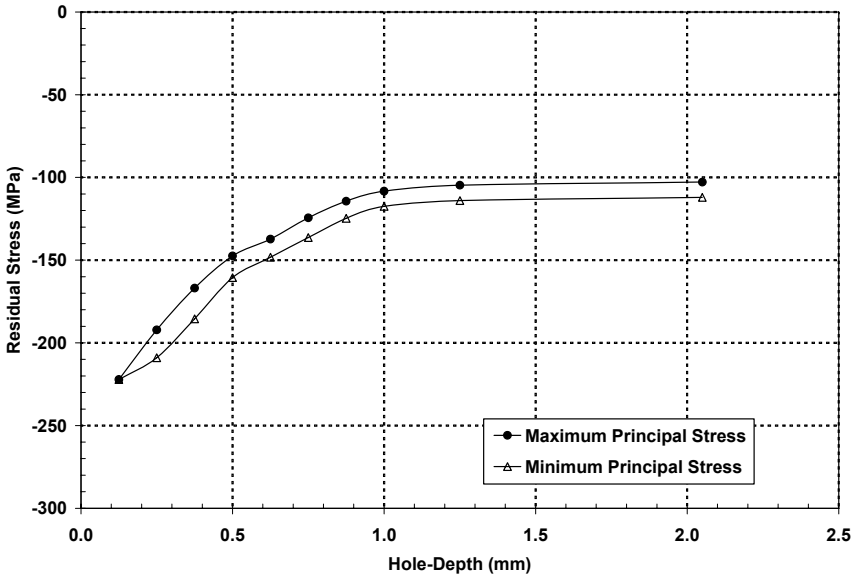

Figure 1.5- Typical stress profile in a shot-peened steel specimen [1.77]

Since in the present work, laser shock peening has been investigated in detail, more emphasis is given to the description of this technique here.

1.4.2.2) Laser Shock Peening

Laser shock peening was first used by Battelle Columbus Laboratories in 1974 [1.78]. It is a process in which a solid-state laser beam is pulsed upon a metallic surface, producing a planar shockwave that travels through the material [1.79]. Here laser with a peak power greater that 1 GW is imaged to a spot size of about 5mm×5mm. Energy densities of 50 to 200 joules per cm^2 and pulse durations of 5 to 30 nanoseconds are typical [1.80].

Figure 1.6 illustrates the laser peening process [1.80]. The work piece is first covered by an ablative material, which can be paint or tape, with typical thicknesses of between 1mm to 2mm. It is called ablative since during the peening process, the surface of this material ablates. This layer is then covered by a thick layer of transparent material, usually glass or water, which during the peening process, confines the expansion of the high pressure plasma. As the laser beam irradiates the specimen, high pressure plasma is rapidly formed. Due to the short duration of the irradiation (typically 5 to 30 nanoseconds), the glass or water layer can not move more than a few microns because of its inertia, and therefore confines the pressure which can be roughly a million pounds per square inch (about 6.8 GPa) [1.80].

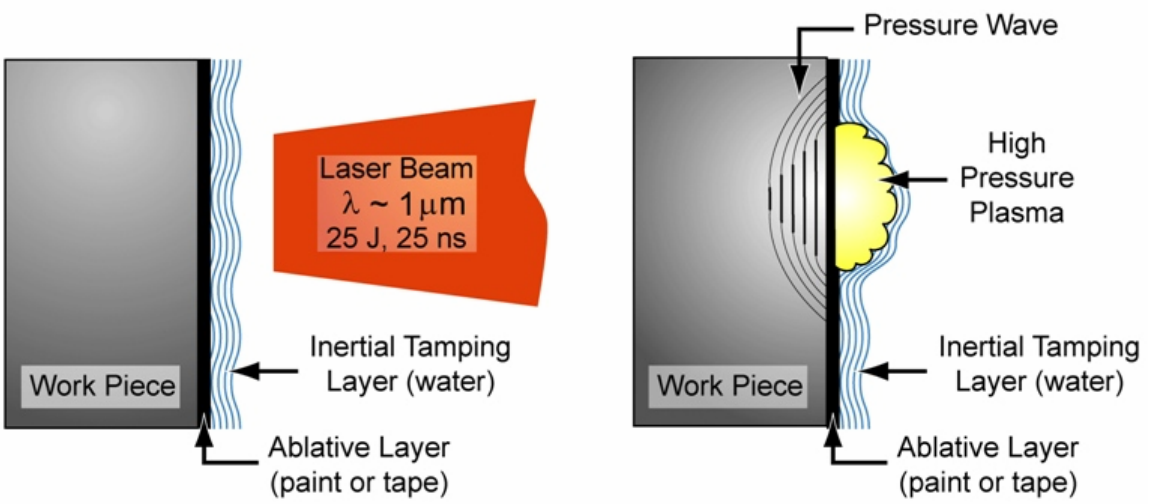

Figure 1.6- Laser shock peening process [1.80]

This pressure sends a shock wave through the work piece which due to its high pressure travels some millimetres in the material and plastically deforms the material in its wake.

Figure 1.7 shows the surface of a steel specimen that has been treated by laser shock peening for the purpose of the present work. Treatment is done in a series of 'spots' of 5mm×5mm each. There is a small amount of overlap between these spots. By a visual comparison with the surface texture of a shot peened specimen made of the same material (figure 1.4) it is clear that the surface texture is relatively unaffected in laser-peened specimens. Though the residual stress across the treated spot is uniform, tensile stress has been observed towards the periphery of the spot and beyond [1.81]. This is required for self-equilibrium of force in the body. However when large areas are peened by overlapping these spots, there is no indication of tensile stress in the overlap regions [1.81].

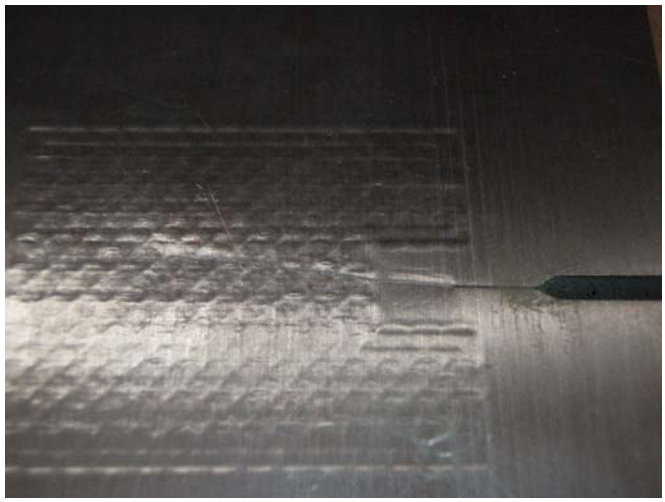

Figure 1.7- Surface texture of a laser chock peened steel specimen

An advantage of laser shock treatment over shot peeening is a higher effective depth of penetration, which means that compressive stresses reach deeper in laser peened specimens. Figure 1.8 shows the depth profile of the residual stress induced in a steel specimen with a thickness of 10mm. This figure is taken from the measurements made in Chapter 4. The stress is measured using neutron diffraction technique.

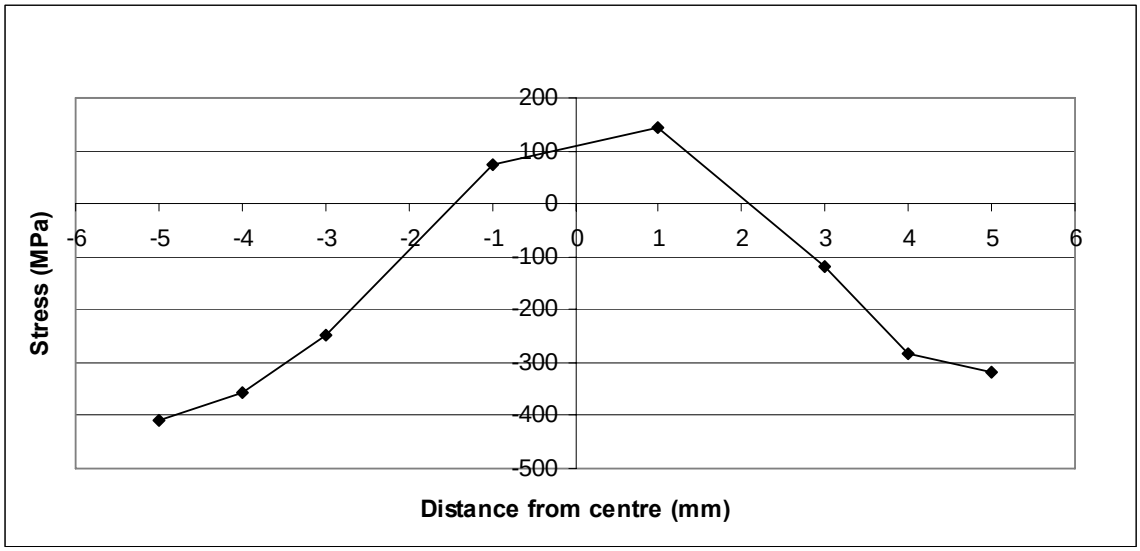

Figure 1.8- Residual stress profile in a 10mm-thick laser peened steel specimen [see Chapter 4]

Hatamleh et al. studied the effects of shot and laser peening on fatigue crack growth in friction stir welded aluminium samples [1.82] and demonstrated the superiority of laser shock peening over shot peening in this application in terms of fatigue life. The laser peening using three layers resulted in a substantial reduction in fatigue life compared with the as-welded and unwelded base material, and shot peening was shown to result in no significant reduction in fatigue crack growth in these samples [1.82].

1.4.3) Measurement of Residual Stress

Residual stresses are known to have a significant effect on fatigue behaviour of components and the performance of the material depends on the magnitude of these stresses. Therefore it is important to have reliable tools and techniques for measurement of the residual stresses in components.

In general, residual stress measurement techniques can be said to be either destructive or non-destructive. Destructive techniques rely on the relaxation, or relief, or residual stresses when part of the stressed material is removed [1.73]. This relaxation usually manifests itself in the form of a change in the displacement, or strain field in the vicinity of the area of interest. Examples of such techniques are the hole drilling method, the

ring core technique and the sectioning method. These techniques are described in the following section.

Non-destructive methods are those techniques which measure the residual stresses without altering the stress field or removing part of the material. Examples of such methods are X-ray and neutron diffraction techniques, and ultrasonic stress measurement methods. These methods are described in the following sections of this chapter.

1.4.3.1) Destructive and Semi-destructive Methods

i) Hole Drilling and Core Methods

Hole drilling methods of residual stress measurement involve drilling a hole through the stressed section, which results in relaxation of the stresses and therefore a change in displacement field around the vicinity of the hole [1.83]. This displacement can be quantified by use of rosette strain gauges [1.84, 1.85], moiré interferometry, laser interferometry based on a rosette of indentations, or holography [1.71]. Typically strain gauges, usually a special three-element strain gauge rosette with a hole in the middle, are placed around the point of interest before drilling, and the change in strain field due to stress relief is measured as a result of material removal. These changes in strain components are then converted to absolute stress values. For a detailed description of the techniques, and recommended guidelines, see ASTM Standard E 837-01 [1.86].

Boag et al [1.87] have studied the occurrence of machining induced stresses due to the drilling process. They found that the drilling speed affects the amount of residual stress induced through drilling: the higher the speed, the lower the levels of induced stresses.

If a specimen is relatively thin [1.83] and a uniform stress profile is expected, through-thickness hole drilling may be used. However, in most application, blind hole drilling is employed [1.84]. In order to obtain the distribution of stress along the depth of the sample, incremental hole drilling is usually used [1.88], where by drilling a hole in a

step-wise manner, the surface displacements of the sample due to stress relief at incremental depths are measured and converted to absolute stress values using a variety of numerical data reduction and analysis procedures [1.86]. It is primarily used for measurements in metallic materials, though Rendler and Vigness have postulated a generalisation to extend the calibrated solution in all elastic, isotropic materials [1.89].

Care must be taken when employing hole drilling method for residual stress evaluation. Accuracy of the measurements taken using the hole drilling technique is sensitive to eccentricity of the hole [1.83]. Rendler and Vigness [1.89] have formulated the relation between the strain gauge readings and residual stresses when the hole is drilled eccentrically. Also, when the stresses vary below the material surface, the accuracy of results depends on the size of depth increments [1.90, 1.86].

Since in this method elastic behaviour is assumed for the material, when residual stresses are high, the drilling may lead to localised plasticity, in which case the response of the material after stress relief is not linear [1.83].

The ring core method is similar, except that a ring core, typically 15mm-150mm internal diameter, is drilled instead of a hole, and displacement in the circular centre area are measured. Since an almost complete relief of surface strains is obtained with this technique, the results show a higher accuracy, and are also insensitive to any minor diameter errors or eccentricity of the annular hole with respect to the strain gauges [1.73]. However, the results obtained using ring core method are much less localised compared to the results from hole drilling [1.71].

The hole-drilling and ring core methods have also been described as “semi-destructive”, since the amount of material removed is small and usually does not affect the behaviour of sample in use [1.83, 1.86]. Current standards recommend that this technique can only be utilised reliably when the stresses do not exceed 50% of the yield strength [1.85, 1.86]. However, studies carried out by Flaman [1.91], indicate that for equal biaxial stresses equal to $0.8\sigma_Y$, the radius of plastic region around the hole is less than 80% of the gauge radius, and therefore the analysis is still valid.

ii) Layer Removal Method

When a layer is removed from a material which contains residual stresses, the balance of the internal stresses and moments is upset. This disturbance in the equilibrium of the material results in a deformation. If the layer removal does not introduce any plasticity in the material, then the new deformation could be said to be the net result of elimination of the residual stresses in the removed section of the specimen. This is the basis of layer removal technique for residual stress measurement. Layer removal is usually done using chemical machining in order to leave the new surface free of removal-induced plasticity [1.92].

1.4.3.2) Non-destructive Residual Stress Measurement Methods

i) Diffraction Methods

Diffraction techniques for residual stress measurement are non-destructive methods that are used for crystalline solids. They are essentially laboratory based methods and therefore restrictions apply when large components are to be tested. They include X-ray and neutron diffraction techniques, the physical principles of which are similar. However, due to different penetration depths of the two beams, their application can be complementary to each other. Usually X-rays provide measurements over a few microns near the surface whereas neutrons, due to their deep penetration (typically many centimetres [1.71]), can be used to measure strains throughout the thickness of a steel component [1.93]. One important advantage of the diffraction residual stress measurement techniques, particularly the X-ray techniques, is their ability to make measurements on a relatively small area.

Physical Principles of X-ray and Neutron Diffraction Methods

A crystalline solid is made of atoms arranged in a three dimensional periodic pattern. The structure of a crystalline solid is determined by its associated space lattice [1.94], the distance between crystallographic planes being a characteristic of the material in a

given environment [1.95]. If a crystalline material is deformed elastically, this lattice spacing changes from the stress-free state. Diffraction methods can, by employing Bragg's law, measure the new lattice spacing and therefore by having the stress-free lattice distance, infer elastic strains.

At a spallation neutron source, a metal target is bombarded with pulses of high energy protons, driving neutrons from the nuclei of the target atoms. By using hydrogenous moderators around the target, the neutrons are slowed down to required speeds.

Powerful X-rays are generated in synchrotrons in an electron storage ring, the actual path of the electrons being polygonal rather than circular. The electron beam is guided from one straight section into the next by dipole magnets while travelling at speeds close to the speed of light [1.96]. Under the action of undulators or wigglers [1.96], the beam is forced into a sinusoidal path and by each deflection radiates X-rays.

When a neutron beam irradiates a crystalline specimen, it is scattered by the atoms. Being charge-neutral particles means that neutrons are scattered by a nuclear interaction with the nuclei of atoms [1.97], whereas X-rays are scattered by the electron cloud surrounding the nucleus.

Bragg's law

Bragg's law simply states that in order for the scattered neutrons to form a constructive pattern, the following relationship has to hold between the diffraction angle θ, beam wavelength λ and lattice spacing d (see figure 1.9):

$$n\lambda = 2d \sin\theta \qquad (1\text{-}23)$$

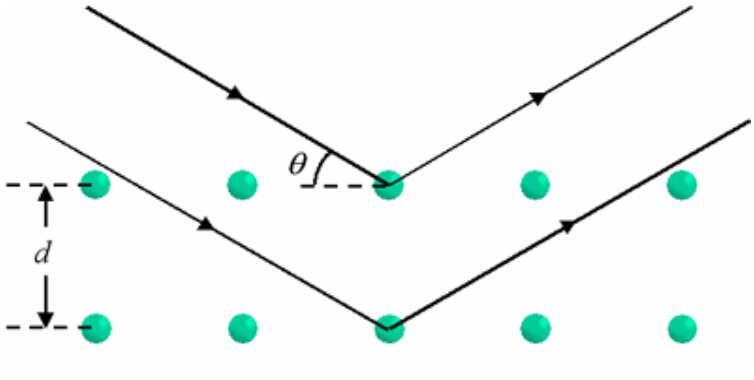

Figure 1.9- Schematic illustration of the parameters used in Bragg's Law

By measuring the diffraction angle, lattice spacing for the area of interest can be found and therefore strains in that direction can be calculated.

ii) Ultrasonic Stress Measurement Method

When part of a material contains stresses, the speed of elastic wave propagation varies and therefore the material exhibits stress induced anisotropy [1.98]. This is the basis of ultrasonic stress measurement technique.

1.4.4) Selecting the Appropriate Measurement Technique

Depending on the application, each of the measurement techniques may be useful in particular cases. Usually the first question is whether partial damage to the specimen is tolerable or not. If hole-drilling can be used, then it is usually the preferred method due to accuracy and low cost of the procedure. One point that should be remembered about diffraction techniques is that whereas hole drilling can be used for any homogenous elastic solid [1.89], diffraction techniques can only be employed for crystalline solids. On the other hand, if an accurate map of stress distribution is required in a thick crystalline sample, neutron diffraction can be a very reliable method. For values of stress very close to the surface, X-ray diffraction is preferable due to its relatively small gauge volume.

Sometimes a combination of two methods can be used. For example, use of X-ray diffraction in conjunction with chemical layer removal method has been effectively used for residual stress evaluation [1.99], which results in an essentially destructive method. Also, when neutrons are used for stress measurement in thick specimens, accurate stress determination in the near surface region is only possible by a complementary X-ray diffraction process [1.100].

1.5) Summary

In this chapter, the backgrounds to the problems of stress intensity factor weight functions and residual stresses were discussed. These are issues that are relevant to the scope of this research. Analysis of crack growth in residual stress fields requires a knowledge of stress intensity factors and of residual stresses and their behaviour. Surface cracks were discussed and their significance in structures was highlighted. It was shown here that there is a need for more reliable stress intensity factor weight functions for surface cracks. Also, residual stresses arising from shot peening and laser shock peening were discussed. Different techniques of residual stress measurements were also explained and their strength and weaknesses were outlined. The interaction of the residual stresses and cracks and the effect of laser shock peening on fatigue crack growth are some of the issues that require further investigation.

The objectives of this PhD research study can be summarised as follows:

1) The development of a reliable weight function for semi-elliptical surface cracks. The desired weight function should be robust and computationally simple.

2) The analysis of fatigue crack growth in residual stress fields arising from surface treatments such as laser peening. The interactions between the crack and the laser peened specimen affect the crack growth and yet this has not been studied in detail before. It is one of the important missions of this research to better understand these interactions.

3) The development of an understanding of the effect of the laser peening process on the specimens and the investigation of the resulting residual stresses due to this process. This is an important step towards the analysis of the crack growth in these fields.

To these end, the subsequent chapters of the thesis have been produced as follows:

Chapter 2 includes a comprehensive study of the weight function technique for stress intensity factor evaluation in surface cracks. A study of the existing weight functions illustrates the need for a robust and reliable weight function. A novel weight function is constructed for the surface cracks under any arbitrary loading condition and its accuracy is verified in this chapter.

Chapter 3 outlines a plan for the experimental investigation of the fatigue crack growth in residual stress fields arising from laser shock peening. The experimental plan is drawn and the test procedure is explained. More specifically, a set of experiments are planned to:

1) Study the effect of surface treatment (laser-shock peening) on fatigue crack growth. If weight functions for the test specimen geometry are known, then by knowing the residual stress field, say by application of neutron diffraction measurement techniques, the growth of the fatigue crack under cyclic loading can be predicted and compared against the observed experimental data. Any discrepancy between the two is to be attributed to mechanisms other than residual stresses. These mechanisms can include surface plasticity or a change in material properties which manifests itself in the form of a change in Paris law exponent [1.101] [3.8]. This is studied in detail in Chapter 5.

2) Study the residual stress distribution in laser peened specimens. This is a necessary requirement for step 1, and is described in detail in Chapter 4.

Neutron diffraction technique was used to analyse the stress field in laser shock peened steel specimens.

3) Develop an understanding of the interaction between the crack and the residual stress field. Some authors have observed a relaxation in the level of residual stresses under cyclic loadings [1.102-1.105][3.11-3.14]. This can also be measured by neutron diffraction measurement and will be discussed in detail in Chapter 4.

Chapter 4 details the experimental study of the residual stress field in laser peened specimens using the neutron diffraction technique. The results of these measurements are analysed and the resulting residual stress field in the specimens is determined.

Chapter 5 analyses the results of the fatigue crack growth tests and combines the findings of Chapter 4 (residual stresses) with the data obtained from the experiments of Chapter 3. The interaction between the crack growth and the laser peening is discussed and the concept of 'effective fatigue stress' is introduced for these specimens.

Chapter 6 draws conclusions from the findings of the previous chapters and presents a discussion of the results. This chapter also includes some recommendations for future work.

References

[1.1] W Schütz, A History of Fatigue, *Engineering Fracture Mechanics*, Vol. 54, No. 2, pp. 263-300 (1996).

[1.2] A Wöhler, Über die Festigkeitsversuche mit Eisen and Stahl, *Zeitschrift für Bauwesen,* Vol. 20, p83 (1870).

[1.3] D E Martin and G M Sinclair, Crack propagation under repeated loading, *Proceedings of Third U.S. National Congress of Applied Mechanics,* pp. 595-604 (1958).

[1.4] A J McEvily, The rate of fatigue-crack propagation in two aluminium alloys, NACA TN 4394 (1958).

[1.5] H F Hardrath and A J McEvily, Engineering aspects of fatigue crack propagation, presented at the Crack Propagation Symposium, Cranfield, England (1961).

[1.6] H W Liu, Crack propagation in thin metal sheets under repeated loading, *The Journal of Basic Engineering*, Vol. 85 p. 116 (1963).

[1.7] A K Head, The growth of fatigue cracks, *The Philosophical Magazine,* Vol. 44(7), p. 925 (1953).

[1.8] P C Paris, M P Gomez and W E Anderson, A rational analytic theory of fatigue, *The Trend in Engineering*, Vol. 13(1), pp. 9-14 (1961).

[1.9] P C Paris and F Erdogan, A critical analysis of crack propagation laws, *Journal of Basic Engineering*, Vol. 85, pp. 528-534 (1963).

[1.10] R J Sanford, Principles of Fracture Mechanics, Prentice Hall (2003).

[1.11] Muskhelishvili, Some Basic Problems of the Mathematical Theory of Elasticity, translated from Russian by J R M Radok, Noordhoff Ltd (1963).

[1.12] N Hasebe and J Iida, A crack originating from a triangular notch on a rim of a semi-infinite plate, *Engineering Fracture Mechanics*, Vol. 10, pp. 773-782 (1978).

[1.13] H Nisitani, Two dimensional problem solving using a digital computer, *Journal of the Japan Society of Mechanical Engineers (JSME)*, Vol. 70, pp. 627-635 (1967).

[1.14] J M Etheridge and J W Dally, A critical review of methods for determining the stress intensity factors from isochromatic fringes, *Experimental Mechanics,* Vol. 17(7), pp. 248-254 (1977).

[1.15] J F Kalthoff, Shadow optical methods of caustics, *Handbook on Experimental Mechanics,* Prentice-Hall, Englewood Cliffs, NJ, pp.430-500 (1987).

[1.16] A J Rosakis and K Ravi-Chandar, On crack-tip stress state: an experimental evaluation of three-dimentional effects, *International Journal of Solids and Structures*, Vol. 22(2), pp. 121-134 (1986).

[1.17] J W Dally and R J Sanford, Strain-gage methods for measuring the opening-mode stress-intensity factor, K_I, *Experimental Mechanics,* Vol. 27(4), pp. 381-388 (1987).

[1.18] D B Barker, R J Sanford and R Chona, Determining *K* and related stress-field parameters from displacement fields, *Experimental Mechanics,* Vol. 25(12), pp. 399-407 (1985).

[1.19] F A Dĭaz, E A Patterson, R A Tomlinson and J R Yates, Measuring stress intensity factors during fatigue crack growth using thermoelasticity, *Fatigue and Fracture of Engineering Materials and Structures,* Vol. 27, pp. 571-583 (2004).

[1.20] J P Gallaghar, Experimentally determined stress intensity factors for several contoured DCB specimens, *Engineering Fracture Mechanics,* Vol. 3, pp. 27-43 (1971).

[1.21] A F Grandt, J A Harter and B J Heath, Transition of part-through cracks at holes into through-the-thickness flaws, Fracture Mechanics, STP 833, ASME, pp. 7-23 (1984).

[1.22] D J Cartwright and D P Rooke, Approximate stress intensity factors compounded from known solutions, *Engineering Fracture Mechanics*, Vol. 6, pp. 563-571 (1974).

[1.23] D P Rooke, An improved compounding method for calculating stress-intensity factors, E*ngineering Fracture Mechanics*, Vol. 23(5), pp. 783-792 (1986).

[1.24] I N Sneddon and M Lowengrub, Crack problems in classical theory of elasticity, John Wiley, New York (1969).

[1.25] M Isida, "Method of Laurent series expansion for internal crack problems", Methods of Analysis and Solution of Crack Problems, Mechanics of Fracture, Vol. 1, G C Sih, ed., Noordhoff Int. Pub., Netherlands, pp. 56-130.

[1.26] M Isida, Effect of width and length on stress intensity factors of internally cracked plates under various boundary conditions, *International Journal of Fracture Mechanics*, Vol. 7(3), pp. 301-316 (1971).

[1.27] H F Bueckner, A novel principle for the computation of stress intensity factors, *Zeitschrift für Angewandte Mathemetik und Mechanik.* Vol. 50(9), pp. 529-546 (1970).

[1.28] J R Rice, Some remarks on the elastic crack-tip stress fields, *International Journal of Solids and Structures,* Vol. 8, pp. 751-758 (1972).

[1.29] G C Sih, P C Paris and G R Irwin, On Cracks in rectilinearly anisotropic bodies, *International Journal of Fracture Mechanics,* Vol. 1, pp. 189-203 (1965).

[1.30] H Tada, P C Paris and G R Irwin, The Stress Analysis of Cracks Handbook, Third Edition (2000), The American Society of Mechanical Engineers.
[1.31] Y Murakami, Stress intensity factors handbook, Pergamon Press, 1987.

[1.32] D P Rooke, Compounding stress intensity factors, The Parthenon Press, 1986.

[1.33] H J Petroski and J D Achenbach, Computation of the weight function from a stress intensity factor, *Engineering Fracture Mechanics,* Vol. 10, pp. 257-266 (1978).

[1.34] P C Paris and G C Sih, Stress analysis of cracks, *ASTM STP* 381 (1965).

[1.35] F Görner, C Mattheck and P Morawietz, Limitations of the Petroski-Achenbach crack opening displacement approximation for the calculation of weight functions, *Engineering Fracture Mechanics,* Vol. 22(2), pp. 269-277 (1985).

[1.36] X Niu and G Glinka, On the "Limitations of the Petroski-Achenbach crack opening displacement approximation for the calculation of weight function"- do they really exist?, *Engineering Fracture Mechanics,* Vol. 26(5), pp. 701-706 (1987).

[1.37] T Fett, C Mattcheck and D Munz, On the calculation of crack opening displacement from the stress intensity factor, *Engineering Fracture Mechanics,* Vol. 27(6), pp. 697-715 (1987).

[1.38] T Fett, Conditions for the determination of approximate COD fields, *Engineering Fracture Mechanics,* Vol. 39(5), pp. 905-914 (1991).

[1.39] R P Ojdrovic and H J Petroski, Weight functions from multiple reference states and crack profile derivatives, *Engineering Fracture Mechanics,* Vol. 39(1), pp. 105-111 (1991).

[1.40] F P Brennan, Evaluation of stress intensity factors by multiple reference state weight function approach, *Theoretical and Applied Fracture Mechanics,* Vol. 20, pp. 249-256 (1994).

[1.41] G R Irwin, Crack-extension force for a part-through crack in a plate, *Journal of Applied Mechanics*, Vol. 29, pp. 651-654 (1962).

[1.42] P M Scott and T W Thorpe, A critical review of crack tip stress intensity factors for semi-elliptic crack, *Fatigue of Engineering Materials and Structures,* Vol. 4 No. 4 pp. 291-309 (1981).

[1.43] J McGowan, Ed., A critical evaluation of numerical solutions to the benchmark surface flaw problem, *Experimental Mechanics*, Vol. 20(8), 253-264 (1980)

[1.44] F Smith, The Surface Crack: Physical Problems and Computational Solutions, pp. 125-152, ASME (Nov 1972).

[1.45] C W Smith, W H Peters, G C Kirby and A Adonian, Fracture Mehcanics, ASTM STP 743, American Society for Testing and Materials, pp. 422-437 (1981).

[1.46] D K Cater, W R Canda and J A Blind, Experimental evaluation of stress-intensity solutions for surface flaw growth in plates, Surface-Crack Growth: Models, Experiments, and Structures, ASTM STP 1060, pp.215-236 (1990).

[1.47] Green and Sneddon: The distribution of stress in the neighbourhood of a flat elliptical crack in an elastic solid, Proceedings of the Cambridge Philosophical Society, Vol. 46(1) pp. 159-163 (1950).

[1.48] J C Newman JR. and I S Raju, An empirical stress intensity factor equation for the surface crack, *Engineering Fracture Mechanics*, Vol. 15(1), pp. 185-192 (1981).

[1.49] A Hosseini and M A Mahmoud, Evaluation of stress intensity factor and fatigue growth of surface cracks in tension plates, *Engineering Fracture Mechanics*, Vol. 22(6), pp. 957-974 (1985).

[1.50] C W Smith and G C Kirby, Stress Intensity distributions for natural cracks approaching benchmark crack depths in remote uniform tension, Fracture Mechanics, ASTM STP 791, American Soceity for Testing and Materials, pp. 269-280 (1983).

[1.51] D L Corn, A study of cracking techniques for obtaining partial thickness cracks of pre-selected depths and shapes, *Engineering Fracture Mechanics*, Vol. 3(1), pp. 45-52 (1971).

[1.52] M Jolles and V Tortoriello, Geometry variations during fatigue crack growth of surface flaws, Fracture Mechanics, ASTM STP 791, American Society for Testing and Materials, pp.I-297-I-307 (1983).

[1.53] X Niu and G Glinka, Theoretical and experimental analyses of surface cracks in weldments, ASTM STP 1060, American Society for Testing and Materials, pp. 390-413 (1990).

[1.54] G Shen and G Glinka, Weight function for a surface semi-elliptical crack in a finite thickness plate, *Theoretical and Applied Fracture Mechanics*, Vol.15, pp. 247-255 (1991).

[1.55] T Fett, C Mattheck and D Munz, On the calculation of crack opening displacement from the stress intensity factor, *Engineering Fracture Mechanics*, Vol. 27(6), pp. 697-715 (1987).

[1.56] X Wang and S B Lambert, Local weight functions for semi-elliptical surface cracks in finite thickness plates, *Theoretical and Applied Fracture Mechanics*, Vol. 23, pp. 199-208 (1995).

[1.57] I V Orynyak, M V Borodii and V M Torop, Approximate construction of a weight function for quarter-elliptical, semi-elliptical and elliptical cracks subjected to normal stresses, *Engineering Fracture Mechanics*, Vol. 49(1), pp. 143-151 (1994).

[1.58] H Tada, P C Paris and G R Irwin, The Stress Analysis of Cracks Handbook, Paris Production Inc. (1985).

[1.59] M Oore and D J Burns, Estimation of stress intensity factors for irregular cracks subjected to arbitrary normal stress fields, *ASME Journal of Pressure Vessel Technology*, Vol. 102, pp. 202-211 (1980).

[1.60] I V Orynyak and M V Borodii, Point weight function method application for semi-elliptical mode-I cracks, *International Journal of Fracture*, Vol. 70, pp. 117-124 (1995).

[1.61] P M Besuner and T A Cruise, Residual life prediction for surface cracks in complex structural details, Journal of Aircraft, Vol. 12(4), pp. 369-375 (1975).

[1.62] P M Besuner, Residual life estimates for structures with partial thickness cracks, Mechanics of Crack Growth, ASTM STP 590, American Society for Testing and Materials, pp. 403-419 (1976).

[1.63] M A Mahmoud, Quantitative prediction of growth patterns of surface fatigue cracks in tension plates, *Engineering Fracture Mechanics*, Vol. 30 (6) pp. 735-746 (1988).

[1.64] M A Mahmoud, Growth patterns of surface fatigue cracks under cyclic bending-a quantitative analysis, *Engineering Fracture Mechanics*, Vol. 31(2) pp. 357-369 (1988).

[1.65] C Mattheck, P Moraweitz and D Munz, Stress intensity factor at the surface and the deepest point of a semi-elliptical surface crack in plates under stress gradients, *International Journal of Fracture*, Vol. 23, pp. 201-212 (1983).

[1.66] T Fett, The crack opening displacement field of semi-elliptical surface cracks in tension for weight functions applications, *International Journal of Fracture*, Vol. 36, pp. 55-69 (1988).

[1.67] T Fett, A procedure for the determination of the weight function for semi-elliptical surface cracks by direct adjustment to reference solutions, *Engineering Fracture Mechanics*, Vol. 43 (4) pp. 519-528 (1992).

[1.68] S J Maddox (1991), Fatigue Strength of Welded Structure – Second Edition, Abington Publishing, ISBN 1855730138.

[1.69] J O Almen, P H Black, Residual Stress and Fatigue in Metals, McGraw Hill Book Company Inc, 1963, ISBN 0486611876.

[1.70] G H Farrahi, J L Lebrun and D Courtain, Effect of Shot Peening on Residual Stress and Fatigue Life of a Spring Steel, *Fatigue and Fracture of Engineering Materials and Structures*, Vol. 18, No. 2, pp. 211-220 (1995).

[1.71] P J Withers and H K D H Bhadeshia, Residual stress, Part 1 – Measurement techniques, *Materials Science and Technology*, Vol.17, pp. 355-365 (2001).

[1.72] P J Withers and H K D H Bhadeshia, Residual stress, Part 2 – Nature and origins, *Materials Science and Technology*, Vol.17, pp. 365-375 (2001).

[1.73] Handbook of Measurement of Residual Stresses, Edited by J Lu, Society for Experimental Mechanics (1996), ISBN 0-88173-229-X.

[1.74] http://www.metalimprovment.com, accessed June 2008.

[1.75] H Berns and L Weber, Influence of Residual Stresses on Crack Growth, in Impact Surface Treatment, Edited by S A Meguid, Elsevier, pp. 33-44 (1984).

[1.76] G R Leverant, B S Langer, A Yuen and S W Hopkins, Surface Residual Stresses, Surface Topography and Fatigue Behavior of Ti-6Al-4V, *Metallurgical Transactions*, American Society for Metals and the Metallurgical Society of AIME, Vol. 10A, pp. 251-257 (1979).

[1.77] Shi Song Ngiam, The Influence of Surface Residual Stress on Fatigue Crack Growth, PhD Thesis, Department of Mechanical Engineering, University College London (Mar 2007).

[1.78] Laser Shock Processing Increases the Fatigue Life of Metal Parts, *Materials and Processing*, Elsevier Science Publishing Co (Sept1991).

[1.79] M R Hill, A T DeWald, A G Demma, L A Hackel, H L Chen, C B Dane, R C Specht, F B Harris, Laser Peening Technology, *Advanced Materials and Processes*, Vol. 161, No. 8 (Aug 2003).

[1.80] L A Hackel and H L Chen, Laser Peenig – A Processing Tool to Strengthen Metals or Alloys to Imrprove Fatigue Lifetime and Retard Stress-Induced Corrosion Cracking, *Laser Science and Technology*, Sep 2003.

[1.81] R A Everett, W T Matthews, R Prabhakaran, J C Newman Jr., M J Dubberly, The Effect of Shot and Laser Peening on Fatigue and Crack Growth in 2024 Aluminum Alloy and 4340 Steel, Langley Research Center Report, NASA /TM-2001-210843 (Dec 2001).

[1.82] O Hatamleh, J Lyons and R Forman, Laser and shot peening effect on fatigue crack growth in friction stir welded 7075-T7351 aluminium alloy joints, *International Journal of Fatigue*, Vol. 29 Issue 3, pp 421-434 (Mar 2007).

[1.83] G S Schajer, M T Flaman, G Roy and J Lu, Hole Drilling and Ring Core Methods, in Handbook of Measurement of Residual Stresses, Society for Experimental Mechanics, Edited by J Lu (1996), ISBN 088173229X.

[1.84] K Sasaki, M Kishida and T Itoh, The accuracy of residual stress measurement by the hole-drilling method, *Experimental Mechanics*, Vol. 37, No. 3, pp. 250-257 (Sept 1997).

[1.85] G S Schajer and M Tootoonian, A new rosette design for more reliable hole-drilling residual stress measurements, *Experimental Mechanics*, Vol. 37, No. 3, pp. 299-306 (Sept 1997).

[1.86] Standard Test Method for Determining Residual Stresses by Hole-Drilling Strian-Gage Method, ASTM International Standard E 837 - 01, American Society for Testing and Materials (2001).

[1.87] J M Boag, M T Flaman and J A Herring, Considerations of Using the Hole Drilling Method for Measuring Residual Stresses in Engineering Components, in Residual Stress in Design, Process and Materials Selection, *Proceedings of ASM's Conference on Residual Stress – Cincinnati, Ohio 27-29 Apr 1987*, Edited by W B Young.

[1.88] P V Grant, J D Lloyd and P S Whitehead, The Measurement of Residual Stresses by the Incremental Hole Drilling Technique, Measurement Good Practice Guide No. 53 – Issue 2, National Physical Laboratory (2006).

[1.89] N J Rendler and I Vigness, Hole-drilling Strain-gage Method of Measuring Residual Stresses, *Experimental Mechanics*, Vol. 6, No. 12, pp. 577-586 (1966).

[1.90] A Niku-Lari, J Lu and J F Flavenot, Measurement of residual stress distribution by the incremental hole drilling method, *Experimental Mechanics*, Vol. 12, No. 2, pp. 175-185 (1985).

[1.91] M T Flaman, Brief investigation of induced drilling stresses in the center-hole method of residual-stress measurement, *Experimental Mechanics*, Vol. 22, No. 1, pp. 26-30 (1982).

[1.92] J F Flavenot, Layer Removal Method, in Handbook of Measurement of Residual Stresses, Society for Experimental Mechanics, Edited by J Lu (1996), ISBN 088173229X.

[1.93] T M Holden and G Roy, The Application of Neutron Diffraction to the Measurement of Residual Stress and Strain, in Handbook of Measurement of Residual Stresses, Society for Experimental Mechanics, Edited by J Lu (1996), ISBN 08173229X.

[1.94] M M Eisenstadt, Introduction to Mechanical Properties of Materials, Macmillan Publishing Co, (1971).

[1.95] M Francios, J M Sprauel, C F Dehan, M R James, F Convert, J Lu, J L Leburn and R W Hendricks, X-ray Diffraction Method, in Handbook of Measurement of Residual Stresses, Society for Experimental Mechanics, Edited by J Lu (1996), ISBN 08173229X.

[1.96] C Riekel, The use of synchrotron radiation for materials research, in Analysis of Residual Stress by Diffraction using Neutron and Synchrotron Radiation, Edited by M E Fitzpatrick and A Lodini, Taylor & Francis (2003), ISBN 0-415-30397-4.

[1.97] M T Hutchings, P J Withers, T M Holden, T Lorentzen, Introduction to the Characterization of Residual Stress by Neutron Diffraction, Taylor & Francis (2005), ISBN 0-415-31000-8.

[1.98] D M Egle and D E Bray, Measurement of Acoustoelastic and Third-order Elastic Constants for Rail Steel, *Journal of the Acoustical Society of America*, Vol. 60, No. 3, pp. 741-744 (Sept 1976).

[1.99] G Vander Voot and J Friel, Developments in Materials Characterization Technologies, ASM International, Materials Park, OH, pp. 103-110 (1996).

[1.100] M E Fitzpatrick, A T Fry, P Holdway, F A Kandil, J Shackleton and L Suominen, Determination of Residual stresses by X-ray Diffraction, Measurement Good Practice Guide No. 52 – Issue 2, National Physical Laboratory (Sept 2005).

[1.101] P C Paris and F Erdogan, A critical analysis of crack propagation laws, *Journal of Basic Engineering*, Vol. 85, pp. 528-534 (1963).

[1.102] G H Farrahi, J L Lebrun and D Courtain, Effect of Shot Peening on Residual Stress and Fatigue Life of a Spring Steel, *Fatigue and Fracture of Engineering Materials and Structures*, Vol. 18, No. 2, pp. 211-220 (1995).

[1.103] O N Romaniv, Relaxation of residual stresses by alternating loads, *Fiziko-Khimichekaya Mekhanika Materialov*, Vol.1, No. 6, pp. 726-729 (1965).

[1.104] W Z Zhuang and G R Halford, Investigation of residual stress relaxation under cyclic load, *International Journal of Fatigue*, Vol. 23, pp.S31-S37 (2001).

[1.105] U P Sinha and D W Levinson, Bending stress relaxation of AISI 1095 steel strip, *Proceedings of ASM's Conference on Residual Stress- In Design, Process and Materials Selection*, Cincinnati, Ohio, 27-29April 1987.

CHAPTER 2

2.0) Surface Crack Stress Intensity Factor Weight Functions

2.1) Introduction

In the previous chapter, a background to the problem of crack growth was given. The significance of the stress intensity factor for fatigue life assessment was emphasised and the existing tools for stress intensity factor derivation were discussed. The lack of an accurate and robust weight function for the determination of stress intensity factors in surface cracks was highlighted and the existing solutions were scrutinised.

In this chapter, the work undertaken on development of weight functions for stress intensity factor (SIF) evaluation in surface cracks is outlined. A thorough background to the problem of surface crack stress intensity factor evaluation is given and the lack of reliable and convenient existing stress intensity factor solutions for semi-elliptical surface cracks is once more emphasised. A new approach is introduced for the calculation of stress intensity factors in surface cracks, and is verified by comparison with Finite Element results for various geometry and loading cases.

The generally accepted Newman-Raju empirical formulae [2.1] are investigated, and surface crack growth behaviour is studied using these SIF equations, leading to aspect ratio variation curves and crack depth/length vs. number of cycles plots for tensile and bending load modes.

Surface crack weight functions should enable one to calculate the stress intensity factor values for surface cracks under different stress distributions; therefore in order to validate the results obtained using weight functions, a reliable reference solution is required for comparison. A Finite Element model of the surface crack is used, which has been modified to accommodate for any arbitrary stress distribution on the crack face. The stress intensity factor values under tension and bending resulted from this model

are verified against Newman-Raju curves for all the different geometries used to ensure the reliability of the Finite Element analyses.

From the two reference solutions of Newman-Raju, the Multiple Reference States (MRS) approach [2.2] is utilised where at each point on the crack front, the surface crack is treated as an edge crack. The results are discussed and the limitations highlighted. It is also argued that the first coefficient, i.e. c_0, is not needed to be known in advance and its numerical value can be directly derived from the reference solutions.

The use of Root Mean Square stress intensity factor (RMS SIF) values for surface crack growth predictions is reviewed. Fett's approximate weight function [2.3] is scrutinised and examined, and its limitations are shown.

A novel RMS SIF weight function is suggested for the surface crack based on the MRS technique. Two reference solutions are taken as Newman-Raju formulae for tension and bending, though these can be any two known solutions. The SIF results from this weight function under different loadings are compared with the Finite Element values. A good agreement is observed.

A Note of Disambiguation

The terms 'one-dimensional' and 'two-dimensional' cracks are frequently used throughout this chapter and the subsequent ones. Very few references refer to edge or through-cracks as 'two-dimensional'; examples of such references are [2.4, 2.5]. However, the majority of authors prefer the use of the term 'one-dimensional' for these cracks because from a mathematical point of view the geometry of these cracks can be characterised by only one variable, i.e. the crack length. Surface cracks or part-through cracks, all of which considered in this work being semi-elliptical in shape, are called 'two-dimensional' herein due to their being characterised by two spatial dimensions, e.g. crack half length and depth.

2.2) Stress Intensity Factors in Surface Cracks

Surface cracks usually occur in components and structures under cyclic loadings such as bending or tension; these cracks usually initiate at defects and minute cracks present on the surface of the material. A stress concentration location such as a rivet, a manufacturing defect such as an inclusion, a weld, or even a scratch on the surface may act as initiating locations for surface cracks.

Surface cracks are more complicated in terms of fracture mechanics analysis compared to one-dimensional cracks (e.g. edge cracks), since they can not be characterised by one unique parameter any more, contrary to the one-dimensional edge or through cracks where a single value of stress intensity factor fully determines the state of stress ahead of the crack tip. Here, on the other hand, stress intensity factor varies along the crack front; this is because the state of stress gradually changes along the crack front from plane stress at the surface points to often a highly tri-axial stress state at the deepest point.

Sneddon [2.6] gives the stress intensity factor for a 'penny-shaped' embedded crack with a radius of a under remote tension as $K = \frac{2}{\pi}\sigma\sqrt{\pi a}$, which compared to the corresponding through-crack problem -i.e., a planar crack of length $2a$, shows that the effect of crack front curvature is to reduce the stress intensity factor value by 36%; this means that the crack curvature has a 'stiffening' effect. The same principle holds for the embedded elliptical cracks where according to Irwin's solution [2.7], the lowest stress intensity value is observed along the major axis where the crack front curvature is maximum, and the lowest SIF value occurs at the minor axis points where the crack front curvature is minimum.

It is observed that surface cracks closely resemble semi-ellipses in shape, and that defects and starter-cracks that are not semi-elliptical, gradually evolve into a semi-elliptical shape [2.8]. Therefore in most of the analyses that have been carried out, surface cracks are modelled as semi-ellipses.

The need for a reliable stress intensity factor solution for surface cracks stems from the fact that similar to one-dimensional cracks, it is believed that fatigue growth of surface cracks under cyclic loading can be quantified using the Paris law, as described in the previous chapter**,** hence the relation between LEFM and two-dimensional fatigue.

As discussed in Chapter 1, Newman and Raju have suggested a simple formula for stress intensity factor values for each point along a semi-elliptical surface crack, in a specimen under cyclic tension and/or bending [2.1]**.** They have based the empirical formulae on the results of numerous different sets of Finite Element analyses. For a point at the crack front with a parametric angle of ϕ, such as the one shown in figure 2.1, the Newman-Raju formula gives the value of SIF as:

$$K_I = (S_t + HS_b)\sqrt{\pi \frac{a}{Q}} F\left(\frac{a}{t}, \frac{a}{c}, \frac{c}{b}, \phi\right) \tag{2.1}$$

Where S_t is a characteristic stress for the tensile plate and S_b is that of the bending plate (anti-plane bending). *H, Q and F* are defined as follows, all based on engineering judgment:

$$Q = 1 + 1.464\left(\frac{a}{c}\right)^{1.65} \qquad \left(\frac{a}{c} \le 1\right)$$

$$F = \left[M_1 + M_2\left(\frac{a}{t}\right)^2 + M_3\left(\frac{a}{t}\right)^4\right] f_\phi g f_w$$

where

$$M_1 = 1.13 - 0.09\left(\frac{a}{c}\right)$$

$$M_2 = -0.54 + \frac{0.89}{0.2 + \left(a/c\right)}$$

$$M_3 = 0.5 - \frac{1.0}{0.65 + \left(a/c\right)} + 14\left(1.0 - \frac{a}{c}\right)^{24}$$

$$g = 1 + \left[0.1 + 0.35\left(\frac{a}{t}\right)^2\right](1 - \sin\phi)^2$$

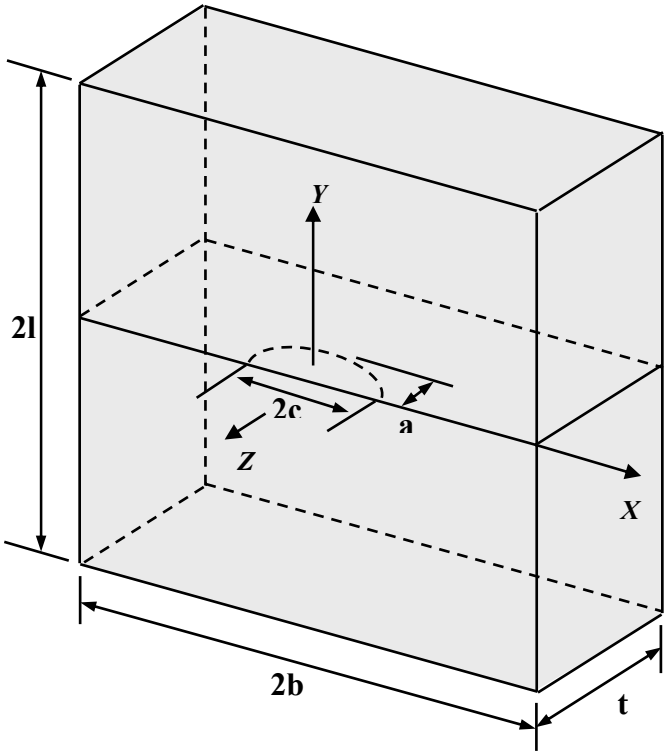

(a)

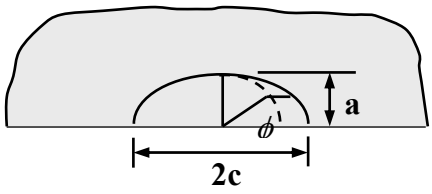

(b)

Figure 2.1- The semi-elliptical surface crack

And the function f_ϕ, an angular function from the embedded elliptical crack [2.9]**,** is

$$f_\phi = \left[\left(\frac{a}{c}\right)^2 \cos^2\phi + \sin^2\phi\right]^{1/4}$$

The finite-width correction factor has been chosen from [2.10] as

$$f_w = \left[\sec\left(\frac{\pi c}{2b} \sqrt{\frac{a}{t}} \right) \right]^{1/2}$$

$$H = H_1 + (H_2 - H_1)\sin^p \phi$$

Where

$$p = 0.2 + \frac{a}{c} + 0.6\frac{a}{t}$$

$$H_1 = 1 - 0.34\frac{a}{t} - 0.11\frac{a}{c}\left(\frac{a}{t}\right)$$

$$H_2 = 1 + G_1\left(\frac{a}{t}\right) + G_2\left(\frac{a}{t}\right)^2$$

$$G_1 = -1.22 - 0.12\frac{a}{c}$$

$$G_2 = 0.55 - 1.05\left(\frac{a}{c}\right)^{0.75} + 0.47\left(\frac{a}{c}\right)^{1.5}$$

Newman and Raju claim that for $a/t \leq 0.8$, equation 2-1 is within ±5% of the finite element results [2.1]. For a plate with a thickness of 6*mm* and width of 200*mm*, the stress intensity factor variation for two different surface cracks is shown in figure 2.2, both under tension and under bending loading.

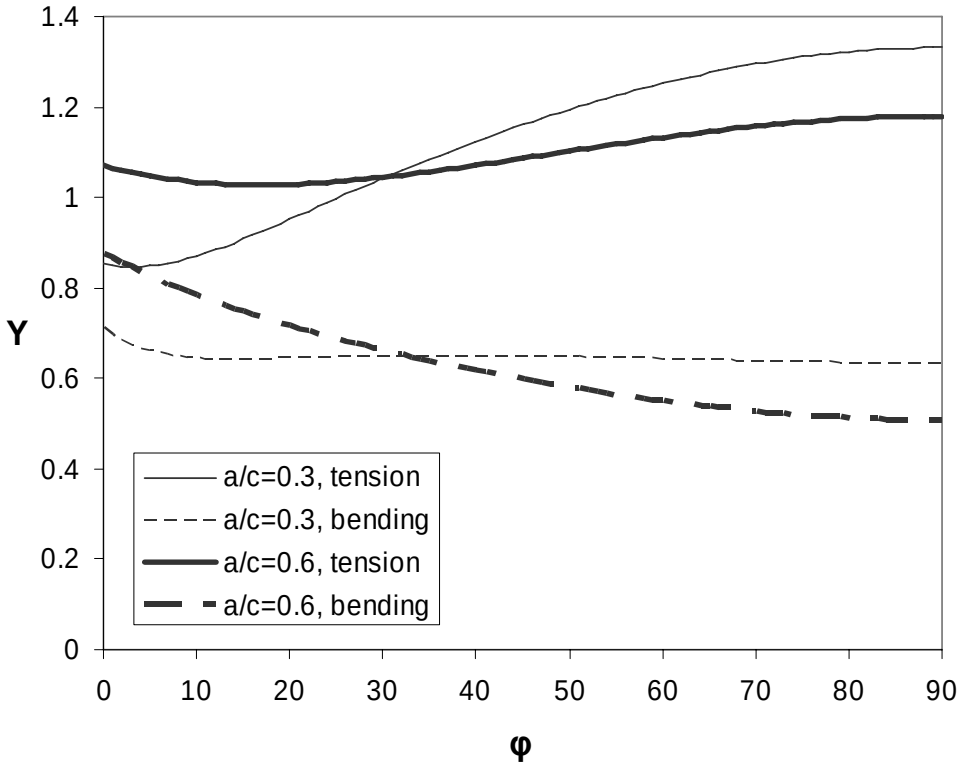

Figure 2.2- Newman and Raju's solution for surface cracks under bending and tension

2.3) Determination of Fatigue Life of Cracked Components using Stress Intensity Factors

2.3.1) Introduction- Integration of Paris Law

Remaining fatigue life of a component is the time it takes for an existing crack to grow to a critical size under cyclic loading. For one-dimensional cracks, starting from Paris law [2.11]:

$$\frac{da}{dN} = C(\Delta K)^m$$

where C and m are material properties derived from CT or other fatigue test methods, one can obtain:

$$CdN = \frac{da}{(\Delta K)^m} = \frac{da}{\left(Y\Delta\sigma\sqrt{\pi a}\right)^m}$$

$$C\left(\Delta\sigma\sqrt{\pi}\right)^m \int_0^{N_f} dN = \int_{a_i}^{a_f} \frac{da}{Y^m a^{m/2}}$$

$$N_f = \frac{1}{C\left(\Delta\sigma\sqrt{\pi}\right)^m} \int_{a_i}^{a_f} \frac{da}{Y^m a^{m/2}} \tag{2.2}$$

Where N_f is the number of cycles for the crack to grow from a length of a_i to a_f, under constant stress amplitude ($\Delta\sigma = const$). For an exact integration of equation (2.2), the functional dependence of *Y* on the crack length is required. Since this could be a complicated empirical function, or even sometimes expressed is a tabular form, it is possible to assume a constant *Y* for each crack growth increment *da*, and to update this value for each new increment. If the size of the increments is small enough, the error from this approximation would be miniscule and therefore negligible. Figure 2.3 shows a typical crack length vs. number of load cycles curve obtained from fatigue crack growth tests.

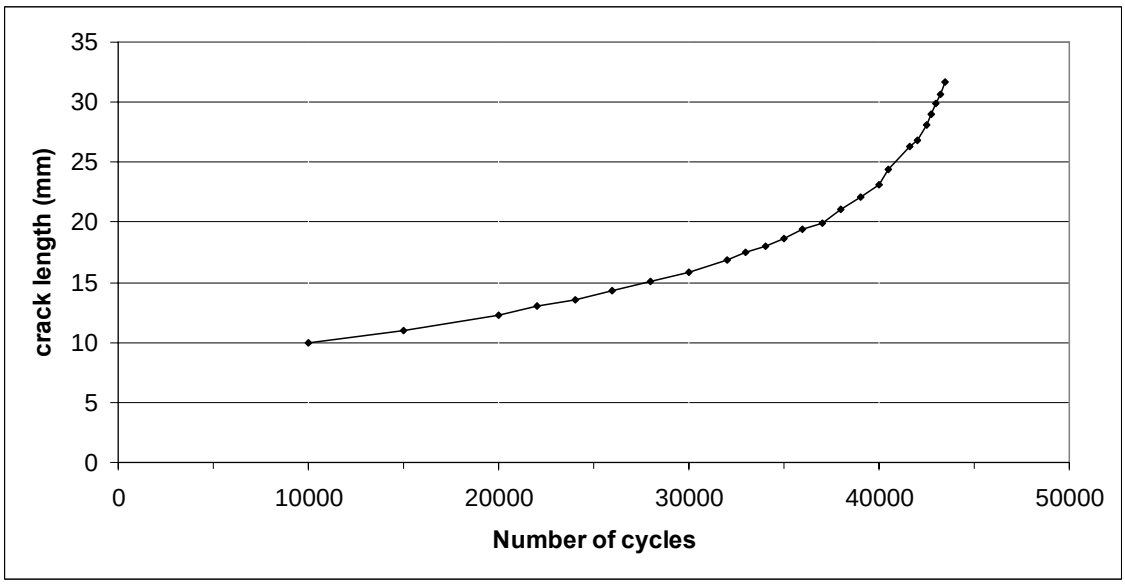

Figure 2.3- Crack length vs. the number of load cycles

2.3.2) Surface Crack Growth

The problem of surface crack growth is more complicated than that of the one-dimensional crack because as mentioned before a unique parameter does not determine the stress behaviour of the crack. Mettheck et al. [2.12] have suggested that if the crack is assumed to retain a semi-elliptical shape during its growth, then knowing only two parameters would fully determine the geometry of the crack, and therefore the problem can be treated as a system with two degrees of freedom.

As mentioned in Chapter 1, Mahmoud [2.13-2.15] has conducted a series of studies where Paris law is used for the deepest point and the surface point, thus calculating the depth and surface length of the crack for a variety of surface cracks. Then a semi-ellipse is passed through these two points which denotes the boundary of the crack. Mathematically speaking, one can write:

$$\frac{da}{dN} = C\left(\Delta K_{DP}\right)^m \quad \text{and} \quad \frac{dc}{dN} = C\left(\Delta K_{SP}\right)^m \tag{2.3}$$

where the subscripts *DP* and *SP* denote the deepest point and the surface point, respectively. Here it is assumed that Paris law coefficients are the same for the two different directions. However, as discussed later in the present chapter, this is open to question. From equation (2.3),

$$CdN = \frac{da}{\left(\Delta K_{DP}\right)^m} = \frac{dc}{\left(\Delta K_{SP}\right)^m} \tag{2.4}$$

Further integration requires knowledge of stress intensity factor values for each increment. Newman and Raju formulae only give the values of K for tensile and bending plates, the stress intensity factor values depending on both a and c for each computational increment. Therefore the two equations in (2.4) can not be solved independently. This means that in order to assess the residual life of components and structures containing surface cracks, stress intensity values as a function of the loading

and crack geometry, i.e. crack depth and half length are required. This method relies on the assumption that SIF values at two points, e.g. the deepest and the surface points, can uniquely determine the growth of the crack.

Crack growth under fatigue can be modelled using either of the two abovementioned stress intensity factor forms, i.e. point-by-point SIF or RMS SIF. It is argued that the two point approach for crack growth (the deepest and surface points) misses an important range of intermediate values of SIF for all other points lying between the surface and the deepest point. There is specially some doubt as to how representative the surface point SIF value is of the overall crack growth in the surface direction. This is the point where, in reality, the highest amount of plasticity is present due to the existence of a plane stress state and lack of stress tri-axiality. Therefore the assumption of fully elastic behaviour for the material, which is the basis of LEFM and weight function methodology, is expected to yield the maximum error at the surface point. It is only by averaging the stress intensity factor that the error may be maintained at a small level. It must be added that the Paris law is a 'phenomenological' approach to the crack growth problem, i.e. one in which the empirical formula is consistent with the theory, but not directly derived from it, and therefore depending on the application it is open to modifications.

The multi-point approach to surface crack growth, assumes that the direction of the growth is normal to the crack front [2.16]. As shown in the following analysis it is observed that a surface crack under cyclic tension would not keep a semi-elliptical shape if the Paris law holds at every single point on the crack front. Therefore, in order to apply the Paris law to a multi-point SIF problem, a slight modification seems to be required.

Before detailing the analysis of surface cracks, the points discussed so far regarding the use of multi-point life predictions for surface cracks are reiterated here in a compact form:

1) The surface point SIF value imposes a problem since at this point there is an immediate transition in the state of stress from three dimensional to biaxial. This area usually encompasses a larger plastic zone as a result of this stress state, which means that this single point does not represent the overall crack behaviour near the surface. Another suggested explanation is the different crack closure along the contour of the crack [2.17, 2.18]. In their experiments, Kim and Song [2.18] observed that the crack opening ratio was about %10 greater at the deepest point than at the surface.

2) It was shown that $C(\phi)$ varies and is a function of crack geometry and loading. An averaged stress intensity factor, when used with the newly proposed form of the Paris law, would essentially eliminate these variations.

3) This new method intrinsically ensures that cracks retain their semi-elliptical shape, and no extra geometrical considerations are required.

4) Assuming a two-point approach to the crack growth problem effectively results in ignoring the value of stress intensity factor at other points along the crack front. Different loadings lead to different stress intensity factor variations, and two different loadings may result in the same SIF values at the deepest and surface points for the two specimens respectively. This, however, does not necessarily mean that the two cracks should evolve identically.

A Study of the Growth of Semi-elliptical Cracks

Assumptions:
1) It is assumed that semi-elliptical cracks, under the action of cyclic tensile loading, generally remain semi-elliptical.

2) It is assumed that incremental growth of the crack at points on the crack front is perpendicular to the crack front.

Figure 2.4 shows a semi-elliptical crack C_1 which, under the action of cyclic loading, has grown into C_2. Δa and Δc denote the growth increments respectively in the depth and half-width of the crack. Point P is an arbitrary point on C_1 with a parametric angle of ϕ, corresponding to point P' on C_2.

Starting from the general equation of an ellipse,

$$\left(\frac{x_p}{a}\right)^2+\left(\frac{y_p}{c}\right)^2=1 \quad \text{and} \quad \left(\frac{x_{p'}}{a+\Delta a}\right)^2+\left(\frac{y_{p'}}{c+\Delta c}\right)^2=1 \tag{2.5}$$

λ is the angle between the x-axis and $\overline{PP'}$ (the normal to the ellipse at P), and can be evaluated as a function of ϕ as

$$\lambda=\tan^{-1}\left(\frac{c}{a}\cot\phi\right) \tag{2.6}$$

The Paris law can be written as follows for point P:

$$\frac{da(\phi)}{dN}=C(\phi)[K(\phi)]^m \tag{2.7}$$

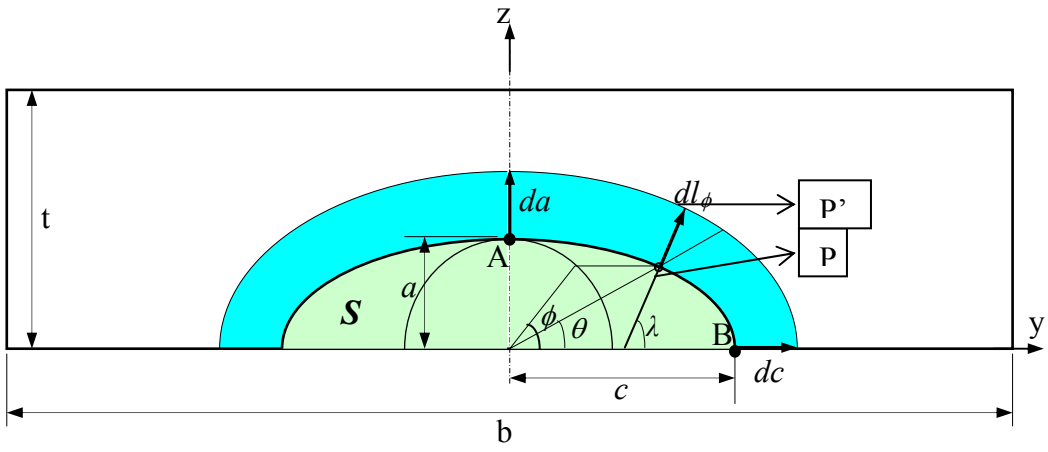

Figure 2.4- Geometrical parameters of the crack

And for the surface point (point B) as:

$$\frac{da}{dN} = C(0)[K(0)]^m \tag{2.8}$$

Dividing equation (2.7) by equation (2.8) eliminates *dN* as:

$$\frac{C(\phi)}{C(0)} = \frac{da(\phi)}{da} \times \left[\frac{K(0)}{K(\phi)}\right]^m \tag{2.9}$$

And for the deepest point:

$$\frac{C(\phi)}{C(\pi/2)} = \frac{da(\phi)}{dc} \times \left[\frac{K(\pi/2)}{K(\phi)}\right]^m \tag{2.10}$$

If the right hand side expression of equation (2.9) and (2.10) is proven not to be constant, then it is evident that $C(\phi)$ is not constant.

In order to evaluate the first ratio on the right hand side of equation (2.9), it is first noted that for small increments of crack growth $da(\phi) \approx \Delta a(\phi) = \overline{PP'}$, $da \approx \Delta a$ and $dc \approx \Delta c$. To express $\overline{PP'}$ as a function of Δa and Δc, equation (2.5) can be used:

$$\left(\frac{x_{p'}}{a+\Delta a}\right)^2 + \left(\frac{y_{p'}}{c+\Delta c}\right)^2 = 1 \tag{2.5}$$

From Figure 2.4 it can be observed that

$$x_{P'} = x_P + \overline{PP'}\cos\lambda = a\cos\phi + \overline{PP'}\cos\lambda$$

and similarly

$$y_{P'} = y_P + \overline{PP'}\sin\lambda = c\sin\phi + \overline{PP'}\sin\lambda$$

Substituting these values in equation (2.5), and rearranging, gives:

$$A \times \overline{PP'}^2 + B \times \overline{PP'} + C = 0 \tag{2.11}$$

where

$$A = \left(\frac{1}{a+\Delta a}\right)^2 \times \cos^2\lambda + \left(\frac{1}{c+\Delta c}\right)^2 \times \sin^2\lambda$$

$$B = 2a\cos\phi\cos\lambda \times \left(\frac{1}{a+\Delta a}\right)^2 + 2c\sin\phi\sin\lambda \times \left(\frac{1}{c+\Delta c}\right)^2$$

$$C = a^2\cos^2\phi \times \left(\frac{1}{a+\Delta a}\right)^2 + c^2\sin^2\phi \times \left(\frac{1}{c+\Delta c}\right)^2 - 1$$

Equation (2.11) gives $\overline{PP'}$ as a function of

$$\overline{PP'} = f(a, c, \Delta a, \Delta c, \phi, \lambda)$$

Bearing in mind that λ itself is a function of *a*, *c*, and ϕ (2.6), this can be simplified as

$$\overline{PP'} = f(a, c, \Delta a, \Delta c, \phi) \tag{2.12}$$

Now from equations (2.9), (2.10) and (2.12) one can get

$$\frac{C(\phi)}{C(0)} = \frac{f(a, c, \Delta a, \Delta c, \phi)}{\Delta a} \times \left[\frac{K(0)}{K(\phi)}\right]^m \tag{2.13}$$

and

$$\frac{C(\phi)}{C\left(\pi/2\right)} = \frac{f(a,c,\Delta a,\Delta c,\phi)}{\Delta c} \times \left[\frac{K\left(\pi/2\right)}{K(\phi)}\right]^m \tag{2.14}$$

Both these equations show that, without a need to solve equation (2.11), in a general case $C(\phi)$ is not constant and can be written as:

$$C(P) = C(a,c,\phi,K(\phi)) \tag{2.15}$$

It should be noted that, from this analysis it is deduced that writing C in the form of $C(\phi)$ is not accurate and could be misleading.

The significance of equation (2.15) is that it introduces a novel concept, namely that the Paris law coefficient C at any point, not only depends on the position of the point (C is a function of ϕ which signifies spatial variability), and on the crack shape (a and c), but also on the loading ($K(\phi)$). Previous authors [2.19, 2.1, 2.16] have emphasised the dependence on geometry but not the load-dependent nature of C. Whereas the dependence of C on ϕ, a and c could be established with relative ease (which may imply the theoretical possibility of a modified Paris law which takes these variations into account), the load dependence nature of this parameter suggests it is not possible to use the Paris law for the deepest and surface (or indeed any two) points along the crack face, since the errors resulting from this source can not be usually (and certainly not easily) evaluated.

The fact that in this form of Paris law $C(\varphi)$ is not constant suggests that Paris law can not be applied in a multi-point analysis unless some special constraint is applied on the geometry, i.e. only two points be analysed and a semi-ellipse be fitted onto them. It can also suggest that by using an averaging process the surface crack growth can be modelled in a simpler manner.

The resulting values of SIF from the point weight functions can be resolved in certain directions to yield a suitable RMS SIF value, which could then be used in conjunction with Paris law to generate reliable predictions of the crack growth.

For arbitrary loadings, similar to one-dimensional cracks, weight functions have been proposed to assist in the calculation of stress intensity factors. The background was discussed in Chapter 1, and the next section gives an in-depth and analytical study of this problem.

2.4) Weight Functions- Arbitrary Loadings

2.4.1) Introduction to Weight Functions for Surface Cracks

As mentioned in Chapter 1, for stress intensity factor calculation in surface cracks, two distinct forms of weight functions have been proposed, namely the point weight functions and the root mean square weight function (RMS WF). The purpose of the point weight function is to determine the value of the stress intensity factor for a specific point on the crack front, whereas the RMS WF calculates the averaged stress intensity factor for a characteristic 'direction' such as the depth direction or the surface direction. As mentioned before, for a semi-elliptical surface crack which retains its general semi-elliptical shape as it grows, two characteristic directions are enough to fully determine the geometry of the crack at any instant. These two directions are taken as the depth direction and the surface direction, as shown in figure 2.5.

Both of these two weight function forms, i.e. the point WF and the RMS WF could be deemed generalisations of the one-dimensional crack weight function.

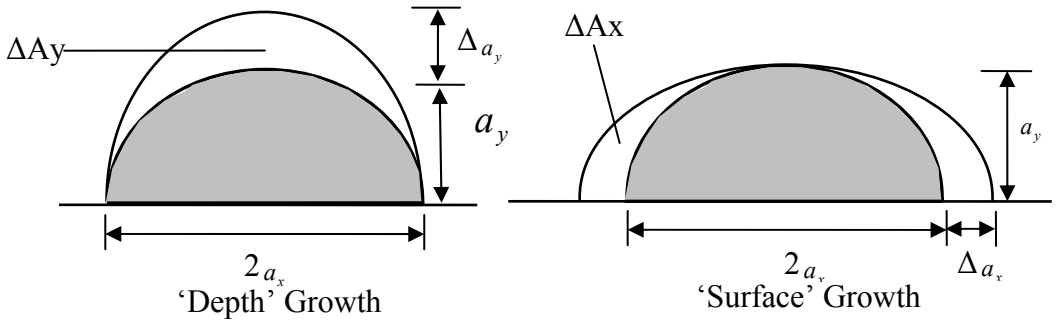

Figure 2.5- The two characteristic growth dimensions

By knowing the point weight function *h(P)* for any point *P* on the crack front, one can calculate the value of the stress intensity factor at that point as:

$$K_P = \int_A h_P(x,y)\sigma(x,y)dA \tag{2.16}$$

where *A* is the area of the crack face. If the Newman-Raju coordinate system is used for the surface crack, as also adopted by Fett [2.3], then each point on the crack front is characterised by its parametric angle ϕ, and equation (2.16) can be rewritten as

$$K_P = \int_A h_{\phi_P}(\rho,\phi)\sigma(\rho,\phi)dA$$

Therefore by knowing *h(x,y)* for all the points on the crack front, *K* distribution may be obtained for the whole crack.

The RMS weight function was defined in Chapter 1. Mathematically, it can be represented as *h* in the following equation

$$\overline{K}_A = \frac{1}{\Delta s_A}\int_{\Delta S_A} K dS_A = \int_A h_A(x,y)\sigma(x,y)dA \tag{2.17}$$

Or, in elliptical coordinate system,

$$\overline{K}_A = \int_A h_A(\rho,\phi)\sigma(\rho,\phi)dA$$

Note that in equation (2.17), ΔS_A represents the increment in area in the '*A direction'* of crack growth, e.g. depth direction, whereas the second integral is taken over *A*, which denotes the whole crack-face area.

2.4.2) Point Weight Functions

As mentioned in Chapter 1, no analytical weight function (point or RMS) currently exists for the surface crack. Attempts on surface crack stress intensity factor weight functions which yield the distribution of *K* at points along the crack front have been mainly focused on developing a weight function for the deepest point, and a separate weight function for the surface point. Shen and Glinka [2.20] have proposed approximate local weight functions for the deepest and the surface points of a semi-elliptical crack based on an approximation of the crack displacement field. As discussed in Chapter 1, this weight function lacks the general characteristics that are required of a reliable weight function. Moreover, as discussed above, the surface point SIF value is not deemed representative of the gross behaviour of the crack near the surface.

The approximate weight function proposed by Orynyak [2.21] was discussed in Chapter 1, and it was concluded that though it produces little error for tensile and bending cases, this weight function would lead to erroneous results where other loadings are involved which contain stress discontinuity etc.

2.4.2.1) MRS Approach for the Surface Crack Point WF

The Multiple Reference State technique for weight function evaluation was introduced in Chapter 1 [2.2]. It seems appropriate to benefit from this technique when two or

more reference solutions exist for stress intensity factors in a crack problem. For a semi-elliptical crack in a simple plate as shown in figure 2.6, two reliable reference solutions for the SIF are known from Newman-Raju. Therefore this approach might be of use with some alterations, bearing in mind that this technique has been developed for one-dimensional cracks only.

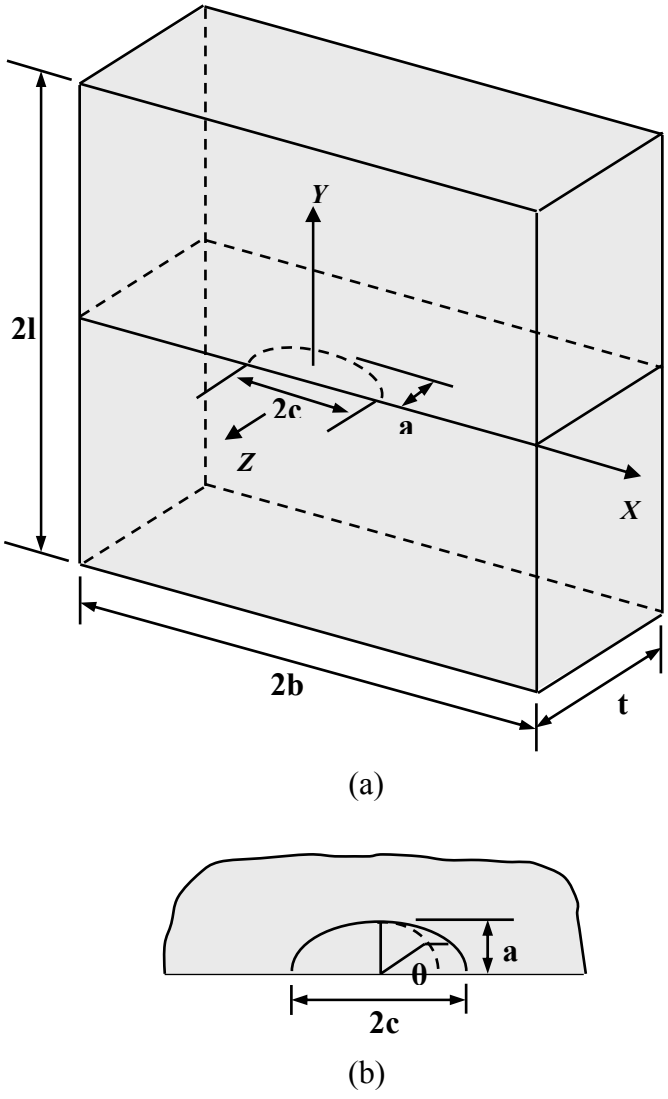

Figure 2.6- A semi-elliptical surface crack on a plate

In this method the functional form of the derivative of the crack profile is assumed to be known as [2.2]:

$$\frac{\partial u(a,x)}{\partial a} = \frac{2\sigma}{H}\sqrt{2}\sum_{j=0}^{M} c_j \left(1-\frac{x}{a}\right)^{j-1/2} \tag{2-18}$$

However, in the case of a one-dimensional crack, the first coefficient is also known from a knowledge of the asymptotic behaviour of the crack profile in the crack-tip region, as

$$c_0 = \frac{F\left(a/t\right)}{2} \tag{2.19}$$

where

$$F\left(\frac{a}{t}\right) = \frac{K}{\sigma_0\sqrt{\pi a}}$$

One major obstacle in generalising this technique to a surface crack is the fact that there is no single *K* value as the stress intensity factor varies along the crack front. If at each point along the crack front, the surface crack is treated as an edge crack having the same length as the local depth of the surface crack (*a*), then the MRS approach could be used in conjunction with Newman-Raju solutions as reference values for each point on the crack front. For this purpose a script *m*-file was developed in MATLAB to test the resulting weight function. Initially the 'depth' was taken as the radial distance, varying between 'a' for the deepest point and 'c' at the surface point. The results were not as accurate as the local depth approach. It should be noted that this method is expected to fail for the cases where the stress distribution varies along the surface direction. This is because, as shown in figure 2.7, by treating the crack as an edge crack at point *P*, only the loading at that specific section along *OP* can be included in the integrals. This is a grave concern and is enough grounds to disqualify this weight function for general SIF determination.

It is trivial that a concentrated load applied on *any point on the crack face* would lead to a non-zero stress intensity distribution along the crack front. Therefore any proposed weight function must be able to take into account the loading everywhere on the crack face.

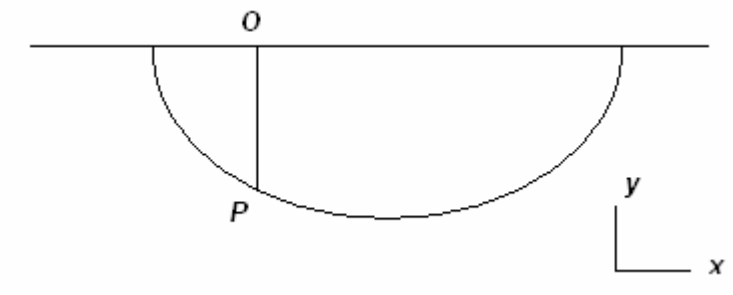

Figure 2.7- Treating the surface crack as an edge crack

2.4.2.2) A Discussion on the Significance of the Leading Term

Considering a case where two reference solutions for the stress intensity factor are known as K_1 and K_2, say under tensile and linear stress loading modes, then from equation 1.3, one gets:

$$\int_0^a H\sigma_1 \frac{\partial u}{\partial a} dx = K_1(a)K_1(a) \tag{2.20}$$

$$\int_0^a H\sigma_2 \frac{\partial u}{\partial a} dx = K_2(a)K_1(a) \tag{2.21}$$

Where $\sigma_1 = const$ and $\sigma_2 = \sigma_1 \frac{x}{a}$

Substituting for $\frac{\partial u}{\partial a}$ in equations (2.20) and (2.21) from equation (2.18), taking once *M*=2 and assuming c_o to be unknown:

$$\int_0^a 2\sqrt{2}\sigma_1^{\,2}\left[\left(c_0\left(1-\frac{x}{a}\right)^{-1/2}+c_1\left(1-\frac{x}{a}\right)^{1/2}\right)\right]dx = K_1(a)K_1(a) \qquad (2.22\text{-a})$$

$$\int_0^a 2\sqrt{2}\sigma_1^{\,2}\left(\frac{x}{a}\right)\left[\left(c_0\left(1-\frac{x}{a}\right)^{-1/2}+c_1\left(1-\frac{x}{a}\right)^{1/2}\right)\right]dx = K_2(a)K_1(a) \qquad (2.22\text{-b})$$

And again M=3, and substituting for c_o from equation (2.19):

$$\int_0^a 2\sqrt{2}\sigma_1^{\,2}\left[\left(\frac{K_1}{2\sigma_1\sqrt{\pi a}}\left(1-\frac{x}{a}\right)^{-1/2}+c_1\left(1-\frac{x}{a}\right)^{1/2}+c_3\left(1-\frac{x}{a}\right)^{3/2}\right)\right]dx = K_1(a)K_1(a) \qquad (2.23\text{-a})$$

$$\int_0^a 2\sqrt{2}\sigma_1^{\,2}\left(\frac{x}{a}\right)\left[\left(\frac{K_1}{2\sigma_1\sqrt{\pi a}}\left(1-\frac{x}{a}\right)^{-1/2}+c_1\left(1-\frac{x}{a}\right)^{1/2}+c_3\left(1-\frac{x}{a}\right)^{3/2}\right)\right]dx = K_2(a)K_1(a) \qquad (2.23\text{-b})$$

From equations (2.22), the two unknown coefficients are derived as:

$$c_0 = \frac{3\sqrt{2}\sigma_1^{\,2}}{4aK_1}\left(\frac{5}{K_2}-\frac{2}{K_1}\right)$$

$$c_1 = \frac{15\sqrt{2}\sigma_1^{\,2}}{4aK_1}\left(\frac{2}{K_1}-\frac{3}{K_2}\right)$$

And from equations (2.23), the two unknown coefficients, i.e. c_1 and c_2 are derived as:

$$c_1 = \frac{15\sqrt{2}\sigma_1^{\,2}}{4aK_1}\left(\frac{7}{K_2}-\frac{2}{K_1}\right)-\frac{5K_1}{\sigma_1\sqrt{\pi a}}$$

$$c_2 = \frac{35\sqrt{2}\sigma_1^{\,2}}{2aK_1}\left(\frac{1}{K_1}-\frac{5}{2K_2}\right)+\frac{35K_1}{6\sigma_1\sqrt{\pi a}}$$

Now, by taking the two reference solutions as K for an edge crack under pure tension (K_1) and an edge crack under pure bending (K_2), one gets

$$K_i = \sigma\sqrt{\pi a}F_i\left(a/b\right) \qquad (i=1,2)$$

Where the *F* solutions are taken, for pure tension as [2.18]

$$F_1\left(a/b\right) = \sqrt{\frac{2b}{\pi a}\tan\frac{\pi a}{2b}}\,\frac{0.752 + 2.02\left(a/b\right) + 0.37\left(1-\sin\frac{\pi a}{2b}\right)^3}{\cos\frac{\pi a}{2b}} \qquad (2.24\text{-a})$$

and for bending as [2.4]

$$F_2\left(a/b\right) = \sqrt{\frac{2b}{\pi a}\tan\frac{\pi a}{2b}}\,\frac{0.923 + 0.199\left(1-\sin\frac{\pi a}{2b}\right)^4}{\cos\frac{\pi a}{2b}} \qquad (2.24\text{-b})$$

Both of the above empirical formulae have a quoted accuracy of 0.5% or better for any value of a/b [2.4]. '*a*' is the depth of the crack and *b* is the width of the specimen.

Substituting equations 2.24 in the equations for c_o, c_1 and c_2 shows that both equations (2.22 and 2.23) generate weight functions that show a maximum difference of about 5%. Therefore it can be concluded that the first coefficient (c_o) does not need be assumed and its numerical value can be directly determined from the reference solutions. While this may be relatively unimportant for the class of one-dimensional cracks where the value of the first coefficient is readily known, it is significant for the case of the surface crack as here the displacement field may not be as easily determined as for the edge crack. Therefore from now on in this study the first coefficient for the surface cracks is directly derived from the reference solutions.

The only point which can not be analysed with this method is the surface point as the local crack depth at this point is zero. Figure 2.8 compares the values of *K* under

tension and bending as a function of the parametric angle using this technique with the Newman-Raju graphs.

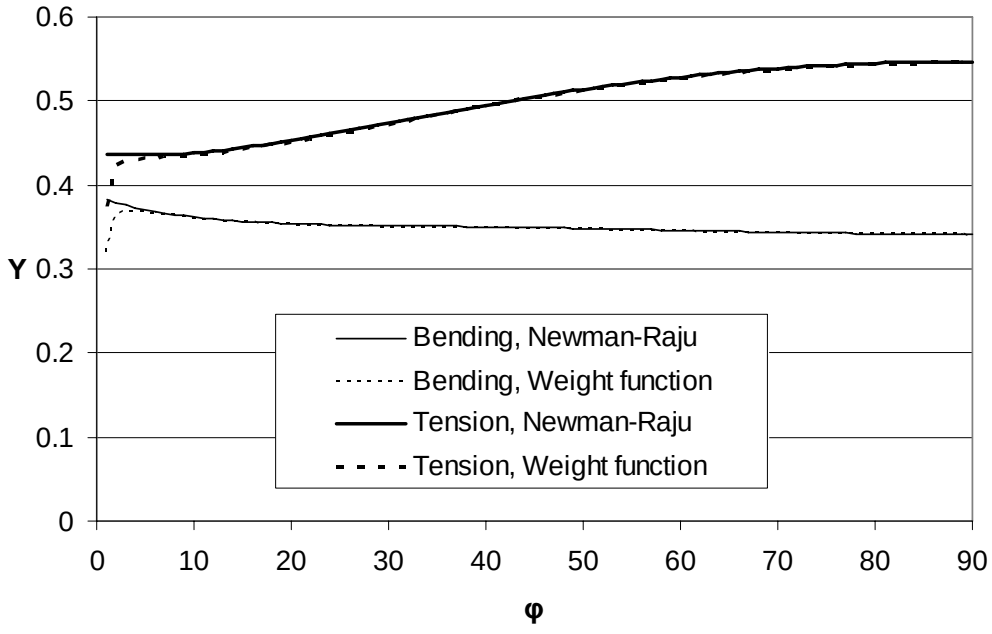

Figure 2.8- The point weight function and Newman-Raju SIF values for a surface crack under tension and bending

2.4.3) RMS Stress Intensity Factor Weight Function

As mentioned in Chapter 1, application of an averaged stress intensity factor value for fatigue life assessment was first proposed by Cruise-Besuner [2.22], where the concept was defined for two-dimensional cracks of elliptical and semi-elliptical shapes. However, the weight function suggested by Besuner [2.23] for RMS stress intensity values, requires an accurate displacement field:

$$h_{ij} = \left(\frac{2\partial\left(Q_m^{\ *} q_m^{\ *}\right)}{H\partial A_i} \right)^{-\frac{1}{2}} \frac{\partial q_j^{\ *}}{\partial A_i}$$

Where q^* is the crack face displacement for the reference crack face loading of σ_{zz}^* and *i* and *j* are the characteristic dimension indices. Q is the normal load. This weight function gives the RMS stress intensity factor as:

$$\overline{K}_i = \left(\frac{2\partial \left[\iint A \sigma_{zz}^* q^* dA \right]}{H \partial A_i} \right)^{-\frac{1}{2}} \iint_A \sigma_{zz} \frac{\partial q^*}{\partial A_i} dA$$

It is obvious that this representation of the weight function has little practical use since accurate displacement fields are not available for semi-elliptical surface cracks. Therefore approximate RMS SIF weight functions should be considered.

Fett [2.3] suggested a method for deriving an approximate RMS SIF weight function based on an approximation of the crack profile, and a number of reference solutions. It is in direct analogy with the work of Ojdrovic and Petroski [2.2], though the unknown coefficients are derived in a somewhat more complicated manner.

Starting from Rice's equation [2.24]

$$\frac{1}{H} \int_{(L)} K_I K_{Ir} \delta l dL = \int_{(S)} \sigma \delta v_r dS \tag{2.25}$$

Here δv_r is a virtual change in the crack displacement of the reference load and δl is the corresponding crack extension perpendicular to the crack front [2.3], the change of area can be determined as

$$\Delta S = \int_{(L)} \delta l dL$$

By substituting this into equation (2.24), one gets:

$$H \int_{(S)} \sigma \frac{\partial v_r}{\partial (\Delta S)} dS = \frac{1}{\Delta S} \int_{(\Delta S)} K_I K_{Ir} d(\Delta S) \tag{2.26}$$

Now depending on the specific crack growth dimension, different weight functions may be introduced. For example for the directions suggested by Cruse and Besuner [2.22], one can define the following weight functions:

$$h_a = \frac{H}{K_{Ir}} \frac{\partial v_r}{\partial a}$$

$$h_c = \frac{H}{K_{Ir}} \frac{\partial v_r}{\partial c}$$

Bearing in mind that for a semi-elliptical crack, for an increase in depth equal to Δa, $d(\Delta S_A) = c\Delta a \sin^2 \varphi d\varphi$ and $\Delta S_A = \frac{1}{2}\pi c \Delta a$, and for an increase in width equal to Δc, $d(\Delta S_B) = a\Delta c \cos^2 \varphi d\varphi$ and $\Delta S_B = \frac{1}{2}\pi a \Delta c$, equation (2.26) can be written as the following two equations for the two different crack growth directions:

$$\frac{1}{c}\int_{(S)} h_a K_{Ir} \sigma dS = \int_0^{\pi} K_I K_{Ir} \sin^2 \varphi d\varphi \qquad (2.27\text{-a})$$

$$\frac{1}{a}\int_{(S)} h_c K_{Ir} \sigma dS = \int_0^{\pi} K_I K_{Ir} \cos^2 \varphi d\varphi \qquad (2.27\text{-b})$$

Fett further assumed the weight functions to be represented by the following series [2.3]:

$$h_a(\rho/r, \varphi) = \sqrt{\left(\frac{2}{\pi a}\right)} \sum_{n=0}^{\infty} f_n(\varphi) \left(1 - \rho/r\right)^{n-1/2} \qquad (2.28\text{-a})$$

$$h_c(\rho/r, \varphi) = \sqrt{\left(\frac{2}{\pi a}\right)} \sum_{n=0}^{\infty} g_n(\varphi) \left(1 - \rho/r\right)^{n-1/2} \qquad (2.28\text{-b})$$

The near-tip field of a semi-elliptical surface crack under tensile loading has been suggested by Fett [2.25] to have the following form

$$u_N(\rho,\varphi) = C_0(\varphi)\left(1-\rho/r\right)^{\nu+1/2}$$

Where

$$C_0(\varphi) = \sqrt{8/\pi}\,\frac{\sigma_0}{H}\,Y\left(\frac{a}{c},\frac{a}{t},\varphi\right)a\left[\left(\frac{a}{c}\right)^2\cos^2\varphi+\sin^2\varphi\right]^{-1/4}$$

Y is the geometric function defined by [2.25]:

$$K = \sigma_0 Y\sqrt{a}$$

Therefore the first terms of the weight functions of equations (2.28) are:

$$f_0(\varphi) = \frac{a^2\sin^2\varphi}{a^2\sin^2\varphi+c^2\cos^2\varphi}\left[\left(\frac{a}{c}\right)^2\cos^2\varphi+\sin^2\varphi\right]^{-1/4} \qquad (2.29\text{-a})$$

$$g_0(\varphi) = \frac{c^2\cos^2\varphi}{a^2\sin^2\varphi+c^2\cos^2\varphi}\left[\left(\frac{a}{c}\right)^2\cos^2\varphi+\sin^2\varphi\right]^{-1/4} \qquad (2.29\text{-b})$$

$$r = \left(a^2\sin^2\varphi+c^2\cos^2\varphi\right)^{1/2}$$

The other coefficients of equations (2.28) are determined from a condition of geometrical compatibility and a number of reference solutions. Using only one reference solution leads to an approximate two-term weight function as follows:

$$h_a\left(\rho/r,\varphi\right) = \sqrt{\left(\frac{2}{\pi a}\right)}\left[\frac{f_0(\varphi)}{\sqrt{\left(1-\rho/r\right)}}+\left(C_1-f_0(\varphi)\right)\sqrt{\left(1-\rho/r\right)}\right] \qquad (2.30\text{-a})$$

$$h_c\left(\rho/r,\varphi\right) = \sqrt{\left(\frac{2}{\pi a}\right)}\left[\frac{g_0(\varphi)}{\sqrt{\left(1-\rho/r\right)}}+\left(C_2-g_0(\varphi)\right)\sqrt{\left(1-\rho/r\right)}\right] \qquad (2.30\text{-b})$$

Where C_1 and C_1 are determined as [2.3]

$$C_1 = \frac{15}{4}\sqrt{\left(\frac{\pi}{2}\right)}\frac{\int_0^{\pi} {Y_r}^2 \sin^2\varphi d\varphi}{\int_0^{\pi} Y_r d\varphi} - 4\frac{\int_0^{\pi} f_0(\varphi) Y_r d\varphi}{\int_0^{\pi} Y_r d\varphi}$$

$$C_2 = \frac{15}{4}\sqrt{\left(\frac{\pi}{2}\right)}\frac{\int_0^{\pi} {Y_r}^2 \cos^2\varphi d\varphi}{\int_0^{\pi} Y_r d\varphi} - 4\frac{\int_0^{\pi} g_0(\varphi) Y_r d\varphi}{\int_0^{\pi} Y_r d\varphi}$$

And using two reference solutions, the three-term weight functions can be expressed as

$$h_a = \sqrt{\left(\frac{2}{\pi a}\right)}\left[\frac{f_0(\varphi)}{\sqrt{\left(1-\rho/r\right)}} + \left(A_0 - A_1\cos 2\varphi\right)\sqrt{\left(1-\rho/r\right)} + \left(C_1 - f_0 - A_0 + A_1\cos 2\varphi\right)\left(1-\rho/r\right)^{3/2}\right]$$

(2.31-a)

$$h_c = \sqrt{\left(\frac{2}{\pi a}\right)}\left[\frac{g_0(\varphi)}{\sqrt{\left(1-\rho/r\right)}} + \left(B_0 - B_1\cos 2\varphi\right)\sqrt{\left(1-\rho/r\right)} + \left(C_2 - g_0 - B_0 + B_1\cos 2\varphi\right)\left(1-\rho/r\right)^{3/2}\right]$$

(2.31-b)

Fett does not give the values of these new coefficients, but they can be calculated by substituting the above equations (equations 2.31) into equations 2.27. The details of these derivations are not shown here. The new coefficients are calculated as

$$A_1 = A_0 - \frac{3}{2}C_1$$

$$B_1 = B_0 + \sqrt{\frac{c}{a}} - \frac{3}{2}C_2$$

$$A_0 = \frac{I_5 I_4 - I_2 I_6}{I_1 I_4 - I_2 I_3}; C_1 = \frac{I_1 I_6 - I_3 I_5}{I_1 I_4 - I_2 I_3}$$

$$B_0 = \frac{J_5 J_4 - J_2 J_6}{I_1 I_4 - I_2 I_3};\ C_2 = \frac{J_1 J_6 - J_3 J_5}{I_1 I_4 - I_2 I_3}$$

$$I_1 = \int_0^{\pi} (1 - \cos 2\varphi) Y_1 d\varphi$$

$$I_2 = \int_0^{\pi} (1 + 2\cos 2\varphi) Y_1 d\varphi$$

$$I_3 = \int_0^{\pi} (1 - \cos 2\varphi) \sin\varphi Y_1 d\varphi$$

$$I_4 = \int_0^{\pi} (1 + 3\cos 2\varphi) \sin\varphi Y_1 d\varphi$$

$$I_5 = \frac{105\pi}{16\sqrt{2}} \int_0^{\pi} \sin^2\varphi {Y_1}^2 d\varphi - 8\int_0^{\pi} f_0 Y_1 d\varphi$$

$$I_6 = \frac{315\pi}{32\sqrt{2}} \left(\frac{t}{a}\right) \int_0^{\pi} \sin^2\varphi Y_1 Y_2 d\varphi - 10\int_0^{\pi} f_0 \sin\varphi Y_1 d\varphi$$

$$J_5 = \frac{105\pi}{16\sqrt{2}} \left(\frac{a}{c}\right) \int_0^{\pi} \cos^2\varphi {Y_1}^2 d\varphi - 8\int_0^{\pi} g_0 Y_1 d\varphi + 2\sqrt{\frac{c}{a}} \int_0^{\pi} \cos 2\varphi Y_1 d\varphi$$

$$J_6 = \frac{315\pi}{32\sqrt{2}} \left(\frac{t}{a}\right) \int_0^{\pi} \cos^2\varphi Y_1 Y_2 d\varphi - 10\int_0^{\pi} g_0 \sin\varphi Y_1 d\varphi + 2\sqrt{\frac{c}{a}} \int_0^{\pi} \sin\varphi \cos 2\varphi Y_1 d\varphi$$

Where Y_1 has been taken as the Newman-Raju solution for tension and Y_2 is the geometric function under a linearly increasing stress state, again taken from Newman-Raju.

Discussion on Fett's RMS Weight Function

Now it is possible to plot the weight functions of equations (2.30) and (2.31) for specific crack geometries. The two-term weight function for the depth direction (2.30-a) and the three term weight function from the (2.31-a) do not show a good agreement. The comparison plots for $\varphi = 0$, 30, 60 and 90 for a crack with an aspect ratio of a/c=0.5 and relative depth of $a/t = 0.3$ are shown in the figure 2.9.

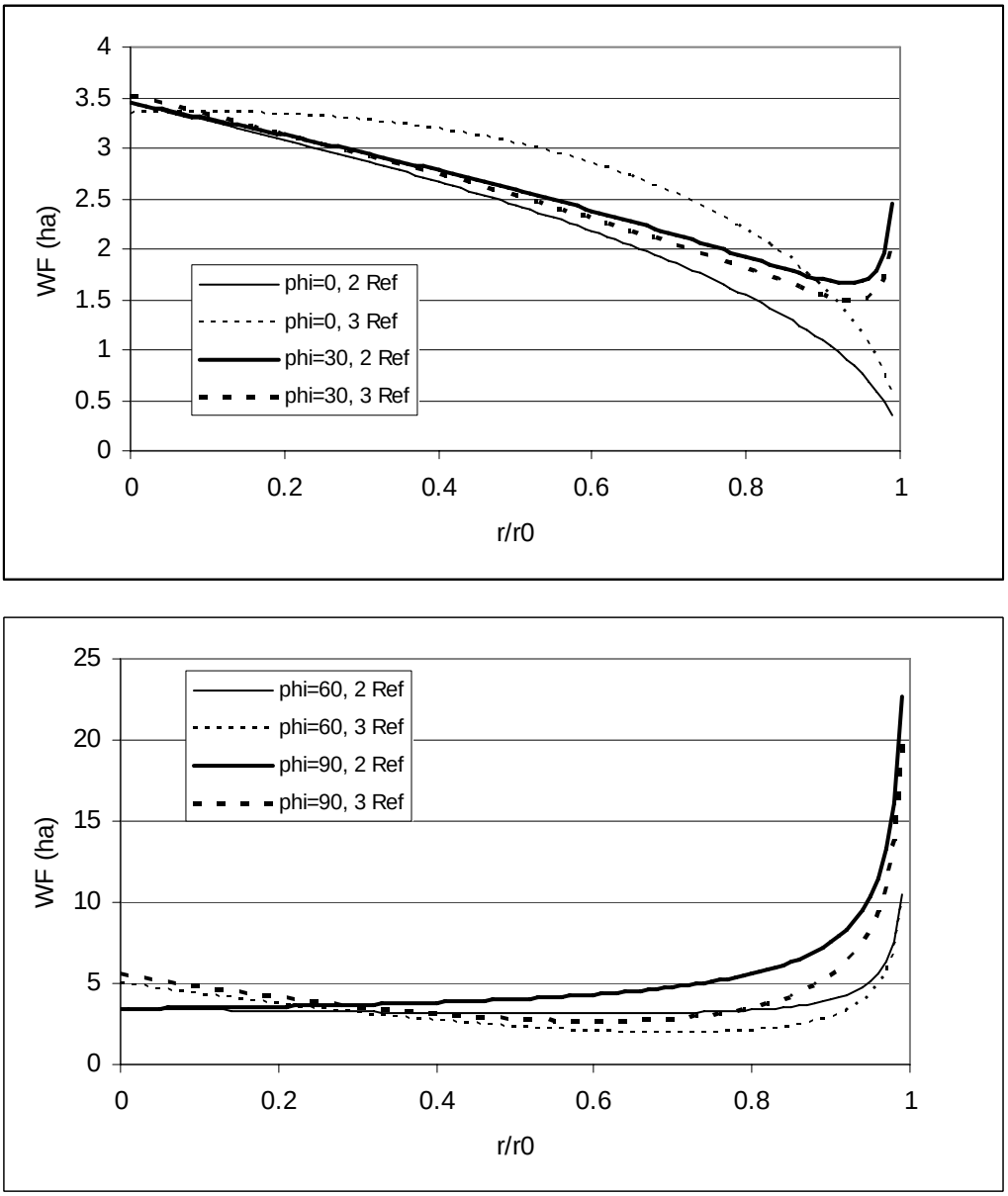

Figure 2.9- A comparison between Fett's weight function values using one and two reference solutions

However, comparison of the two and three term weight functions for the width direction (h_c) for the same crack shows a great difference between the two. For $\varphi = 90^o$, the two term weight function gives negative values for the weight function, which is not possible.

Various studies show that the deviation between the two-term and three-term weight function becomes greater for larger aspect ratios. It is believed that the major

inaccuracy arises from the assumed shape of the displacement field. Fett [2.3] does not give any comparison between the two-term and three-term weight functions for the surface direction (i.e. (2.30-b) and (2.31-b)).

Another drawback of this method of weight function derivation is that it is quite complicated, especially when more than one reference solution is used. It can be concluded here that this weight function, though a logical generalisation of the MRS technique to the two-dimensional crack, is not practical.

Once again it is worth mentioning that the derivation of these weight functions relies on the crack shape being semi-elliptical, therefore they must not be used in situations where the crack shape might deviate from this geometry. Examples of such cracks were observed in the work of Ngiam et al. [2.26].

2.5) A New Approach

One important aspect of the MRS technique in one-dimensional cracks is that the process of COD derivation is circumnavigated and a series representation of the derivative of the COD is assumed. However, the COD field of a one-dimensional crack is simpler than that of a two-dimensional one. Moreover, it should not be forgotten that the one-dimensional MRS technique, though implicitly, relies upon having a plane strain or generalised plane stress state. This is a further reason for using the RMS concept for life predictions when using the two-dimensional weight function.

Starting from

$$H\int_S \sigma_n \frac{\partial u_0}{\partial(\Delta S)} dS = \frac{1}{\Delta S}\int_{\Delta S} K_0 K_n d(\Delta S) \qquad (2.32)$$

And defining the average stress intensity factor as

$$\overline{K}_{nA} = \frac{1}{\overline{K}_{0A}} \frac{1}{\Delta S_A} \int_{\Delta S_A} K_0 K_n d(\Delta S_A) \tag{2.33}$$

And therefore for the reference case, the average SIF would be

$$\overline{K}_{0A}{}^2 = \frac{1}{\Delta S_A} \int_{\Delta S_A} K_0{}^2(\phi) d(\Delta S_A)$$

Now by defining m_A as

$$m_A = \frac{H}{K_0} \frac{\partial u_0}{\partial(\Delta S_A)}$$

equation (2.33) becomes

$$\overline{K}_{nA} = \frac{1}{\overline{K}_{0A}} \int_S \sigma_n m_A K_0 dS$$

for the 'A' direction, and the same could be derived for the 'B', or surface' direction. So again from equation (2.33), for the 'A' direction, it follows:

$$\frac{2H}{\pi c} \int_S \sigma_n \frac{\partial u_0}{\partial(\Delta a)} dS = \frac{2}{\pi c \Delta a} \int_{\Delta S_A} K_0 K_n d(\Delta S_A)$$

where the following geometric relations can be derived:

$$d(\Delta S_A) = \Delta a_p dx$$

$$\Delta a_P = \Delta a \sqrt{1 - \frac{x^2}{c^2}}$$

$$dS = dxdy$$

$$H \int_{-c}^{c} \int_0^a \sigma_n \frac{\partial u_0}{\partial(\Delta a)} dydx = \int_{-c}^{c} K_0 K_n \sqrt{1 - \frac{x^2}{c^2}} dx \tag{2.34}$$

So far no assumption has been introduced. Now if the derivative of the crack face displacement is assumed to be approximately expressed by the following finite series

$$\left.\frac{\partial u_0}{\partial(\Delta a)}\right|_{\varphi} = \frac{\sigma_0}{H}\sum_{j=0}^{m} C_j f(x,y)^{j-\frac{1}{2}}$$

then equation (2.34) can be written as

$$\int_{-c}^{c}\int_{0}^{a} \sigma_0\sigma_n \sum_{j=0}^{m} C_j f(x,y)^{j-\frac{1}{2}} dydx = \int_{-c}^{c} K_0 K_n \sqrt{1-\frac{x^2}{c^2}}dx$$

Following the MRS methodology as introduced by Ojdrovic-Petroski [2.2] for the one-dimensional cracks, by letting

$$W_{ij} = \int_{-c}^{c}\int_{0}^{a} \sigma_0\sigma_i(x,y) f(x,y)^{j-\frac{1}{2}} dydx$$

$$p_i = \int_{-c}^{c} K_0 K_i \sqrt{1-\frac{x^2}{c^2}}dx$$

and using *m* reference solutions, the following set of simultaneous equations is obtained

$$\sum_{j=0}^{m} W_{ij} C_j = p_i \qquad (2.35)$$

Based on an analogy to the one-dimensional weight function, the following functional form has been chosen for *f*:

$$f(x,y) = \left(1-\frac{y}{a}\right)\left(1-\frac{|x|}{c}\right)$$

It was argued that in the multiple reference state technique an *a priori* knowledge of the leading term coefficient is not crucial since this can simply be calculated from the

resulting equation. Obviously when this coefficient is known, it is only more accurate to include it in the equations and calculate one more coefficient from the reference solutions [2.27]. It can be proven that the sensitivity of the chosen COD derivative to the value of coefficients, calculated as (bearing in mind that $0 \le f \le 1$):

$$\frac{\partial}{\partial C_j}\left[\frac{\partial u_0}{\partial(\Delta a)}\right] = \frac{\sigma_0}{H} f^{j-\frac{1}{2}}$$

is maximum when j=0. This means that the first coefficient has to be chosen carefully and if its exact value is not known, it is best to be left as an unknown and to be derived from the set of equations. However, by using two reference solutions only two unknown coefficients can be derived, and hence one could assume an arbitrary value for the third coefficient, i.e. C_2 and the first two coefficients would automatically adjust.

Therefore equation (2.35) could be rewritten, for m=2, as

$$\sum_{j=0}^{2} W_{ij} C_j = p_i$$

$$\sum_{j=0}^{1} W_{ij} C_j = p_i - W_{i2} C_2 = q_i$$

From which the unknown coefficients are derived as

$$C_0 = \frac{q_1 W_{21} - q_2 W_{11}}{W_{10} W_{21} - W_{20} W_{11}} \quad \text{and} \quad C_1 = \frac{q_2 W_{10} - q_1 W_{20}}{W_{10} W_{21} - W_{20} W_{11}}$$

Therefore the weight function is derived as

$$\frac{H}{\sigma_0}\frac{\partial u_0}{\partial(\Delta a)} = \sum_{j=0}^{m} C_j \left(1 - \frac{|x|}{c}\right)^{j-\frac{1}{2}} \left(1 - \frac{y}{a}\right)^{j-\frac{1}{2}}$$

Now the stress intensity factor can be calculated, using the above weight function in the Cartesian coordinate system, as

$$\overline{K}_{nA} = \frac{2}{\pi c}\frac{1}{\overline{K}_{0A}}\int_S \sigma_0 \sigma_n \sum_{j=0}^{m} C_j \left(1-\frac{|x|}{c}\right)^{j-\frac{1}{2}} \left(1-\frac{y}{a}\right)^{j-\frac{1}{2}} dS$$

where m is the number of reference solutions. For semi-elliptical surface cracks it is usually taken as two as Newman-Raju formulae give two reliable SIF solutions.

2.6) Verification of the Weight Function Results

In order to verify the results of the weight function which was derived in the previous section, it is important to have a reliable and accurate tool for comparison. Finite Elements analysis of stress intensity factors in surface cracks gives an invaluable tool for this purpose. A series of three-dimensional models was created and different loadings were applied on each model. The following sections describe the modelling process. The Finite Elements software ABAQUS 6.5-1 was used for this study; Appendix A outlines the method used by this software for K and J evaluation.

2.6.1) Verification of the Weight Function Results - Developing a Finite Element Model for Arbitrary Loadings

2.6.1.1) Introduction to the Principle of Superposition for Surface Cracks

It is often found that the crack is subjected to non-uniform loadings such as a steep stress gradient or partial loading due to residual stresses. Before proceeding any further, it would be helpful to study the problem of a loaded crack more closely.

Figure 2.10 shows the principle of superposition as applied to stress intensity factors in surface cracks under fully elastic conditions.

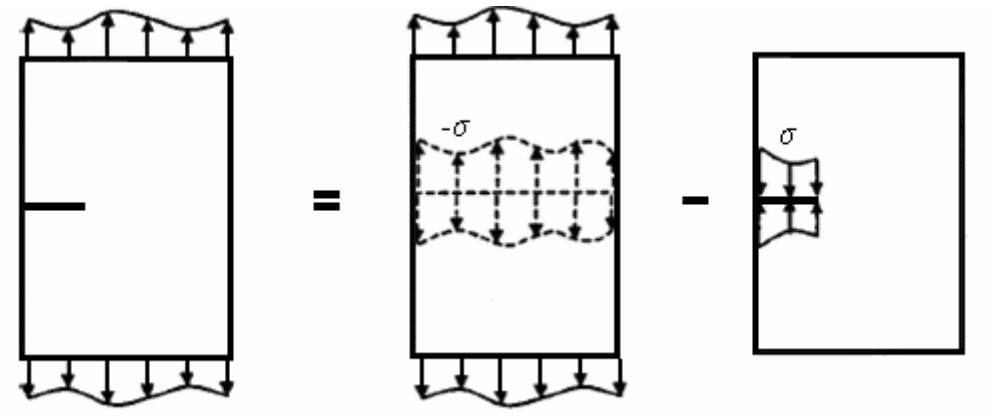

Figure 2.10- Principle of Superposition for an elastic body with a crack

Remote boundary loading is applied to the specimen on the left hand side of the equality sign. This specimen represents the original case which needs to be analysed. In the first specimen of the right hand side, in addition to the same applied boundary loading, another distributed stress $-\sigma$ is applied on the two crack-faces, which closes the crack. It is clear that σ is the stress that would have been produced on the same plane under the same boundary conditions had the crack not existed. As the crack has been fully closed here, the value of the stress intensity factor is zero everywhere along the crack front. Once again it should be noted that plasticity is neglected here. The crack faces in the second specimen on the right hand side are loaded under σ to equate the two sides of the equation. Therefore one concludes that in a fully elastic specimen with a crack, the effect of remote boundary loading on stress intensity factors can be replicated by ignoring the boundary conditions and applying a distributed load directly on the crack faces. Moreover, this distributed load has to be the stress distribution in the un-cracked specimen under the same boundary conditions.

The weight function approach to SIF calculation, which was discussed in Chapter 1, relies upon the abovementioned fact. It is nearly always easier to determine the stress distribution on the crack plane in the un-cracked specimen rather than in the cracked body.

At this point it seems reasonable to develop a reliable source of stress intensity factor values for the surface crack for comparison purposes. It is only by comparing the

weight function results with reliable reference values that the weight functions can be validated. Newman and Raju formulae represent two such reliable SIF solutions. For other loading cases, Finite Element method has been chosen in this study because of the advantages mentioned in Chapter 1**.** All the finite element analyses are carried out in ABAQUS version 6.5-1.

Surface cracks with different geometric parameters (i.e. aspect ratio and relative depth) are modelled using a FORTRAN mesh-generator which creates three-dimensional finite element meshes of the surface crack such as the one shown in figure 2.11. A MATLAB script *m*-file has been developed which facilitates application of arbitrary stress distribution on the face of the crack. The superposition concept discussed above permits the loading to be applied directly on the crack face.

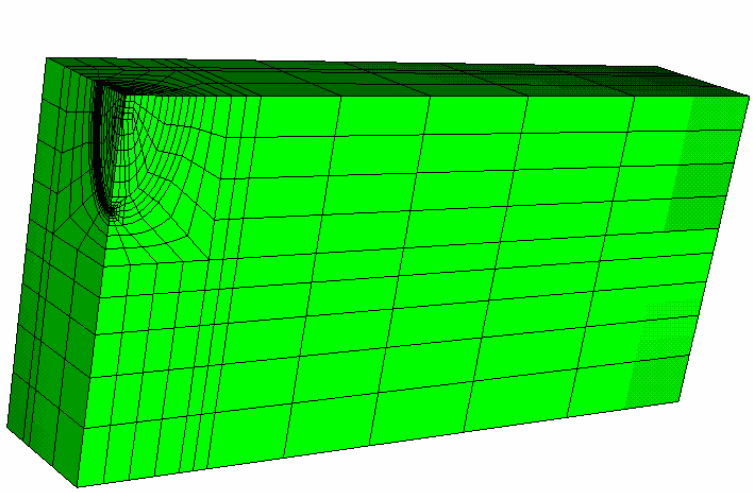

Figure 2.11- The finite element mesh of the quarter-model

2.6.1.2) Application of an Arbitrary Stress on the Crack Face

Figure 2.12 shows the finite element mesh of the surface crack face. The arbitrary stress distribution is to be applied on the quarter-elliptical area.

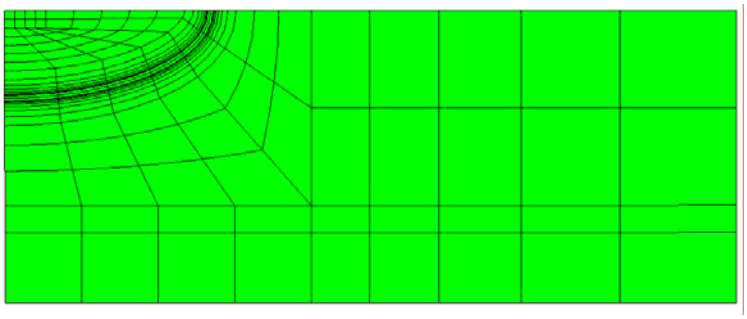

Figure 2.12- The *x-y* plane of the three-dimensional Finite Element mesh

Only a quarter of the specimen has been modelled here, which means only loadings that are symmetrical with respect to the *y* axis can be applied. One face of a typical element is shown in figure 2.13.

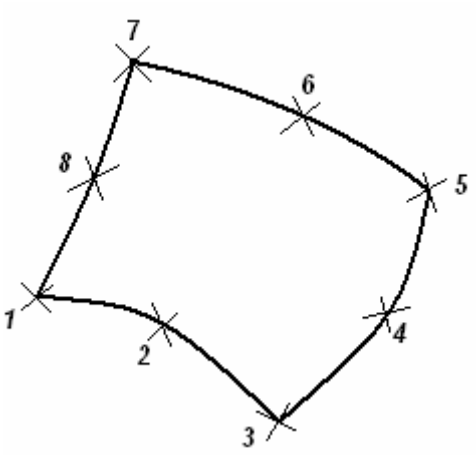

Figure 2.13- The load face of a typical element

Here, the numbers 1-8 denote local node numbers. Each boundary can be expressed as a quadratic polynomial, i.e. a parabola. An automated routine has been developed, which when given the crack-face element numbers as input, searches the ABAQUS input file for each element number and finds the appropriate element face (i.e. the free face where the loading should be applied), and then extracts the node numbers of the boundaries of this face from the elements data file. After retrieving the global coordinates of these nodes from the node definition file, parabolas are fitted to the boundaries of each element. For example, assuming that the global coordinates of the nodes shown in figure 2.13 are known, for the boundary consisting of nodes 1-2-3; x_1, y_1, x_2, y_2, x_3 and y_3 would be known values from the input file. A parabolic relation

of the following form is assumed to define each boundary, where *a*, *b* and *c* are unknown parameters:

$$y = ax^2 + bx + c$$

Having the following matrix equation:

$$\begin{bmatrix} x_1^{\,2}, x_1, 1 \\ x_2^{\,2}, x_2, 1 \\ x_3^{\,2}, x_3, 1 \end{bmatrix} \begin{bmatrix} a \\ b \\ b \end{bmatrix} = \begin{bmatrix} y_1 \\ y_2 \\ y_3 \end{bmatrix}$$

the unknown coefficients are derived as:

$$\begin{bmatrix} a \\ b \\ b \end{bmatrix} = \begin{bmatrix} x_1^{\,2}, x_1, 1 \\ x_2^{\,2}, x_2, 1 \\ x_3^{\,2}, x_3, 1 \end{bmatrix}^{-1} \begin{bmatrix} y_1 \\ y_2 \\ y_3 \end{bmatrix}$$

The same procedure is applied for the other three boundaries. In the next step, the face area of each individual element is calculated by a simple double-integration within these boundaries. Finally, knowing the required stress distribution σ, the equivalent uniform element face-pressure for element *i* can be obtained as:

$$P_i = \frac{1}{A_i} \int_A \sigma(x, y) dA$$

A_i is the area of the element face. The whole procedure is repeated for every single element on the crack face.

Note: this method is an approximation, and could lead to inaccurate results for a coarse mesh and steep stress gradients. The accuracy of this method has been checked for different crack geometries by comparing the SIF results under bending with Newman-

Raju values; for the tensile loading case, the method does not introduce any inaccuracy in applying the load. Obviously, the overall accuracy of the analysis also depends on other factors such as mesh density. For all the surface cracks that are studied in this chapter, the SIF results from FE for bending have been within ±1% of the Newman-Raju stress intensity factor values for bending.

2.6.2) Verification of the Weight Function Results – Comparison with Finite Elements Solutions

A wide range of crack aspect ratios for the semi-elliptical surface crack were modelled using the Finite Element model. For the tensile and bending cases, the weight function results show a near-exact match with the computed FE RMS SIFs. This is expected as the tensile and bending cases have been used as references in constructing the weight function. For validation purposes, two more types of loading have been used, namely $\sigma = \sigma_0\left(\frac{a-y}{a}\right)^2$, denoted as loading 1, and $\sigma = \sigma_0\left(\frac{a-y}{a}\right)^3$, denoted as loading 2. Figure 2.14 shows a comparison between the RMS SIF values obtained using the weight function and the FE results, for different surface cracks with a fixed a/t of 0.3. It is observed that the weight function result for tension and bending coincide exactly with Newman-Raju values. This is expected as Newman-Raju values are used for reference solutions. For the two other loading cases that have been shown, i.e. $\sigma = \sigma_0\left(\frac{a-y}{a}\right)^2$ and $\sigma = \sigma_0\left(\frac{a-y}{a}\right)^3$, a good agreement is observed between the weight function results and the results obtained from finite elements method.

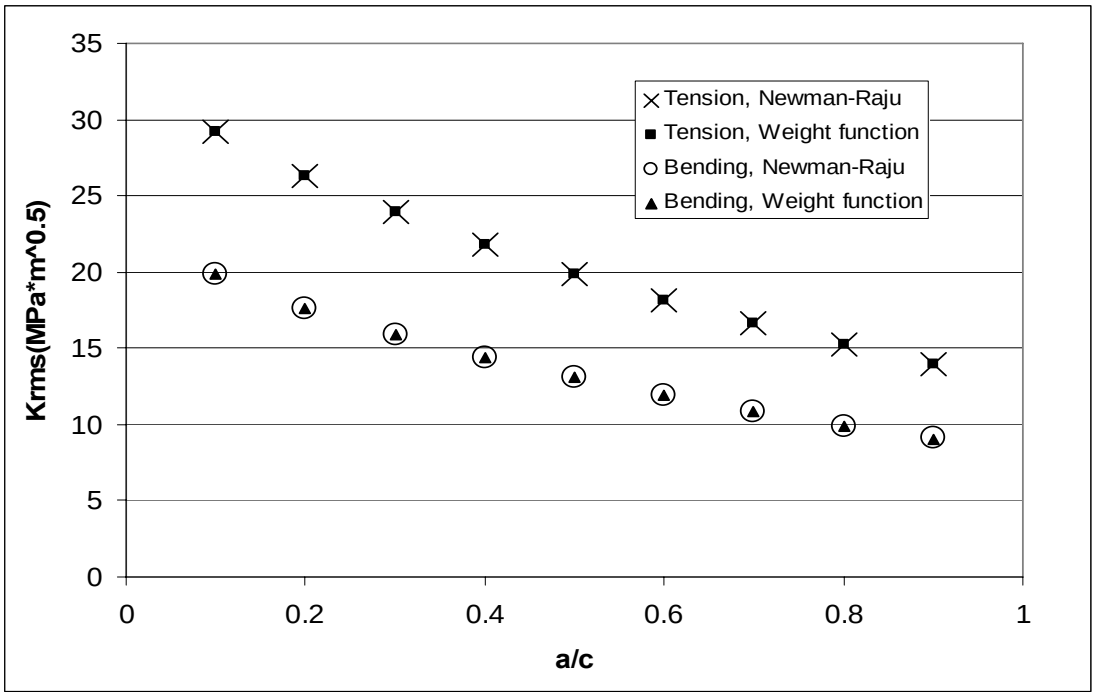

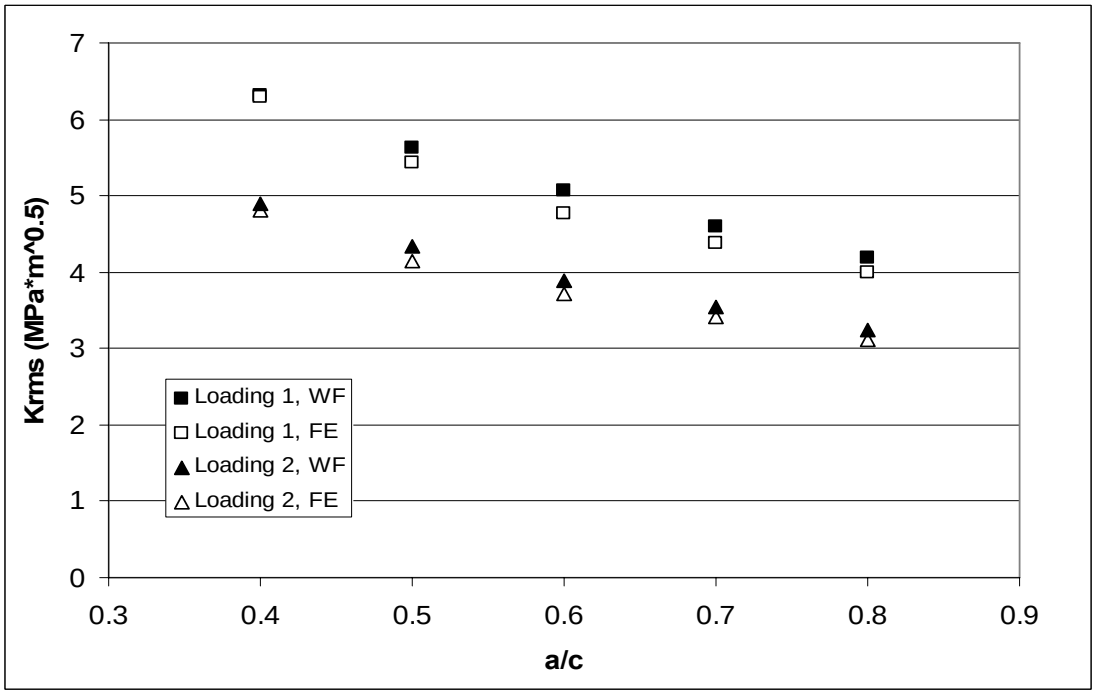

Figure 2.14- Comparison between the weight function and the finite elements results for different loadings

2.7 Summary

In this chapter, two different approaches to the problem of surface crack growth analysis were discussed: the point-by-point growth approach using the Paris law, and the RMS analysis using a modified form of the Paris law. It was argued that the point-by-point analysis suffers from a fundamental intrinsic flaw, namely that the Paris law coefficient in this case is not constant and depends, among other things, on the loading and therefore may result in unknown errors when applied for arbitrary loadings where its dependence on the load is not established.

The RMS SIF approach in fatigue life prediction was discussed and its advantages over the two point method enumerated. The lack of existing reliable and accurate weight functions for the RMS SIF in surface cracks was stressed and in view of this, a new weight function for the surface crack was proposed. This weight function is based on the Multiple Reference States principle [2.2] and is far less complicated than the existing methods, and therefore suitable for incremental crack growth analyses where as the crack grows, values of SIF for a large number of different crack geometries are required.

The results from this weight function were compared with finite element solutions for a wide range of crack geometries and loading and a good agreement was observed in all the cases.

In order to study the effect of arbitrary loadings on crack growth, the next chapter proposes a set of experiments in which specimens which include non-uniform stresses are subjected to cyclic loading. To analyse the results of the experiment, the one-dimensional weight function method based on MRS technique is to be used. Laser shock peening is chosen as the preferred treatment for the purpose of this study because the resulting residual stress field is typically several times deeper than the field achievable by shot peening (see Chapter 1). Also, due to the increased depth of penetration the residual stresses can be easily measured using the neutron diffraction

stress measurement technique, and the laser peening process creates much less surface roughness than shot peening.

References

[2.1] J C Newman and R J Raju, An empirical stress-intensity factor equation for the surface crack, *Engineering Fracture Mechanics*, Vol. 15(1-2), pp. 185-192 (1981).

[2.2] R P Ojdrovic and H J Petroski, Weight functions from multiple reference states and crack profile derivatives, *Engineering Fracture Mechanics*, Vol. 39(1), pp. 105-111 (1991).

[2.3] T Fett, A procedure for the determination of the weight function for semi-elliptical surface cracks by direct adjustment to reference solutions, *Engineering Fracture Mechanics*, Vol. 43(4), pp. 519-528 (1992).

[2.4] H Tada, P C Paris and G R Irwin, The Stress Analysis of Cracks Handbook, Third Edition (2000), The American Society of Mechanical Engineers.

[2.5] R J Sanford, Principles of Fracture Mechanics, *ISBN*-10: 0130929921Prentice Hall (2003).

[2.6] I N Sneddon, The Distribution of Stress in the Neighbourhood of a Crack in an Elastic Solid, *Proceeding of the Royal Society A*, 187, pp. 229-260 (1946).

[2.7] G R Irwin, Crack Extension Force for a Part-Through Crack in a Plate, *Journal of Applied Mechanics,* 29, pp. 651-654 (1962).

[2.8] D K Cater, W R Canda and J A Blind, Experimental evaluation of stress-intensity solutions for surface flaw growth in plates, Surface-Crack Growth: Models, Experiments, and Structures, *ASTM STP 1060*, pp.215-236 (1990).

[2.9] A E Green and I N Sneddon, The distribution of stress in the neighbourhood of a flat elliptical crack in an elastic solid, *Proceedings of the Cambridge Philosophical Society*, Vol. 46(1), pp. 159-163 (1950).

[2.10] J C Newman, Predicting failure of specimens with either surface cracks or corner cracks at holes, *NASA TN D-8244* (1976).

[2.11] P C Paris and F Erdogan, A critical analysis of crack propagation laws, *Journal of Basic Engineering*, Vol. 85, pp. 528-534 (1963).

[2.12] C Mattheck, P Morawietz and D Munz, Stress intensity factor at the surface and t the deepest point of a semi-elliptical surface crack in plates under stress gradients, *International Journal of Fracture*, Vol. 23, pp. 201-212 (1983).

[2.13] M A Mahmoud, Quantitative prediction of growth patterns of surface fatigue cracks in tension plates, *Engineering Fracture Mechanics*, Vol. 30(6), pp. 735-746 (1988).

[2.14] M A Mahmoud, Growth patterns of surface fatigue cracks under cyclic bending-A quantitative analysis, *Engineering Fracture Mechanics*, Vol. 31(2), pp. 357-369 (1988).

[2.15] M A Mahmoud, Surface fatigue crack growth under combined tension and bending loading, *Engineering Fracture Mechanics*, Vol. 36(3), pp. 389-395 (1990).

[2.16] Wu Shang-Xian, Shape change of surface crack during fatigue growth, *Engineering Fracture Mechanics*, Vol. 22(5), pp. 897-913 (1985).

[2.17] Putra I S and Schijve J, *Fatigue and Fracture of Engineering Materials and Structures*, Vol. 15, pp. 323-338 (1992).

[2.18] Kim J H and Song J H, *Fatigue and Fracture of Engineering Materials and Structures*, Vol. 15, pp. 477-489.

[2.19] Corn D L, A study of cracking techniques for obtaining partial thickness cracks of pre-selected depths and shapes, *Engineering Fracture Mechanics,* Vol. 3, pp. 45-52 (1971).

[2.20] G Shen and G Glinka, Determination of weight functions from reference stress intensity factors, *Theoretical and Applied Fracture Mechanics*, Vol. 15(3), pp. 237-245 (1991).

[2.21] I V Orynyak and M V Borodii, Point weight function method application for semi-elliptical mode-I cracks, *International Journal of Fracture*, Vol. 70, pp. 117-124 (1995).

[2.22] P M Besuner and T A Cruise, Residual life prediction for surface cracks in complex structural details, Journal of Aircraft, Vol. 12(4), pp. 369-375 (1975).

[2.23] P M Besuner, Residual life estimates for structures with partial thickness cracks, Mechanics of Crack Growth, ASTM STP 590, American Society for Testing and Materials, pp. 403-419 (1976).

[2.24] J R Rice, Some remarks on the elastic crack-tip stress fields, *International Journal of Solids and Structures,* Vol. 8, pp. 751-758 (1972).

[2.25] T Fett, The crack opening displacement field of semi-elliptical surface cracks in tension for weight functions applications, *International Journal of Fracture*, Vol. 36, pp. 55-69 (1988).

[2.26] F P Brennan and S S Ngiam, Fatigue Crack Shape Control under Bending by Cold Working, *International Conference on Fatigue Crack Paths, Parma*, 14 - 16 September 2006.

[2.27] F P Brennan, Evaluation of stress intensity factors by multiple reference state weight function approach, *Theoretical and Applied Fracture Mechanics,* Vol. 20, pp. 249-256 (1994).

CHAPTER 3

3.0) Experimental Investigation of Fatigue Crack Growth in Laser Shock Peened Specimens

3.1) Introduction

Chapter 2 discussed the concept of weight functions for stress intensity factor derivation and proposed a novel technique for SIF assessment in surface cracks under non-uniform stress fields. The accuracy of the proposed weight functions was illustrated through comparison with finite element results. Important practical examples of the non-uniform type of loading are components containing residual stresses. These could either exist in the component as a result of the manufacturing, assembly etc. (such as residual stresses in welded parts [3.1]), or be intentionally 'added' to the component to enhance its behaviour. Examples of these residual stresses are those induced by shot and laser peening, which were discussed in Chapter 1.

As pointed out in Chapter 1, shot peening and laser peening are effective techniques that have been used for fatigue crack retardation [3.2, 3.3]. It is believed that through the compressive residual stresses that are created in the material, these treatments affect the stress intensity factors and can therefore retard the growth of fatigue cracks [3.4] and delay the crack initiation phase [3.2]. Various studies confirm the beneficial effect of these methods in components that are prone to cyclic fatigue [3.2, 3.3]; see Chapter 1 for more details.

However, the advantage of these methods, though undeniably apparent, has not been conclusively quantified in terms of the residual stress field. There are two main reasons for this absence of analytical approach:

1) The extent to which residual stress measurement methods can be utilised for these stress fields is somehow limited. In the case of shot-peening, the relatively shallow depth of reach of these stress fields (in the order of 1mm) and the steep gradients of the stress distribution (see figure 3.1) mean that accurate measurements are only possible using X-ray diffraction. Hole drilling strain-gauge techniques have been used on shot peened specimens but as discussed in Chapter 1, since the residual stresses at the surface are very close to yield [3.6, 3.7], the accuracy of this technique is questionable [3.7]. For this same reason in the case of laser-peened specimens, X-ray (for surface layers) and neutron diffraction methods are the only non-destructive residual stress measurement techniques that can be reliably used. No study has yet been conducted to show an agreeable comparison between the diffraction and hole drilling strain gauge measurements of these stresses in laser-peened specimens, and therefore any incremental hole drilling measurement should be accompanied by benchmark values obtained from other techniques such as neutron diffraction or layer removal methods.

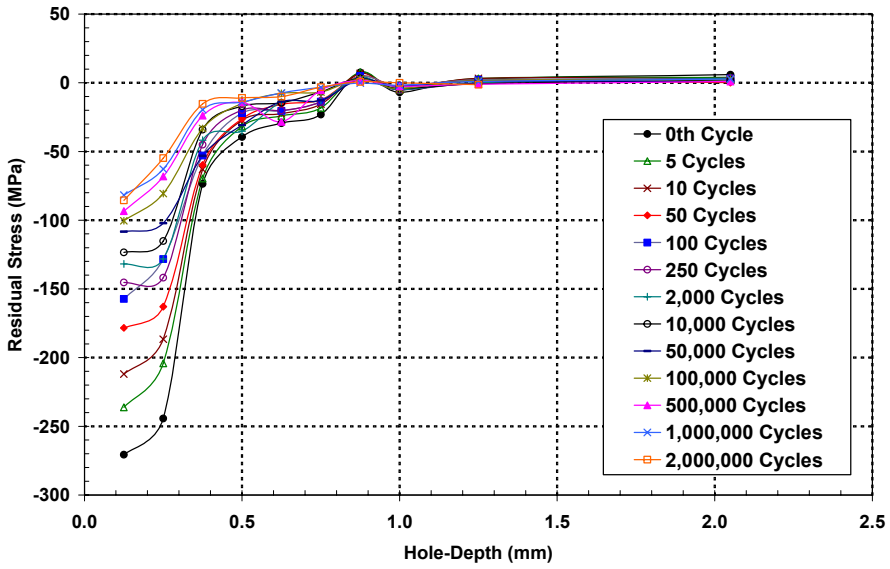

Figure 3.1- Typical stress profiles in a shot-peened steel specimen under a cyclic load measured using incremental hole drilling [3.5]

2) The study of the combined effect of a residual stress field and the externally applied load on fatigue crack growth requires knowledge of stress intensity factors for the particular geometry-stress combination in question. This stress field can be a non-

uniform distribution of stresses due to loading and residual stresses. Knowing the applied and residual stress fields in a particular specimen, one still requires knowledge of SIFs for different crack lengths to accurately predict the fatigue crack growth, which is done by using the Paris Law [3.8]. In simple situations where the stress intensity factors for the applied stress, and those due to the residual stress field are known separately, such as the tensile specimen with a 'fictitious' uniform compressive residual stress distribution shown in figure 3.2, the effective SIF is simply found by adding the two separate SIFs, for example from Brown-Srawley [3.9]. However, due to the necessary internal balance of forces, residual stress fields of this simple form are not practically found, and the residual stress profile often shows a compressive-to-tensile distribution such as the one shown in figure 1.8, which complicates the SIF evaluation. In situations like this, weight functions are a reliable solution to this problem.

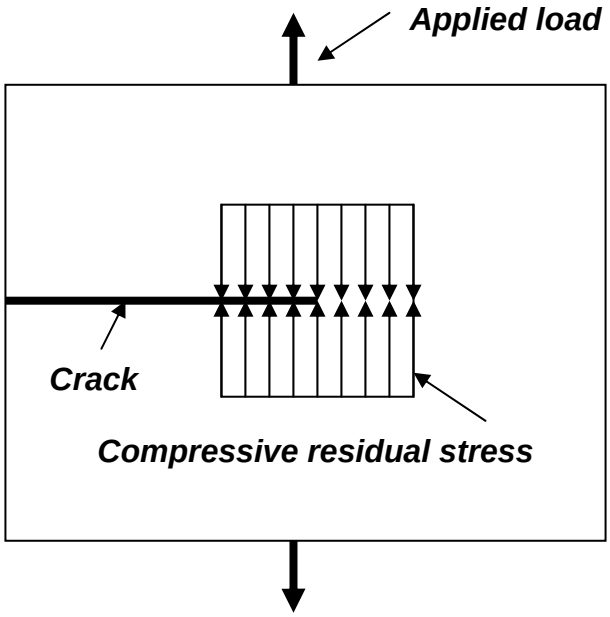

Figure 3.2- A simple residual stress field in a tensile specimen

Due to the combination of the two main reasons mentioned, a full and conclusive study of the peening effects on fatigue crack growth has not yet been carried out.

It should be emphasised that the above arguments are based on the assumption that it is solely through the introduction of residual stresses that surface peening techniques retard the growth of cracks. Though not explicitly stated, it seems to be the current

belief that the effective interaction of the peened specimen with fatigue crack growth is the effect of the residual stresses on the SIFs [3.10]. However, as mentioned in Chapter 1, Farrahi et al. [3.11] concluded that the three main factors affecting mechanical properties of the shot peened part are the compressive residual stresses induced in the superficial layers, the quality of the surface finish of the part, and the increase in yield stress of the shot peened material due to strain hardening of the surface. The interaction between fatigue crack growth and the two latter factors has not been vigorously studied [3.11, 3.2].

In this chapter and in the subsequent ones, the aim is to better understand the effect of laser peening on fatigue crack growth. More specifically, a set of tests are planned to:

1) Study the effect of surface treatment (laser-shock peening) on fatigue crack growth. If weight functions for the test specimen geometry are known, then by knowing the residual stress field, say by application of neutron diffraction measurement techniques, the growth of the fatigue crack under cyclic loading can be predicted and compared against the observed experimental data. Any discrepancy between the two is to be attributed to mechanisms other than residual stresses. These mechanisms can include surface plasticity or a change in material properties which manifests itself in the form of a change in Paris law exponent [3.8]. This is studied in detail in Chapter 5.

2) Study the residual stress distribution in laser peened specimens. This is a necessary requirement for step 1, and is described in detail in Chapter 4. Neutron diffraction technique was used to analyse the stress field in laser shock peened steel specimens.

3) Develop an understanding of the interaction between the crack and the residual stress field. Some authors have observed a relaxation in the level of residual stresses under cyclic loadings [3.11-3.14]. This can also be measured by neutron diffraction measurement and will be discussed in detail in Chapter 4.

Figure 3.3 shows a block diagram of the different possible interactions between these phenomena. In this figure, LSP stands for Laser Shock Peening, RS for Residual Stress and FCG for Fatigue Crack Growth,

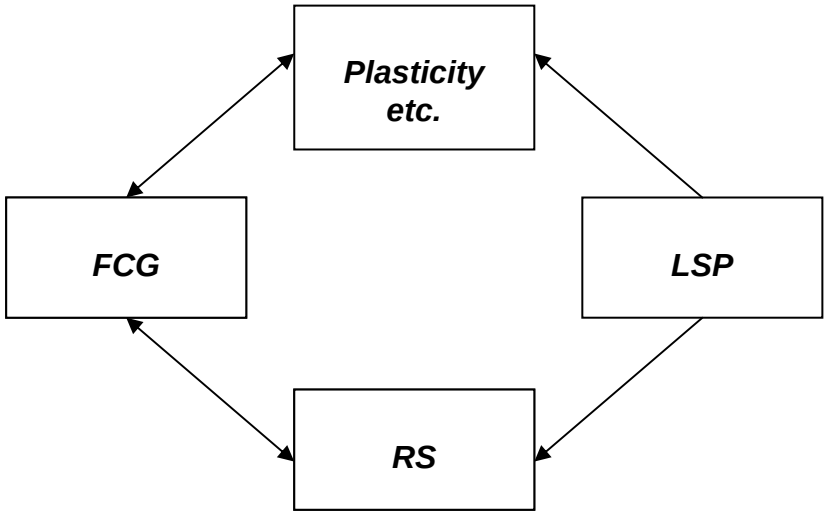

Figure 3.3- Block diagram of the possible interactions between laser shock peening and fatigue crack growth

The proposed analysis methods for each of these interactions are as follows:

1) LSP→RS: using neutron diffraction; this is dealt with in detail in Chapter 4.
2) RS→FCG: numerically, using weight functions; this is analysed Chapter 5.
3) FCG→RS: using neutron diffraction, as discussed in Chapter 4.
4) Plasticity→FCG: comparison between experimental and numerical results, which is studied in Chapter 5.

The next part of this chapter describes the planning of a test programme that covers these studies.

3.2) Planning the Tests

For the purpose of this study, fatigue specimens are tested under cyclic loading. Due to their simplicity, single edge notch tensile specimens (SENT) were deemed suitable. Partial laser peening treatments on specimens as shown in figure 3.4 were planned. By growing fatigue cracks into the peened region, the rate of crack growth can be measured in these regions and analysed to compare the crack growth properties of this region against the results of the CT test. It is believed that compressive stresses induced by laser shock peening should retard, or perhaps even stop the growth of the crack.

Various factors were taken into consideration for design of the dimensions and load levels. The thickness of these specimens was determined, by considering the depth of penetration of laser peening in steels, as 10mm. In order to better understand the effect of laser peening on fatigue crack growth, two different cyclic load levels were chosen, based on the capacity of the available test machines, as 50kN and 90kN. And by a simple stress and stress intensity factor analysis, the width for both specimens was chosen as 100mm. The size and shape of the notch, and other parameters of the test were chosen based on ASTM Standard E 647-05 [3.15] and partly on BS ISO 12108:2002 [3.16].

The specimens were made of BS EN 10025 Grade S275JR steel [3.17]. This material was used in a previous study [3.18] in which the specimens' surfaces were partly shot peened and the distribution of residual stresses due to shot peening was investigated. CT tests had been done on this material and therefore standard crack growth properties (i.e. C and m in Paris Law) for this material are known [3.18]. Figure 3.4 shows the overall dimensions of the new specimens.

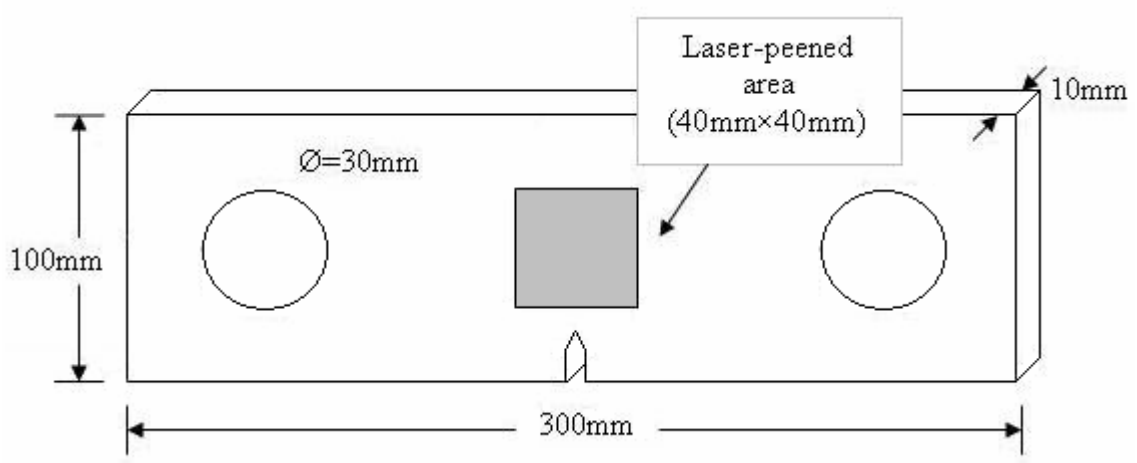

Figure 3.4- Dimensions of the fatigue specimens

3.3) Test Procedure

For the purpose of this study, a total of four steel specimens with identical overall dimensions were prepared. These specimens were made from BS EN 10025 Grade S275JR steel [3.17] and were ground and polished.

3.3.1) Pre-cracking of Specimens

For the study of fatigue crack growth behaviour, two of the specimens included identical single-edge starter notches, with the dimensions of the notches shown in figure 3.5. Before laser peening the specimens, pre-cracks were grown in the notched specimens. From standard CT tests on the material [3.5], the material coefficients for Paris Law were calculated as $C = 1.26 \times 10^{-10}$ and $m = 4.162$, where crack growth rate is measured in *mm*/cycle. Based on recommendation of BS ISO 12108:2002 [3.16], the threshold is defined as the stress intensity factor range corresponding to a growth rate of 10^{-8} mm/cycle, which, when substituted in the Paris Law [3.8]:

$$\left(\frac{da}{dN}\right)_{th} = C\left(\Delta K_{th}\right)^{m} \tag{3.1}$$

gives $\Delta K_{th} = 2.86 MPa\sqrt{m}$ as the predicted threshold stress intensity factor. To ensure crack growth, any precracking load has to result in higher values of SIF. However, for crack initiation from the notch tip, higher values of SIF are applied to the specimen, though according to standards [3.15], a good notch made to the recommended length and tip radius can be treated as a crack of the same length. Both of the notched specimens were precracked under a tensile load range of 5-50 kN ($\Delta\sigma = 45 MPa$), and after around 2.5 million load cycles, the desired pre-crack lengths were achieved in both specimens.

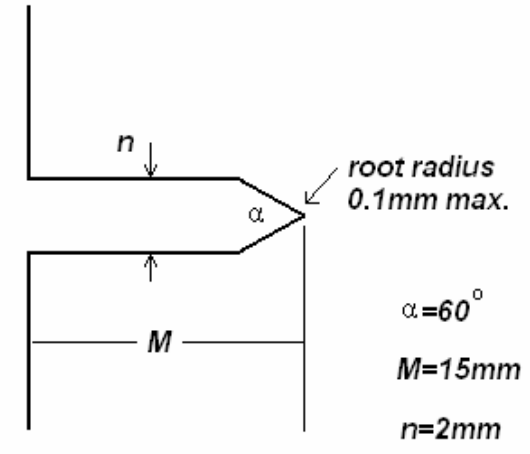

Figure 3.5 showing notch dimensions

3.3.2) Laser Shock Peening of Specimens

All of the specimens were sent to Metal Improvement Company [3.19] to be partially laser-peened. The laser beam spot sizes used were 3×3 mm, the energy focused on each spot 16.2 J and the pulse width was 18ns. For a description of these parameters see Chapter 1. Figure 3.6 shows the dimensions of the specimens and the laser peened regions. The top figure shows the geometry of specimens A and B and the bottom figure shows the geometry of specimens 1 and 2.

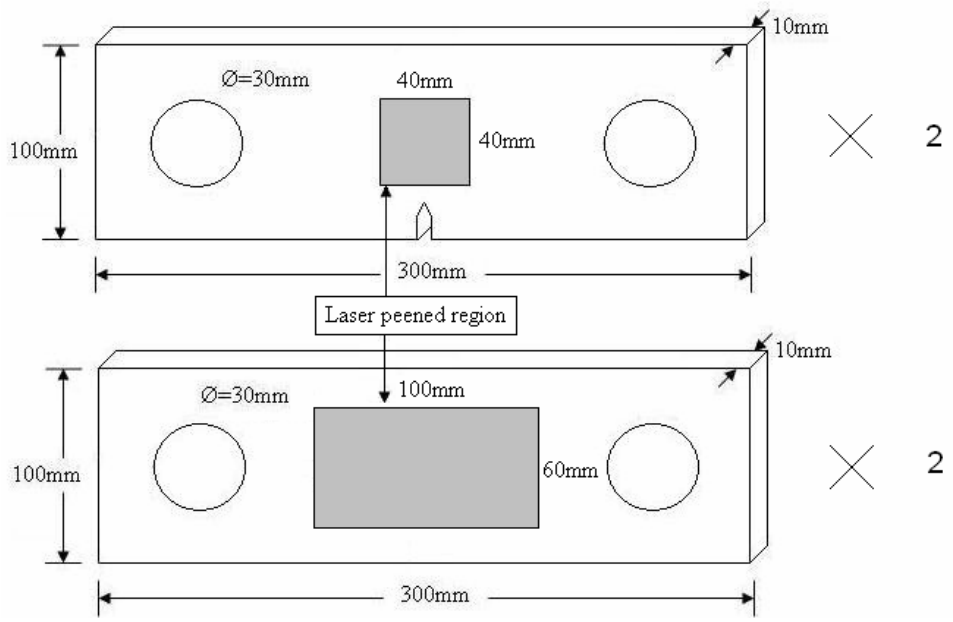

Figure 3.6- Laser-peened specimen dimensions

3.3.3) Fatigue Crack Growth Tests

Use of edge-crack specimens requires freedom of rotation at the supports to accommodate for any asymmetry in compliance and prevent any asymmetry in stresses due to bending. To this end, universal joints (see figure 3.7) were specially designed and made for this set of tests to allow rotation in two directions. This double pin and clevis configuration is thought to eliminate any undesirable effects due to misalignment of the test machine.

Test started with specimen A, which was pre-cracked under a tensile cyclic load between 5kN to 50kN with a frequency of 3Hz. Crack growth was monitored by a travelling microscope which was attached to a digital caliper. This test set-up is shown in figure 3.7.

Figure 3.7- The test setup

The measured crack lengths vs. number of cycles for specimen A were as shown in figure 3.8. Here, the crack length measurements were taken every 2000 load cycles up to 160000 cycles and every 1000 cycles thereafter. The tests were stopped for each measurement and during these measurements the static loads were kept at the mean value of the cyclic loading. To avoid any abrupt load effect on the crack tip, the applied load during the first 5 cycles of restarting the tests was in the form of a sinusoidal load with an increasing amplitude in the form of a linear ramp. Test on specimen A was stopped after 190000 load cycles; this was because the crack had reached the desired length.

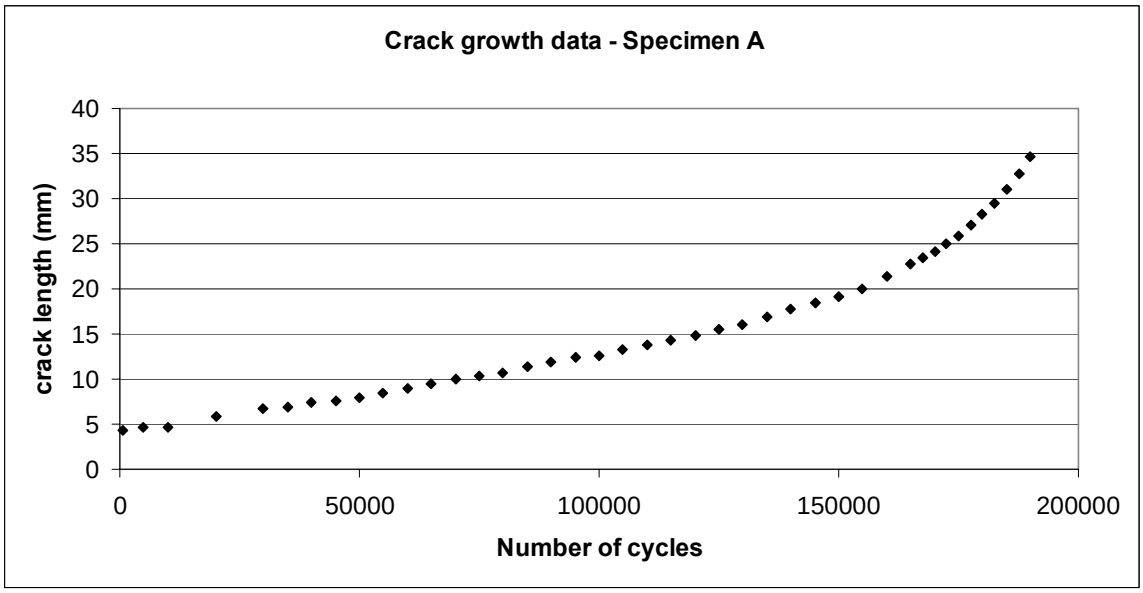

Figure 3.8- Fatigue crack growth data (a-N curve) for specimen A

The next specimen to be tested was specimen B. This time the load range was between 5kN and 90kN. As with specimen A, crack lengths were measured using the travelling microscope-digital caliper set-up. The plot of crack length vs. number of load cycles for specimen B is shown in figure 3.9.

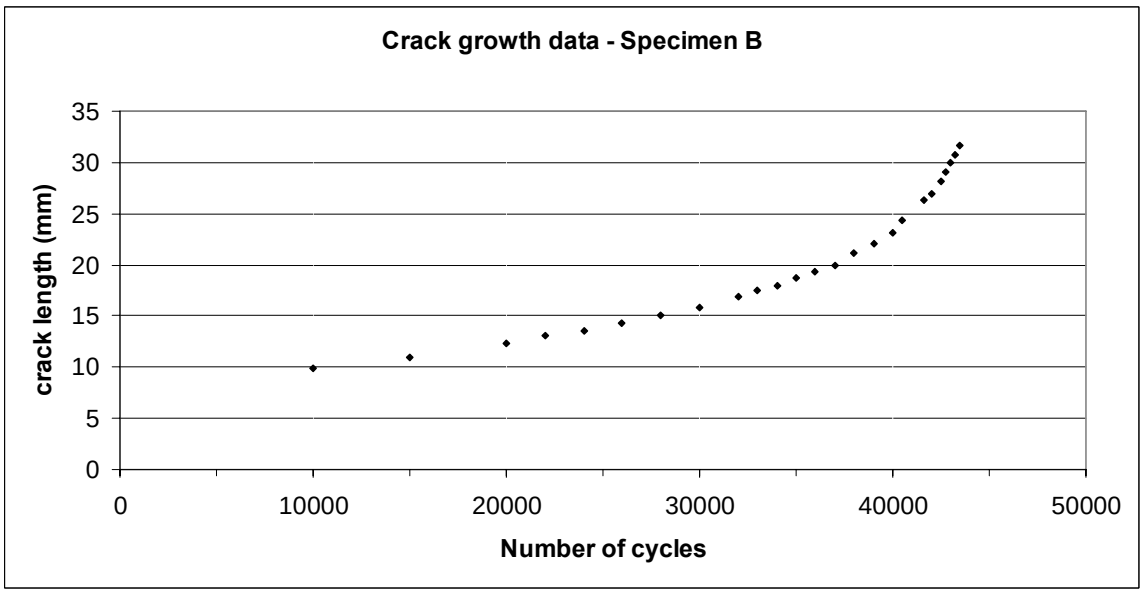

Figure 3.9- Fatigue crack growth data (a-N curve) for specimen B

The test was stopped after 43000 cycles of load since the growth rate was deemed too fast and the crack length was as desired.

3.4) Summary

This chapter detailed the plan and the procedure for the fatigue crack growth experiments in laser peened specimens. As mentioned in Chapter 2, laser peening was chosen primarily due to its deep penetration. As examples of non-uniform stress fields two specimens, both partly laser peened, were loaded under different cyclic load levels and the crack growth data were obtained. These data, along with the residual stress measurement results of Chapter 4, will be used in Chapter 5 to analyse the effect of laser shock peening on crack growth behaviour through a study where the experimental results will be compared against the predicted numerical crack growth behaviour.

References

[3.1] S J Maddox (1991), Fatigue Strength of Welded Structure – Second Edition, Abington Publishing, ISBN 1855730138.

[3.2] G R Leverant, B S Langer, A Yuen and S W Hopkins, Surface Residual Stresses, Surface Topography and Fatigue Behavior of Ti-6Al-4V, *Metallurgical Transactions*, American Society for Metals and the Metallurgical Society of AIME, Vol. 10A, pp. 251-257 (1979).

[3.3] Laser Shock Processing Increases the Fatigue Life of Metal Parts, *Materials and Processing*, Elsevier Science Publishing Co (Sept 1991).

[3.4] H Berns and L Weber, Influence of Residual Stresses on Crack Growth, in Impact Surface Treatment, Edited by S A Meguid, Elsevier, pp. 33-44 (1984).

[3.5] Shi Song Ngiam, The Influence of Surface Residual Stress on Fatigue Crack Growth, PhD Thesis, Department of Mechanical Engineering, University College London (Mar 2007).

[3.6] K J Marsh (Editor), Shot Peening: Techniques and Application, Engineering Materials Advisory Services Ltd, ISBN 0 947817 64 6 (1993).

[3.7] Standard Test Method for Determining Residual Stresses by Hole-Drilling Strian-Gage Method, ASTM International Standard E 837 - 01, American Society for Testing and Materials (2001).

[3.8] P C Paris and F Erdogan, A critical analysis of crack propagation laws, *Journal of Basic Engineering*, Vol. 85, pp. 528-534 (1963).

[3.9] B Gross, J E Srawley and W E Brown Jr, Stress-intensity factors for a single-edge-notch tension specimen by boundary collocation of a stress function, NASA Technical Note, NASA TN D-2395, Lewis Research Center, Cleveland, Ohio (Aug 1964).

[3.10] O Hatamleh, J Lyons and R Forman, Laser and shot peening effect on fatigue crack growth in friction stir welded 7075-T7351 aluminium alloy joints, *International Journal of Fatigue*, Vol. 29 Issue 3, pp 421-434 (Mar 2007).

[3.11] G H Farrahi, J L Lebrun and D Courtain, Effect of Shot Peening on Residual Stress and Fatigue Life of a Spring Steel, *Fatigue and Fracture of Engineering Materials and Structures*, Vol. 18, No. 2, pp. 211-220 (1995).

[3.12] O N Romaniv, Relaxation of residual stresses by alternating loads, *Fiziko-Khimichekaya Mekhanika Materialov*, Vol.1, No. 6, pp. 726-729 (1965).

[3.13] W Z Zhuang and G R Halford, Investigation of residual stress relaxation under cyclic load, *International Journal of Fatigue*, Vol. 23, pp.S31-S37 (2001).

[3.14] U P Sinha and D W Levinson, Bending stress relaxation of AISI 1095 steel strip, *Proceedings of ASM's Conference on Residual Stress- In Design, Process and Materials Selection*, Cincinnati, Ohio, 27-29April 1987.

[3.15] Standard Test Method for Measurement of Fatigue Crack Growth Rates, ASTM International Standard E 647 - 05, American Society for Testing and Materials (2005).

[3.16] British Standard BS ISO 12108:2002, Metallic materials- Fatigue testing- Fatigue crack growth method, BSI (November 2003).

[3.17] British Standards Institute, "BS EN 10025:2004 – Hot Rolled Products of Non Alloy Structural Steels", British Standards Institute, 2004.

[3.18] Muhamad Saifuldin ABDUL MANAN, Fracture Mechanics Analysis of Multiple Edge Cracks, PhD Thesis, Department of Mechanical Engineering, University College London (Feb 2008).

[3.19] http://www.metalimprovment.com, accessed June 2008.

CHAPTER 4

4.0) Experimental Determination of Residual Stress using Neutron Diffraction Technique

4.1) Introduction

Chapter 3 discussed the experimental procedure for fatigue crack growth in laser peened specimens. It was pointed out that in order to study the interaction between fatigue crack growth and the residual stresses, accurate measurement of residual stresses is essential since evaluation of stress intensity factors requires reliable residual stress values. It was also discussed that another possible interaction is the relaxation, or decay, of residual stress magnitudes due to cyclic loading; this phenomenon is explained in the present chapter.

Different techniques of residual stress measurement were discussed in Chapter 1 and it was concluded that diffraction techniques offer reliable albeit costly results. The use of neutron diffraction for residual stress measurement was described in Chapter 1. In this chapter, results of the neutron diffraction measurement of residual stresses in the laser peened specimens are shown and analysed. These measurements were taken at the ISIS Engin-X facility at Rutherford Appleton Laboratories in Harwell [4.1].

It has been shown [4.2] that residual stresses may show a tendency to decreasing in magnitude under cyclic loadings. Hence a brief background to this phenomenon is presented in the present chapter. The measurements showed no relaxation of residual stress levels during the tests.

The raw data obtained from neutron diffraction measurements are analysed and results are presented in terms of the appropriate stress components, which give an insight into not only the effect of laser peening on the specimen but also the interaction between the

crack and this non-uniform residual stress field. These results are also used in the next chapter (Chapter 5) where the crack growth behaviour is studied.

4.2) Residual Stress Relaxation under Cyclic Loading

Many authors have observed a decay in the magnitude of residual stresses in specimens that were under cyclic loads [4.2-4.5]. This relaxation behaviour has been observed both for tensile [4.6] and in compressive residual stresses [4.5]. The exact mechanism for this phenomenon is not known, and most of the proposed models are empirical in the sense that they have been obtained by fitting curves to the experimental results. Some investigators [4.7] have associated the residual stress relaxation with the Bauschinger effect [4.8] during direct cyclic loading, though these models are not reliable predictive tools. The Bauschinger effect is the lowering of the yield stress when deformation in one direction is followed by deformation in the opposite direction [4.9]. It is believed that this phenomenon is due to the fact that dislocations pile up on slip planes at barriers in the crystal; the pile-ups results in a *back stress* [4.10] which opposes the applied stress on the slip plane [4.9].

Since compressive residual stresses are usually beneficial in term of fatigue, it is important to be aware of their possible decay over time. A design incorporating beneficial residual stresses against fatigue may, after a certain number of loading cycles, no longer be safe.

A detailed study by Zhuang et al [4.11] has found that the relaxation due to cyclic loading is mainly influenced by: (1) initial magnitude of the residual stress field, (2) fatigue stress amplitude and number of cycles, and (3) material cyclic stress-strain behaviour and degree of cyclic work hardening or softening; the intensity of relaxation increases with increase in the amplitude of the alternating stresses. However, since the neutron diffraction measurements carried out in the current research (see the next section) show no significant relaxation of residual stresses in the fatigue specimen, the proposed residual stress models are not mentioned here.

4.3 Neutron Diffraction Measurements

4.3.1 Experimental Set up

The theoretical background to the neutron diffraction method for residual stress measurement was explained in Chapter 1. The set up is shown in figure 4.1. The specimen is placed in the path of the neutron beam at an incident angle of 45°. The positioning system (positioner) allows for rotation about one axis (normal to the floor in this set-up) and translational movements of the specimen platform in three directions. To set the specimen in the required position, a point on the surface of the specimen is positioned at the required coordinate using a looking-through optical positioning system and the position of the mid-plane of the specimen is found by measurement of diffraction of neutrons along the thickness of the specimen. This relieves the user of the cumbersome task of manually locating the mid-plane of the specimen. The two slightly curved metallic surfaces to either sides of the specimen in figure 4.1 are neutron detectors, or 'detector banks'. Since the set up has two banks (called the north and south banks), it is capable of simultaneous measurement of two perpendicular strain components for each beam position. For example, the set up shown in figure 4.1 is set to measure the longitudinal (i.e. along the length of the specimen) and normal (through-thickness) components of elastic strain.

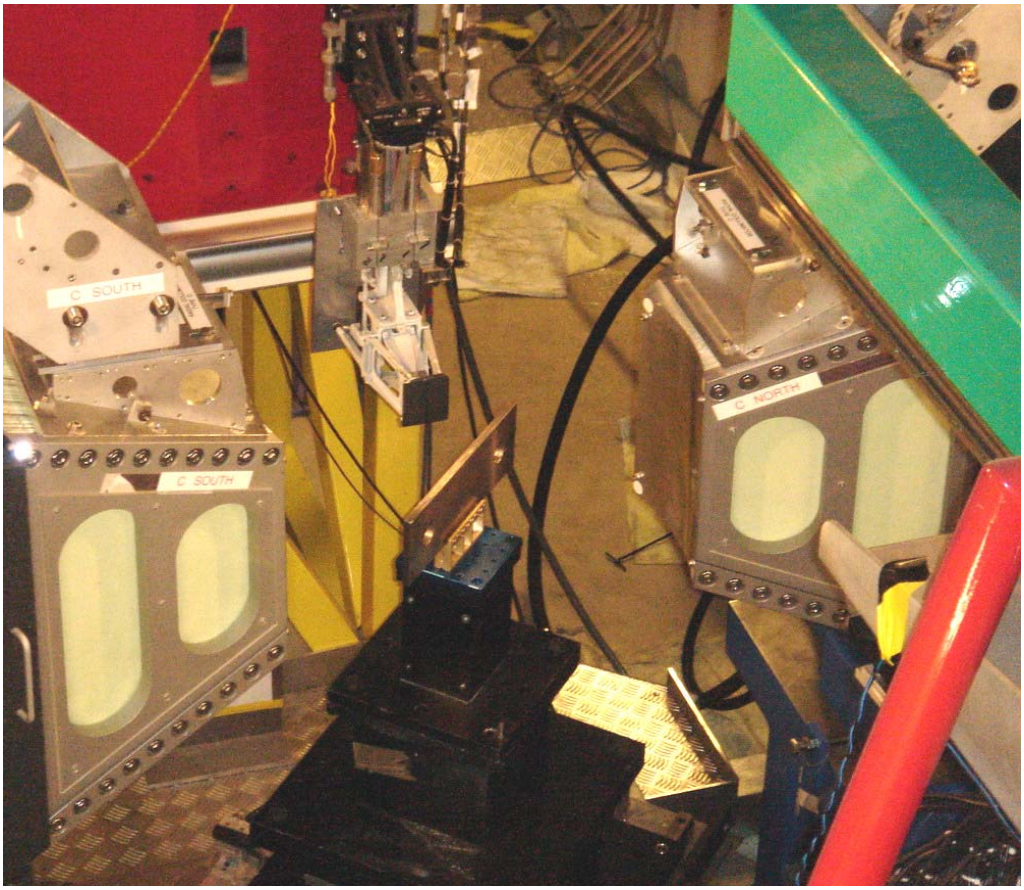

Figure 4.1- Test specimen set up in ISIS Engin-X neutron diffraction facility

It should be noted here that since it is eventually the stress components that are to be inferred, the measured strain components have to be converted to stresses. This is discussed in the following section.

4.3.2) Deriving Stress Values from Strain Components

In a homogeneous, isotropic, elastic material, the relations between normal strain and normal stress components are expressed by the generalised Hooke's law [4.12] as:

$$\varepsilon_x = \frac{1}{E}(\sigma_x) - \frac{\upsilon}{E}(\sigma_y + \sigma_z)$$

$$\varepsilon_y = \frac{1}{E}(\sigma_y) - \frac{\upsilon}{E}(\sigma_z + \sigma_x) \qquad (1)$$

$$\varepsilon_z = \frac{1}{E}(\sigma_z) - \frac{\upsilon}{E}(\sigma_x + \sigma_y)$$

From which, solving for stress components gives:

$$\sigma_x = \frac{\upsilon E}{(1+\upsilon)(1-2\upsilon)}\left(\varepsilon_x + \varepsilon_y + \varepsilon_z\right) + \frac{E}{(1+\upsilon)}\varepsilon_x$$
$$\sigma_y = \frac{\upsilon E}{(1+\upsilon)(1-2\upsilon)}\left(\varepsilon_x + \varepsilon_y + \varepsilon_z\right) + \frac{E}{(1+\upsilon)}\varepsilon_y \qquad (2)$$
$$\sigma_z = \frac{\upsilon E}{(1+\upsilon)(1-2\upsilon)}\left(\varepsilon_x + \varepsilon_y + \varepsilon_z\right) + \frac{E}{(1+\upsilon)}\varepsilon_z$$

In a laser shock peened specimen, far from the effects of the boundaries (e.g. peen boundary or cracks), the residual strain components in the two in-plane directions are assumed to be equal. This is due to the nature of the peening process where no preference is given to either of these directions during peening. This assumption will effectively reduce the neutron diffraction measurement time for the points that are far from the boundaries as only two components of strain are sufficient to determine the longitudinal stress component.

For such points $\varepsilon_x = \varepsilon_y$ and equation 2 gives the axial component of stress in terms of the normal and axial strain components as:

$$\sigma_y = \frac{2\upsilon E}{(1+\upsilon)(1-2\upsilon)}\left(2\varepsilon_y + \varepsilon_z\right) + \frac{E}{(1+\upsilon)}\varepsilon_y \qquad (3)$$

For positions close to the crack face or the peen boundary, all three components of strain should be used to calculate stresses because being in the vicinity of the boundaries may mean that the in-plane strain field is not longer isotropic, i.e. the in-plane components of strain (ε_x and ε_y) are not necessarily equal.

4.3.3) Measurement Points

In total, three specimens were tested using the neutron diffraction technique. Two of these specimens, named specimen 1 and specimen 2, were un-notched and had large identical leaser peened sections (see figure 4.2a), and the third specimen was previously fatigue tested and contained a crack which had grown in the laser peened area (see figure 4.2b). This fatigue specimen had undergone 190000 cycles of tensile loading between 5kN to 55kN (specimen A as discussed in Chapter 3).

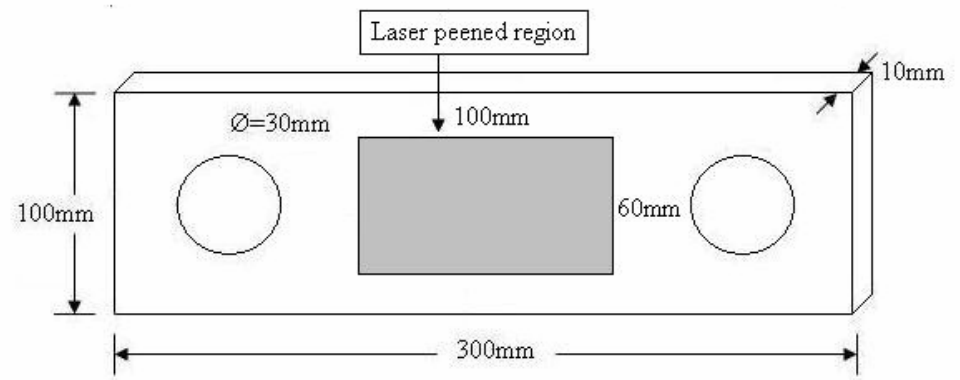

Figure 4.2a- Specimens 1 and 2

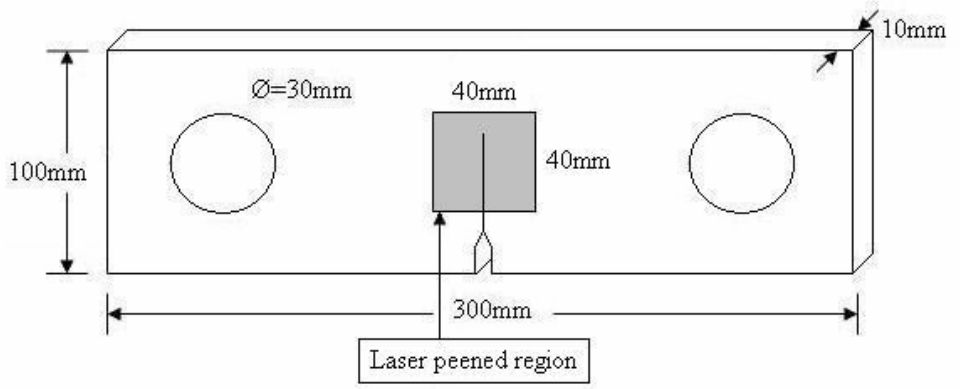

Figure 4.2b- Specimen A

Specimen 1 was never put under any loading, and specimen 2 had undergone ten tensile cycles of 5kN – 55kN (corresponding to 5MPa – 55MPa).

In order to obtain a through-thickness profile of residual stress in the laser peened region, a series of measurement points were chosen for specimens 1 and 2. Since the measurements were taken far from any surface boundaries, as discussed in section 4.3.2 only two strain components need to be measured, namely the normal and the longitudinal strain components. In test 1, for both specimens 1 and 2, eight different

points symmetrical with respect to the mid-plane and lying on a line normal to the plane of the specimens were chosen for this purpose and strain measurements were taken. Because the effect of laser peening on the specimen is supposed to be symmetrical with respect to the mid-plane of the specimen, it may appear that only the points on one half of the specimen thickness could be measured and then strain values for the other side be taken as the symmetrical image of these. However, this assumption is not based on any hard facts and the stress state may not be symmetrical. One reason for this is that although the intensity of the laser beam used for each spot is equal, the procedure is done on each side separately, and not simultaneously. The stress results actually show a slight skewed distribution which is discussed in section 4.3.6.

To highlight any error due to the surface effect, i.e. proximity of the gauge-volume to the surface of the specimen, after a first set of measurements, both specimens were taken out of the set up and put back in with the reverse side facing the oncoming neutron beam. This exercise should both underline any errors due to the surface effect and also emphasise the repeatability of the measurement procedure. Results of these measurements are discussed in the 4.3.5. Table 4.1 shows the coordinates of these points, the origin is at the centre of the specimen lying on the mid-plane. Because two of these points are very close to the surface (points 1 and 8), small gauge volumes were used for this test which increased the duration of the measurements. Measurement of strains at each point took around 15-20 minutes.

Point number	coordinates (mm)
1	(0,0,4.95)
2	(0,0,4)
3	(0,0,3)
4	(0,0,1)
5	(0,0,-1)
6	(0,0,-3)
7	(0,0,-4)
8	(0,0,-4.95)

Table 4.1 showing coordinated of the eight points for test 1 (specimens 1 and 2)

To better understand the effect of laser peening on the specimen in terms of the resulting residual stress field, the stress profiles on either sides of the boundary of the peened region need to be measured. These measurements should help in understanding the behaviour of the residual stress field as it transitions from the peened region to the unpeened material. This was done in 'test 2', the coordinates of these points are shown in table 4.2; the 'peened' points were 2mm from the boundary and in the peened region, and 'unpeened' points were 2mm from the boundary outside the peened region. Again the z coordinate denotes the distance from the mid-plane. These measurements were taken on specimen 1.

Point number	z-coordinate (mm)
1	4
2	3
3	2
4	1
5	0
6	-1
7	-2
8	-3
9	-4

Table 4.2 showing coordinates for the points in test 2

In the next set of measurements, specimen A was tested. As mentioned before, specimen A had undergone 190000 cycles of tensile loading. It was considered possible that the magnitude of residual stresses may have decreased due to the relaxation action of the repeated loading (see section 4.2). A methodology was devised where it is possible to establish the dependence of residual stress magnitude on the number of load cycles for a given specimen with a crack. This is based on the idea of 'crack stress shielding' effect and does not require measurement during loading, a cracked specimen can be analysed to reveal the history of residual stress relaxation, and therefore this technique eliminates the need to interrupt the loading for taking measurements.

However, the stress profile for a point on the fatigue specimen, remote from the crack but within the peened region, shows no significant change in the level of residual stresses compared with the un-cycled specimen. As no decrease in the residual stress level due to repeated loading was observed, this study is not discussed here.

4.3.4) Raw Data and Interpretation of Strain Results

SScanSS [4.13] is a software package designed to simulate the neutron diffraction test procedure for ISIS Engin-X facility. Here a digital model of the specimen can be built either by the geometry creation facility or from a direct laser surface scan of the actual specimen and then be imported to the program. Prior to the test, this software can be used for the following [4.13]:

i) A model of the sample to be measured is generated, either by LASER scanning, exporting from a CAD package, or from within SScanSS.
ii) The user positions the required measurement points within the sample model.
iii) The virtual instrument is selected and modified to reflect the user's choices of (optional) hardware items such as collimators, jaw settings etc.
iv) The sample model is positioned within the virtual instrument and the scan is simulated. This simulation is performed in order to: a) determine how the sample should be oriented in order to measure the required components, b) determine feasibility, (are all measurement points accessible), and c) estimate count times (can the measurement be performed in the available time).

After choosing the measurement points and the gauge volumes, this software can be used to optimise the actual test in terms of duration by a sensible choice of measurement sequence, i.e. in which order the points should be measured. This is achieved simply by trying different point orders and comparing the overall durations for each scenario, which depend, along with the gauge volume used, on the length of the path of the neutron beam inside the material, and the number of required positional adjustments of

the specimen; a shorter beam path means less scatter by the material, and fewer positional adjustments will simply reduce the amount of manual labour required. A model of each specimen was created and the sequence of measurements which gave the minimum time was obtained after running several analyses using SScanSS. The resulting sequence was used in the actual test at the Engin-X facility.

The first set of experiments was carried out to determine the d-spacing of the stress-free material. This was simply achieved by taking measurements on a virgin material specimen, i.e. on the unpeened section and far from the effect of peening. This value is then used to determine strain values. Readings from banks 1 and 2, when analysed (using the Open Genie® software), give the crystal spacing value in the stressed region, which is used to calculate the strain in that particular direction using the simple formula

$$\varepsilon = \frac{d}{d_0}.$$

Depending on which component of stress is to be calculated, these strains are substituted in equations 2 or 3.

There are a few points that should be borne in mind when interpreting the strain data. After taking the measurements in each specimen, the specimen was taken out and put back in with the reverse side facing the beam, and the same points were measured again. This is to ensure that the effect of proximity of the gauge volume to the surface in minimised; this proximity effect is called 'surface effect' [4.14]. For the points near the surface, when the values of strain from the two set of measurements are different, a common practise to rectify this issue is to average the values of the strains measured for that point from the two tests.

When all three components of strain are needed for stress determination, the specimen should be tested twice; each test gives two perpendicular components of the strain. After the first set of measurements, which measure say longitudinal and normal strains, the specimen is rotated 90˚ and the test repeated for the same points, this time resulting

in the transverse and normal strains. To ensure that the same points have been measured, and that the specimen has not rotated from the desired position (i.e. same points with the same orientations are measured), the normal component of strain for each point from the two set of measurements must match. If these components do not match, it means that the specimen has translated or rotated from the desired position and after making the required adjustments to the position of the specimen the test should be repeated.

4.3.5) Stress Calculations

The results of the measurements, when converted to stresses, are discussed here. The component of stress that is of interest when dealing with fatigue crack growth analysis in LEFM is the stress component acting perpendicular to the crack face, which in the case of this test is the longitudinal stress, denoted henceforth by σ_{xx}. The coordinate system used is shown in figure 4.2. Unless explicitly stated, this is the coordinate system that will be used in the present chapter and in Chapter 5.

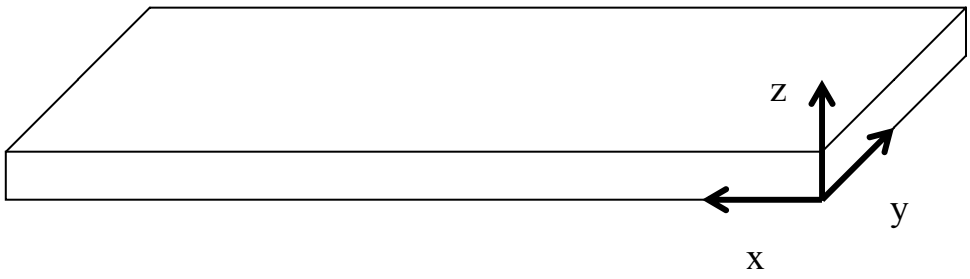

Figure 4.2- The coordinate system

Figures 4.3 and 4.4 show the obtained stress distribution for test 1. These figures show the classic compressive-to-tensile trend for each of the two faces of the specimen.

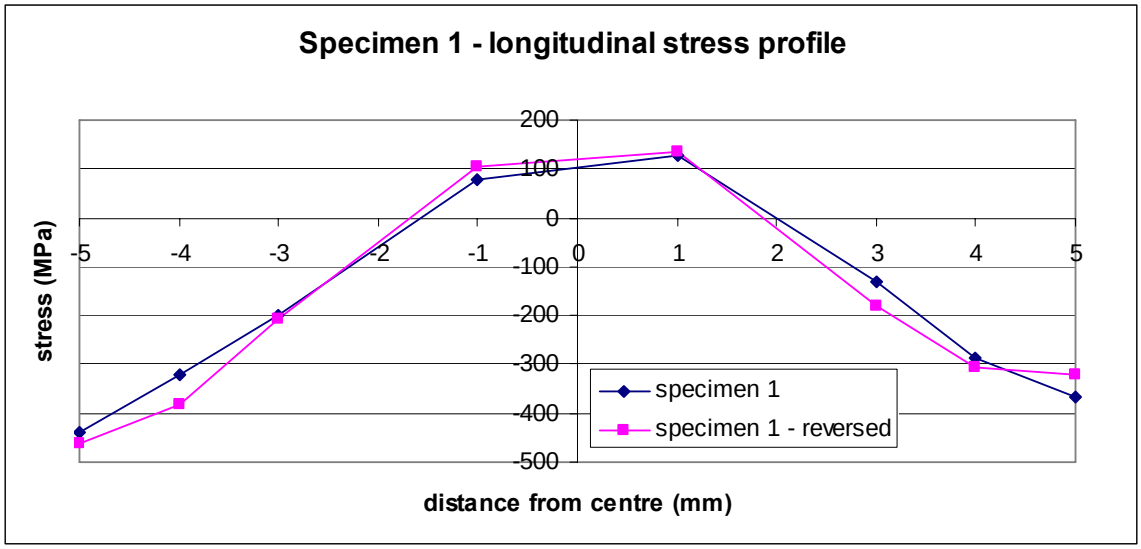

Figure 4.3- Residual stress distribution profile in specimen 1 at the centre of the laser peened region.

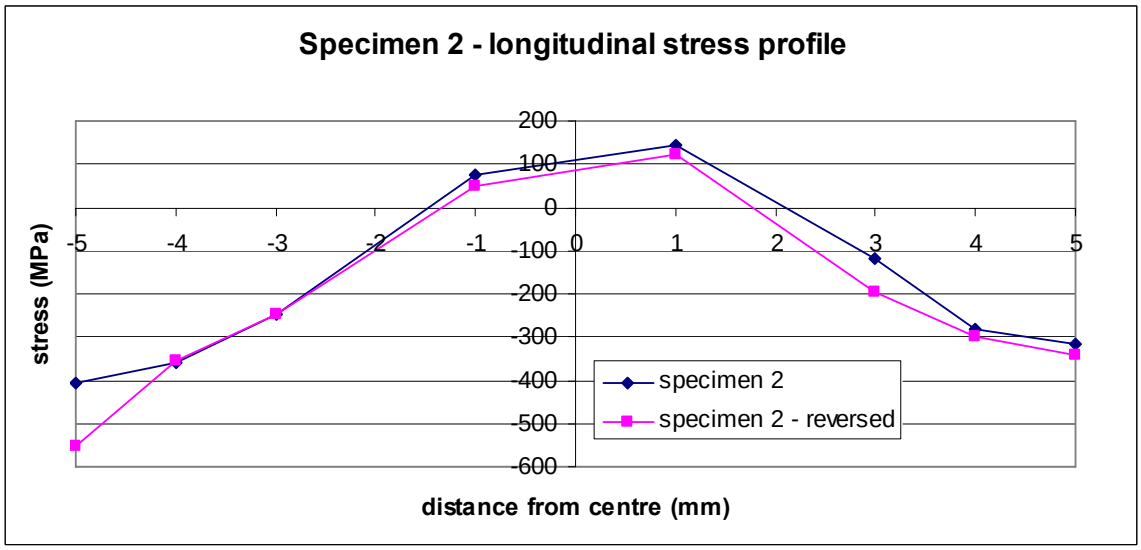

Figure 4.4- Residual stress distribution profile in specimen 2 at the centre of the laser peened region.

A number of salient observations have been made which all help in understanding the residual stress field behaviour and also in affirming self consistency of the results. These are discussed in detail in this section.

1) The first point to notice in these two figures is the congruency between the two sets of readings for each specimen, i.e. initial and reversed measurement. In figure 4.4, the only noticeable exception to this agreement is the surface point in specimen 2 (-5mm

from the mid-plane) and this can be attributed to the surface effect. The surface effect is slightly apparent in figures 4.3 and 4.4 for the surface point which is 5mm from the mid-plane, though since the difference between the two readings in this position is small, it may be attributed to any slight misalignment or mis-positioning of the specimen rather than the surface effect. Anyhow, the results do seem to be repeatable as a good agreement is observed between the two sets for each specimen.

2) One important aspect of these figures is the similarity of the trends and magnitudes of the residual stresses in the two specimens. This is partly due to a high degree of repeatability of the laser shock peening process, and also shows that the relaxation effect of ten cycles of tensile stress on specimen 2 is negligible.

Regarding the stress relaxation due to cyclic loading, one point which concludes the study is the point on the peened region on the fatigue specimen, far from the crack and other boundaries. Figure 4.5 shows the stress distribution profile for this point. This specimen, specimen A (see Chapter 3), had undergone 190000 cycles of tensile stress in the range of 5MPa to 55MPa.

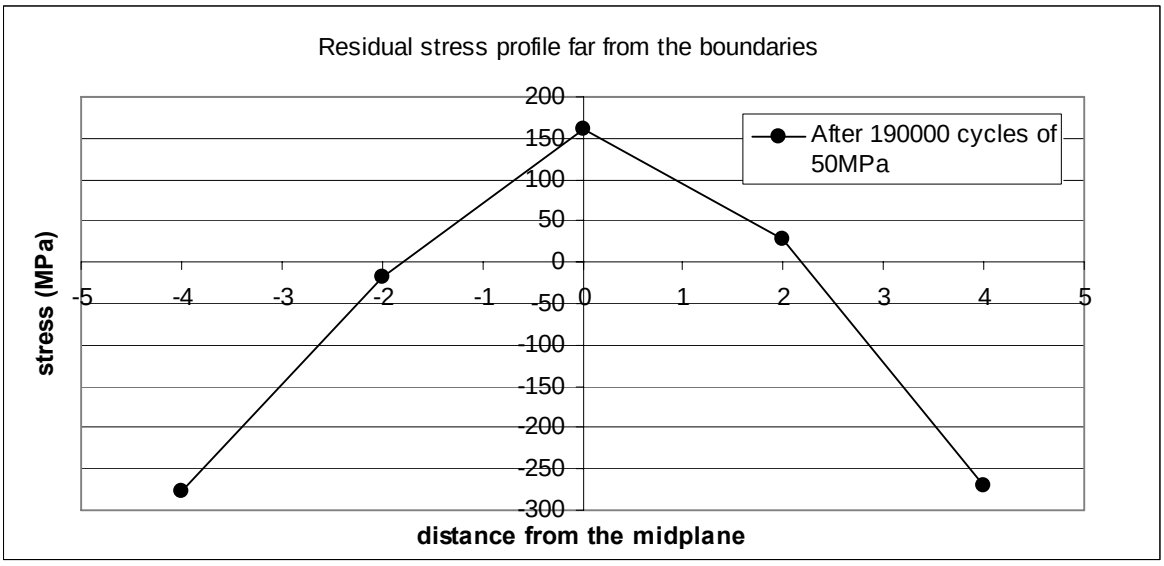

Figure 4.5- Residual stress distribution profile in specimen A, in the peened region far from the effect of boundaries.

Since the results of figures 4.3 and 4.5 are from different specimens, to clarify the comparison between the stress values, these are both plotted in the same graph (figure 4.6). It must be emphasised that the lines shown are just for clarity and the actual data consist only of the points shown.

One notable point is the relatively elevated level of stresses in specimen A compared to specimen 1. This may either be resulted from a slightly different peening intensity, or can indeed be related to the effect of repeated tensile load on the specimen. Nevertheless, the level of residual stresses in both specimens is such that by the existing data one can only conclude that if relaxation has indeed occurred, it is relatively small in magnitude and therefore negligible

.

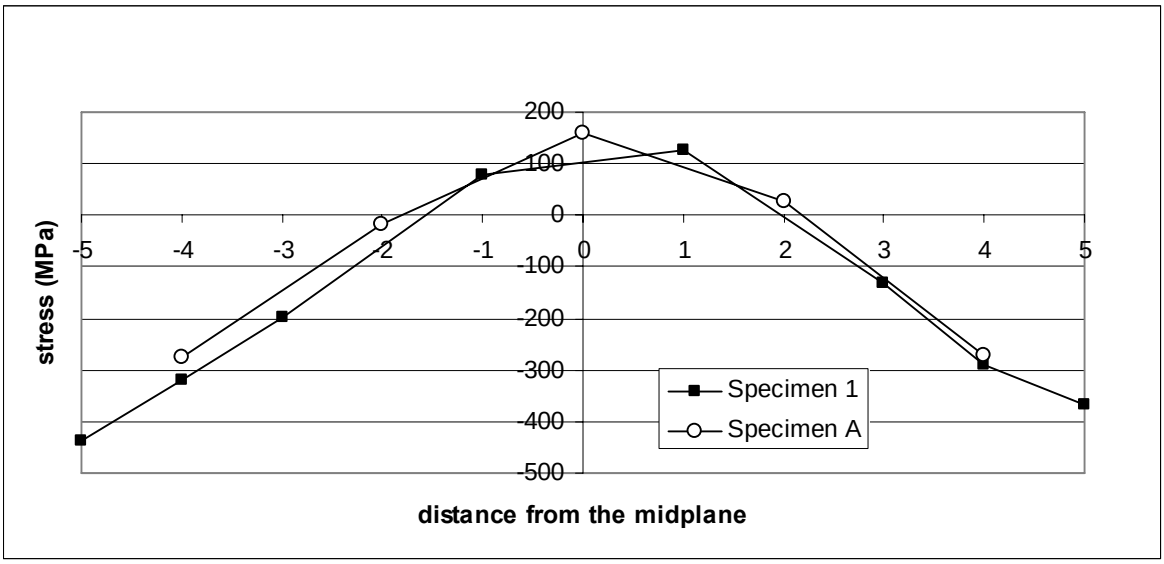

Figure 4.6- Comparison between residual stress profile in specimens 1 and A.

3) It can be seen from the stress profiles of figure 4.3, 4.4 and 4.5 that the net effect of the peening processing can be said to be a negative stress, i.e. the net resultant force on the section of the specimen is a compressive force. To satisfy the equilibrium of the forces at each section, the overall resultants of forces and of bending moments have to be zero, i.e. the total compressive *force* at any cross section balances the total tensile *force*. This means that outside the peened region exists an area with tensile residual stresses whose task is to equilibrate the forces. This phenomenon is rarely encountered in shot peened specimens since due to their relatively small depth of reach; the overall

effect in terms of resultant forces in shot peened specimens is either neutral or a very small compressive force which only requires a small area of equilibrating tensile stresses which do not usually extend beyond the peened region. However, in laser peened specimens, this effect may be significant. Therefore in the next test (test 2), the residual stress profile just outside the boundary of the peened area was determined. The positions of the points that were measured are shown in table 4.2. Figure 4.7 shows the stress distribution profile at a point just outside and another point just inside the peened region on specimen 1. The stress profile outside the peened boundary shows a tensile residual stress which is relatively uniform in magnitude. Apart from this test, there was not enough time at the Engin-X facility for a thorough measurement of the residual stress field outside the laser peened region. To establish how far this tensile residual stress extends requires accurate measurements but a great deal can be learnt by applying simple assumptions and using basic principles.

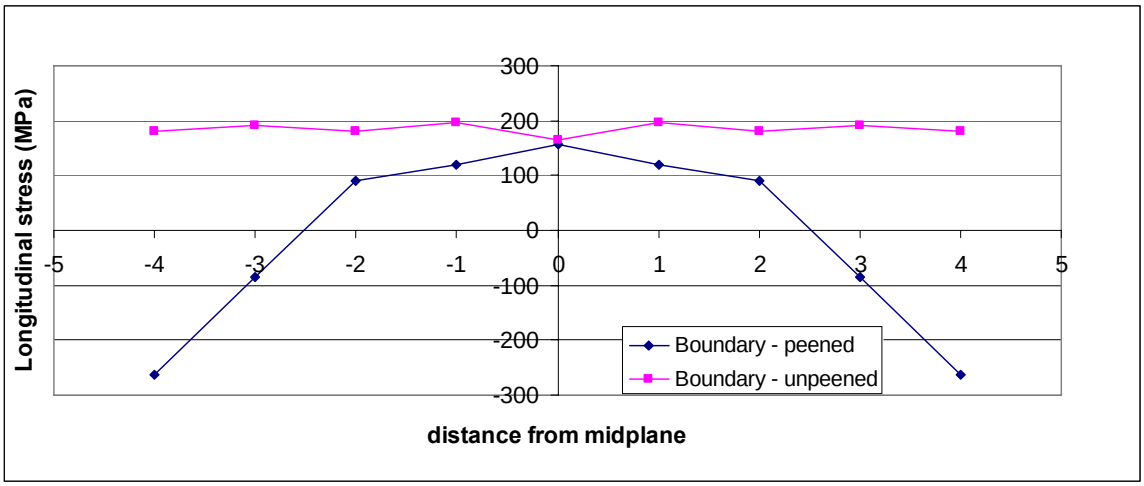

Figure 4.7- Residual stress profile just outside and inside the peened region

To study this phenomenon, by assuming that the specimen is cut at a distance of x_0 from one end, as shown in figure 4.8a, the stresses (or body forces) acting on this cut face act as surface forces. The free body diagram of the left hand side body is shown in figure 4.8b.

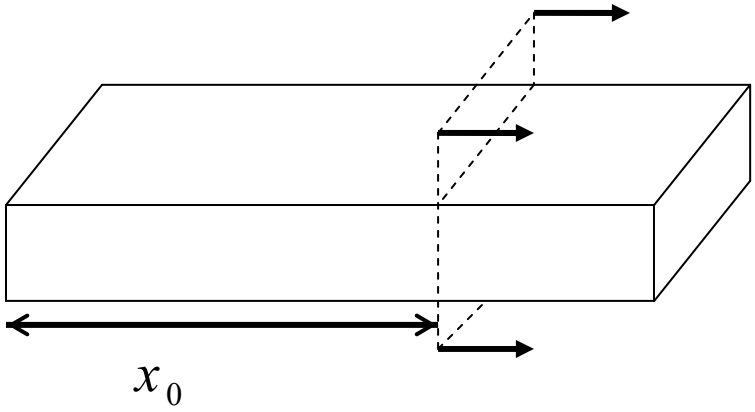

Figure 4.8a showing an arbitrary section of the laser peened specimen

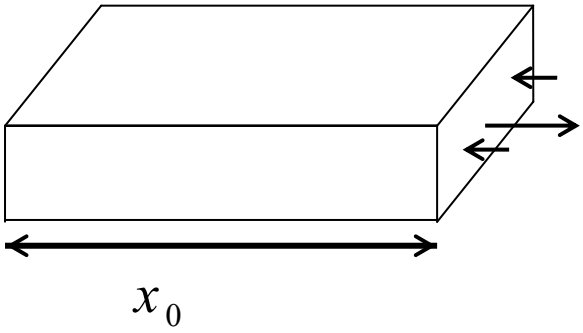

Figure 4.8b showing the free body diagram of the cut block

To satisfy the conditions of equilibrium, $\sum F_x = 0$ and $\sum M_y = 0$. The stresses responsible for the longitudinal component of force, i.e. F_x are the longitudinal stresses, therefore the equilibrium equations can be written in terms of this stress component as:

$$\sum F_x = \int_{A(x_0)} \sigma_x dA = 0 \tag{4}$$

And

$$\sum M_y = \int_{A(x_0)} z\sigma_x dA = 0 \tag{5}$$

Figure 4.9 shows the cross section of the specimen with the forces acting on this surface. If the residual stresses in the peened region of the specimen, i.e. for any point where $y_1 \le y \le y_2$, are assumed to be have the same distribution profile as shown in figure 4.3, then the longitudinal stress field within this region is fully known. This assumption is only valid if the cut has been made far from the two boundaries, i.e. for x_0 values that are near the middle of the specimen. It can then be said that only the stress state at the two remaining areas outside the peened region is unknown (see figure 4.9). Due to the symmetry of the specimen and the treatment, only half of the block shown in figure 4.9 needs to be considered. The coordinate system is the same as shown in figure 4.2.

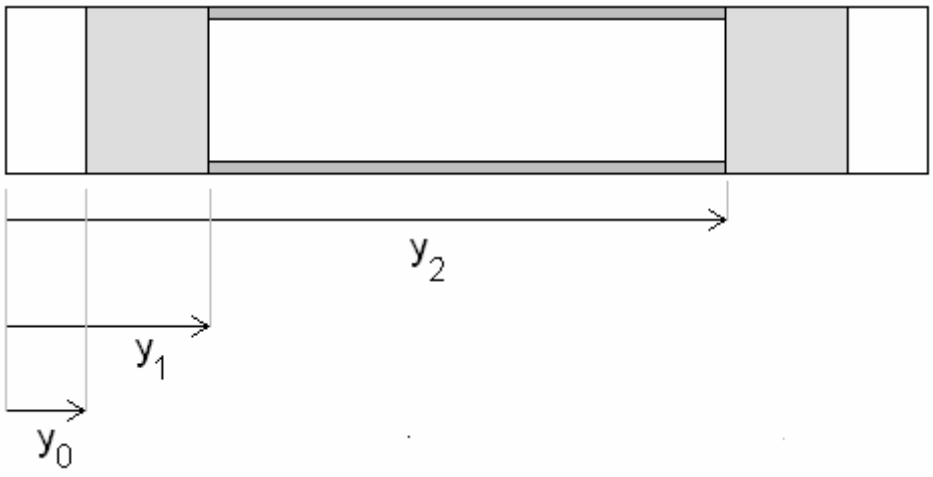

Figure 4.9- Cross section of the specimen

The second simplifying assumption is to assume that the tensile stresses in the $y_0 \le y \le y_1$ range are uniform and equal to the ones measured and shown in figure 4.7. If the specimen is now assumed to be in equilibrium, the length of this tensile stress region can be found from a simple balance of forces. y_0 is the distance on which these tensile stresses act and is an unknown, which can be found from:

$$\sum F_x = \int_{A(x)} \sigma_x(y,z)dA = 0$$

$$\int_{A(x_0)} \sigma(y,z)dA = \int_{y=0}^{y=y_0}\int_{z=0}^{z=z_0} \sigma dzdy + \int_{y=y_0}^{y=y_1}\int_{z=0}^{z=z_0} \sigma dzdy + \int_{y=y_1}^{y=\frac{y_1+y_2}{2}}\int_{z=0}^{z=z_0} \sigma dzdy = I_1 + I_2 + I_3 = 0 \qquad (6)$$

Where z_0 is the thickness of the specimen, i.e. 10mm.

The first integral is zero because this region is assumed to be stress-free. The other two integrals can be evaluated as:

$$I_2 = \int_{y_0}^{y_1}\left[\int_0^{z_0} \sigma(z)dz\right]dy = (y_1 - y_0)\int_0^{z_0} \sigma(z)dz = (y_1 - y_0)J_1$$

Here J_1 can be evaluated numerically from the stress results shown in figure 4.3.
The third integral in equation 6 can be evaluated as:

$$I_3 = \int_{y_1}^{\frac{y_1+y_2}{2}} \left(\int_0^{z_0} \sigma dz\right)dy = \left(\frac{y_2 - y_1}{2}\right)\sigma \times z_0$$

Now by substituting these results back into equation 6,

$$(y_1 - y_0)z_0\sigma + \left(\frac{y_2 - y_1}{2}\right)J_1 = 0 \qquad (7)$$

From figure 4.7, the value of the uniform tensile stress is found, by averaging the stress results, as σ=184MPa, and J_1 is evaluated from the stress values shown in figure 4.3, by integrating the stress values over the thickness, as:

$$J_1 = \int_0^{z_0} \sigma_x(z)dz = \text{-1208 mmMPa.}$$

Therefore from equation 7, y_0=19.6mm, which means that the tensile stress is extended along the whole width of the specimen. This may have a profound effect on the crack growth; this will be discussed in Chapter 5.

4.3.6 An Observation on the Distribution of Residual Stresses in Laser Peened Specimens

One interesting feature common between the stress profiles shown in figures 4.3 and 4.4 is that the stress distribution is not symmetrical with respect to the mid-plane of the specimen: it is skewed toward one face. This is believed to be due to the nature of the laser peening process, where one face is treated first and then the specimen is reversed and the same treatment (i.e. the same laser beam intensity) is applied to the other face.

When one side is treated, due to the action of the compressive surface residual stresses, it will deform and bend inwards. Now if the other face is treated with the same energy, part of the compressive stresses on the first side would have to relax and the plate will then become flat. This relaxation is partly due to introduction of new tensile stresses in the middle of the specimen. Each face of the specimen, when laser peened, will generate tensile stresses in the mid-section of the specimen. Also, the compressive plastic strains at the surface have to relieve in order to allow the specimen to turn back to its original flat shape. This means that the side that was peened first would end up having slightly lower residual stress magnitudes. Therefore the left hand side face of the specimens in figures 4.3 and 4.4 (the side where z=-5mm) were laser shock peened first.

4.4) Summary

Neutron diffraction technique was used for measurement of residual stresses in three specimens, one of which contained a crack. Measurements showed no significant relaxation of residual stress magnitude and therefore it is assumed that in the fatigue tests that were carried out (see Chapter 3) no relaxation has occurred.

Measurements show that in laser peened specimens, a tensile core extends beyond the peened area whose task is to equilibrate the forces acting at each section in the specimen. Simple analyses found that this extension may be considerable; in the present study nearly all of the un-peened region contains relatively high tensile stresses.

Values of residual stresses were measured at various positions in the specimens and a good understanding of the residual stress field inside the specimens is thought to have been achieved. This knowledge is imperative for the task of analysing the fatigue crack growth in these specimens and for understanding the mutual interactions of the crack, applied loads and residual stresses.

The results of this chapter will be used in Chapter 5 where the fatigue crack growth in laser peened regions is studied.

References

[4.1] http://www.isis.rl.ac.uk (Accessed July 2008).

[4.2] W Soete, Measurement and Relaxation of Residual Stresses, *Welding Journal*, Vol. 28, No. 8, pp. 354-364 (1949).

[4.3] R L Mattson and W S Coleman, Effect of shot peening variables and residual stresses on fatigue life of leaf spring specimens, *Transactions of the Society of Automotive Engineers*, Vol. 62, pp. 546-556 (1954).

[4.4] J Morrow and G M Sinclair, Cycle-dependent Stress Relaxation, In: *Symposium of Basic Mechanisms of Fatigue*, ASTM STP 237, American Society for Testing and Materials, pp. 83-109 (1958).

[4.5] R W Landgraf and R A Chernenkoff, Residual Stress Effects on Fatigue of Surface Processed Steels, In: *Analytical Methods for Residual Stress Effects in Fatigue*, ASTM STP 1004, American Society for Testing and Materials, pp.1-12 (1988).

[4.6] U P Sinha and D W Levinson, Bending Stress Relaxation of AISI 1095 Steel Strip, In: *Proceedings of ASM's Conference on Residual Stress- In Design, Process and Materials Selection*, Cincinati, Ohio, USA, Edited by W B Young (April 1987).

[4.7] O N Romaniv, Relaxation of Residual Stresses by Alternating Loads, *Fiziko-Khimicheskaya Mechanika Materialov*, Vol. 1, No. 6, pp. 726-729 (1965).

[4.8] J Bauschinger, *Zivilingur*, Vol. 27, pp.289-347 (1881).

[4.9] G E Dieter, Mechanical Metallurgy, McGraw Hill Publishing Company, ISBN 0-07-016893-8 (1986).

[4.10] E H Edwards, J Washburn and E R Parker, Stress Induced Movement of Crystal Boundaries, *Transactions of AIME*, Vol. 197, p.1525 (1953).

[4.11] W Z Zhuang and G R Halford, Investigation of residual stress relaxation under cyclic load, *International Journal of Fatigue*, Vol. 23, pp. S31-S37 (2001).

[4.12] P P Benham, R J Crawford, C G Armstrong, Mechanics of Engineering Materials, Prentice Hall, ISBN: 0582251648 (1996).

[4.13] J James, J Santisteban, M Daymond and L Edwards, SScanSS Standard Manual (April 2005).

[4.14] A D Evans, A King, T Pirling, G Bruno and P J Withers, Near Surface Residual Stress Determination of Laser Shock Peening by Neutron Diffraction, *Journal of Neutron Research*, Vol. 11 Issue 4, pp. 229-233 (Dec 2003).

CHAPTER 5

5.0) Fatigue Crack Growth in Laser Peened Specimens- Analysis of Test Results

5.1) Introduction

In Chapter 3, the rationale for the fatigue tests of laser peened specimens as specimens containing non-uniform stress fields was discussed. The test procedure and instrumentation were explained and preliminary results obtained from these tests were shown. It was argued that an accurate map of the residual stress field in the specimens is required in order to analyse the results of the tests.

Chapter 4 introduced the strategy to measure the stress values at relevant points in the specimens using neutron diffraction technique. The process of the measurement was explained and results obtained from these measurements were analysed, and a fairly comprehensive understanding of the residual stress field in the laser shock peened specimens was achieved.

Having an accurate map of the residual stress field inside the laser shock peened specimens now makes it possible to analyse the effect of these stresses on the fatigue crack growth. Residual stresses manifest their effect on fatigue crack growth via the stress intensity factor values, and weight functions allow accurate determination of SIF values in these specimens. Numerical simulations of the crack growth, under the action of applied and residual stresses yield crack growth rates which are not necessarily the same as the rates observed in the experiments. As discussed in Chapter 3, any discrepancy between the 'numerical' and 'experimental' rates is likely to be due to factors other than the residual stresses.

A comparison between the fatigue crack growth test data and numerical predictions of crack growth facilitates the understanding of the way laser peening really affects crack growth. This numerical analysis, using weight functions, can only include the effect of *applied* and *residual stresses* on the crack growth rate, whereas the results of the experiment show the actual interaction between the peening (of which residual stresses are only a part) and crack growth.

Numerical analyses of crack growth for these specimens require knowledge of residual stresses. Before undertaking the neutron diffraction tests, as a preliminary study in order to devise a plan for the experiments and develop a computer algorithm, a hypothetical value of -275MPa was chosen for the residual stress in the laser peened area, and load levels were chosen based on this residual stress value. This hypothetical value, being the lowest possible stress encountered in the elastic region, was chosen so that crack growth in both specimens was guaranteed.

Also, provision was made to include any cycle-dependent relaxation of this stress in the model. This mechanism ensured that even with the highest possible initial values of compressive residual stresses, which can in certain circumstances completely stop the crack, the relaxation would cause the crack to continue to grow after the magnitude of the residual stress has decreased due to cyclic loading. This phenomenon is discussed in Chapter 4, where following neutron diffraction measurements of the actual residual stress field, these values were used to analyse the crack growth. However, no relaxation of residual stresses was observed in these tests (see Chapter 4). As the stress field in the crack plane is non-uniform, weight functions may be used to evaluate the stress intensity factors as the crack grows.

5.2) Developing a Weight Function for the Single Edge Notched Specimen

As mentioned in Chapters 1 and 2, multiple reference states (MRS) method [5.1] has been successfully used to calculate stress intensity factors for one dimensional edge and through cracks. Brennan [5.2] used this technique with the two stress intensity factor

solutions of Gross-Brown-Srawley [5.3, 5.4] for tensile and bending loads and demonstrated self-consistency of the method, i.e. results from the weight function for linear stress distributions agree with those of Gross-Brown's. However, the weight functions derived using the MRS technique are not verified for arbitrary loadings.

By assuming that the crack face displacement can, being symmetrical with respect to the crack mid-plane, be expressed in the following form:

$$u_r(a,x) = \frac{\sigma a}{E'} \sum_{j=1}^{J} F_j(a) \left[1 - \left(\frac{x}{a} \right)^2 \right]^{j-\frac{1}{2}} \tag{1}$$

Wu [5.5, 5.6] derived the weight function for a single edge crack with length a in a finite width (W) plate as:

$$m(a,x) = \frac{1}{\sqrt{2\pi a}} \sum_{i=1}^{5} \beta_i(a) \left(1 - \frac{x}{a} \right)^{i-\frac{3}{2}} \tag{2}$$

Where values of $\beta_i(a)$ are known and have been shown in Appendix C.

Now by knowing this weight function, stress intensity factors can be calculated as:

$$K = f\sigma\sqrt{\pi a W} \tag{3}$$

Where f is:

$$f = \int_0^a \frac{\sigma(x)}{\sigma} \frac{m(a,x)}{\sqrt{\pi a}} dx = \frac{1}{\sqrt{2\pi a}} \int_0^a \frac{\sigma(x)}{\sigma} \sum_{i=1}^{5} \beta_i(a) \left(1 - \frac{x}{a} \right)^{i-\frac{3}{2}} dx$$

This weight function has been verified against many different solutions for the edge crack. However, it can be recognised from Appendix C that the amount of numerical calculations necessary for each crack length is more than that required for the multiple

reference states approach. However, this solution can be used to compare with the results of the MRS method and check for possible inaccuracies. Once the MRS weight function is verified against the well-established Wu's weight function [5.5], it can be used confidently for SIF evaluation in edge cracks under arbitrary loadings.

To this end, by using the solutions of Gross-Brown-Srawley for tensile and bending plates [5.4] as two reference states, the weight function can be calculated in the following manner [5.2]:

$$K = \int_0^a g(x,a)\sigma(x)dx \tag{4}$$

$$g(x,a) = \frac{2\sigma_0}{K_1(a)}\sqrt{2}\sum_{j=0}^{m} C_j\left(1-\frac{x}{a}\right)^{j-\frac{1}{2}} \tag{5}$$

If m=2, then from Brennan [5.2] (see Chapter 2):

$$C_0 = \frac{K_1}{\sigma_0\sqrt{\pi a}}\ ;\ C_1 = \frac{q_1 w_{22} - q_2 w_{12}}{w_{11}w_{22} - w_{21}w_{12}}\ \text{; and}\ C_2 = \frac{q_2 w_{11} - q_1 w_{21}}{w_{11}w_{22} - w_{21}w_{12}} \tag{6}$$

And also

$$q_i = C_0\left[K_i(a)\sqrt{\frac{\pi a}{2}} - w_{i0}\right] \tag{7}$$

and $w_{ij} = \int_0^a \sigma_i(x)\left(1-\frac{x}{a}\right)^{j-\frac{1}{2}} dx$, where indices i and j denote the reference states.

For i=1, by assuming $\sigma_1(x) = \sigma_0$ for pure tension, Gross–Srawley [5.4] derived the following empirical formula for single edge notch specimens under tension:

$K_i = \sigma\sqrt{\pi a}F_i\left(\frac{a}{W}\right)$ and

$$F_1\left(\frac{a}{W}\right) = 1.122 - 0.231\left(\frac{a}{W}\right) + 10.550\left(\frac{a}{W}\right)^2 - 21.71\left(\frac{a}{W}\right)^3 + 30.382\left(\frac{a}{W}\right)^4 \quad (8)$$

And for *i*=2, for a specimen under pure bending load, $\sigma_2(x) = \sigma_0\left(1 - \frac{2x}{W}\right)$ and from Brown [5.7]:

$$F_2\left(\frac{a}{W}\right) = 1.122 - 1.40\left(\frac{a}{W}\right) + 7.33\left(\frac{a}{W}\right)^2 - 13.08\left(\frac{a}{W}\right)^3 + 14.0\left(\frac{a}{W}\right)^4 \quad (9)$$

Now by using equations 8 and 9, the coefficients in equation 5 can be found from equations 6.

The weight functions obtained using this technique where compared against those derived by Wu [5.5], and an excellent agreement was observed for different crack lengths. As mentioned before, using the MRS method is mathematically more straightforward and involves fewer and simpler numerical operations, and therefore this will be the preferred weight function which is used for the analyses in the subsequent sections.

5.3) Numerical Analysis of Fatigue Crack Growth of Edge Cracks under Arbitrary Loadings

The numerical approach to modelling the crack growth in the specimens is described in this section. An incremental numerical code developed in MATLAB® was used to predict the growth of edge cracks in specimens under arbitrary loading. As discussed in Chapter 3, this arbitrary stress can be the superposition of an externally applied tensile load and a residual stress field within the specimen. It was also discussed in Chapter 4

that residual stresses may relax under cyclic loading; therefore this cycle-dependent behaviour of residual stress magnitude should also be included in the numerical model. Weight functions, obtained from Brown-Srawley SIF values [5.3, 5.4] using the MRS techniques are incorporated in this code to evaluate stress intensity factor values.

This incremental prediction method works as shown in figure 5.1. The algorithm is as follows:

Starting from a pre-cracked specimen with a precrack length of a_0, for each ΔN number of load cycles the stress intensity factor value is calculated. The stress distribution is a superposition of the externally applied tensile stress and the residual stresses that exist in the specimen. Using the Paris law, with the coefficients obtained from the CT tests (see Chapter 3) the crack growth increment (Δa) is evaluated and the new crack length is updated. The new crack length is used for SIF evaluation after another ΔN number of load cycles. This incremental increase in crack growth is continued for each loop until the crack length reaches the maximum desirable length, at which point the analysis is stopped.

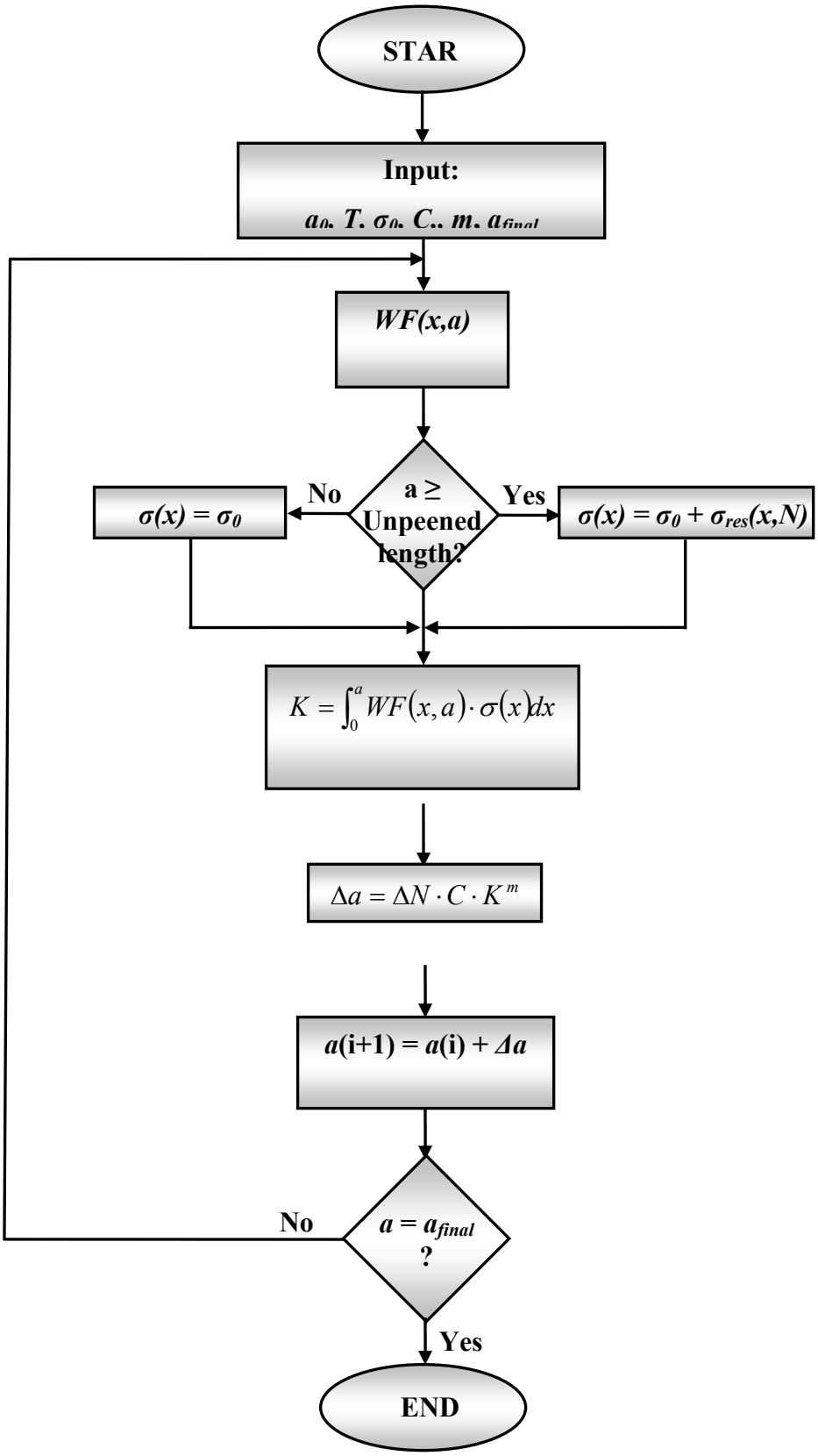

Figure 5.1 showing the flowchart of the incremental crack growth simulation

Notes:

i) Fixed intervals of ΔN are used.

ii) ΔN is assumed to be small enough for ΔK to be zero (i.e. for K to be constant) during each interval.

iii) Though a cycle-dependent residual stress is provisioned in this code, since relaxation of residual stresses was deemed negligible (see Chapter 4), the residual stress field used in this model was assumed to be invariant with respect to load cycles and therefore would not change during the analysis. Nevertheless it is important to note that the amount of the relaxation of residual stresses, as modelled by previous authors (see Chapter 4), is dependent on the effective (applied and residual) stresses present in the material. As the crack grows, the state of stress ahead of the crack changes. Imagine a single edge notch specimen under a cyclic tensile load with constant amplitude, i.e., $\Delta F = const$. As the crack's length increases, the magnitude of the stresses present at the crack tip increases (which is basically why K increases with crack length). Therefore the material ahead of the crack actually experiences a cyclic tensile stress with an ever increasing magnitude ($\Delta\sigma \neq const$). In the presence of a residual stress field, it is this increasing 'applied stress' that causes the relaxation of the residual stress.

iv) It is worth noting here that the growth of the fatigue crack would inevitably affect the state of the residual stress field ahead of the crack. This is because as shown in Chapter 4, the tensile core of the specimen is imperative for keeping the force balance at each cross section. As the crack advances, the newly cracked part of the specimen would no longer have this tensile core because the material has lost its integrity. This will in turn affect the compressive stress field ahead of the crack. The crack-stress interaction in laser peened specimens as described here is a complicated phenomenon and deserves a separate study. However, when using weight functions, it is the state of the stress in the *un-cracked* body that is the determining factor for stress intensity values [5.8]. Therefore this interaction between the crack and residual stresses ahead of it can be overlooked in an analysis such as the present one i.e. where no residual stress

relaxation is observed. However, this interaction is important when dealing with a stress-dependent relaxation phenomenon.

The developed code will be used to interpret the results of the fatigue growth tests. The crack growth data results from the tests have to be analysed and be transformed to more useful forms. Traditionally, ΔK vs. $\frac{da}{dN}$ and Y vs. $\frac{a}{T}$ plots are used for interpretation of fatigue crack growth tests. The raw data (i.e. crack length vs. number of load cycles) were shown in Chapter 3. In the following section, these data will be further analysed.

5.4) Analysis of the Fatigue Test Results

Figures 5.2 and 5.3 show the crack growth data directly measured from the experiments. In order to obtain the crack growth rate for each increment, i.e. for calculation of $\frac{da}{dN}$ from *a* vs. *N* data, several techniques can be used such as the *secant method* or the *incremental polynomial method*. Whereas numerical integration techniques are usually straightforward and fairly robust, one should be very careful when differentiating numerically [5.9]. The secant method is the most basic differentiation technique for a set of data [5.10]. In this method the derivative is obtained as:

$$\left(\frac{da}{dN}\right)_{\bar{a}_i} = \frac{a_{i+1} - a_i}{N_{i+1} - N_i}$$

Where the averaged crack length ($\bar{a}_i = \frac{1}{2}\left(a_{i+1} + a_i\right)$) is used for calculating ΔK.

ASTM Standard E647 [5.11] recommends the use of an incremental seven-element polynomial method. This is the technique used in this study as in most cases this method evens out the local irregularities from the actual experimental data [5.10]. A Fortran® recipe of this technique is outlined in ASTM E647 [5.11]. Therefore for each crack length *a*, the $\frac{da}{dN}$ value can be evaluated from the *a* vs. *N* data.

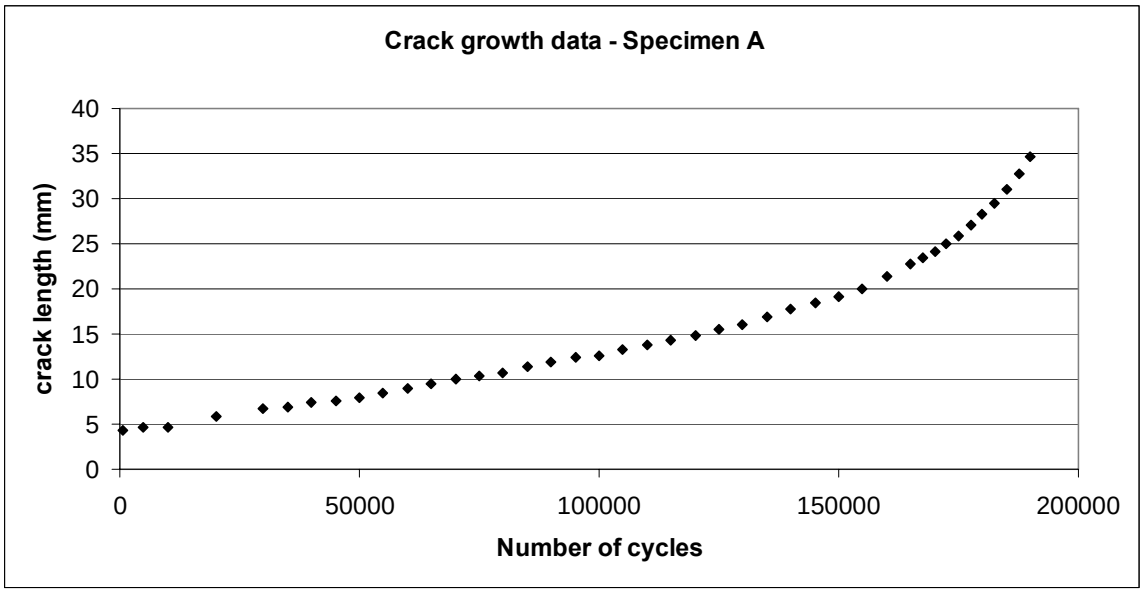

Figure 5.2- Fatigue crack growth data (a-N curve) for specimen A

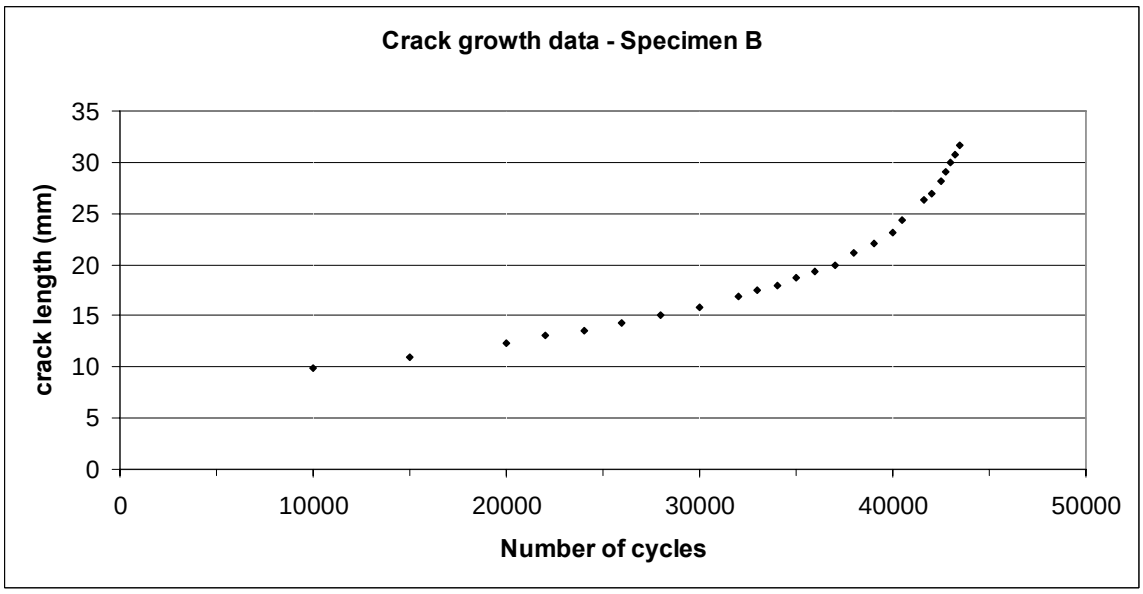

Figure 5.3- Fatigue crack growth data (a-N curve) for specimen B

In order to evaluate K for each crack length, there are two options available. The first option is to use the Paris law [5.12] coefficients (which are known from CT tests for this material), and calculate the K value corresponding to the $\frac{da}{dN}$ value for that crack length. However, the accuracy of these K values would depend on the accuracy of the experimental $\frac{da}{dN}$ values. Also, these values are dependent on the Paris law coefficients

C and *m*. The second option would be to use a weight function and to calculate the stress intensity factor for each crack length based on the stress field acting on the crack plane. In the current study, the values of *K* obtained from the first method are called 'experimental *K*' and the values determined using the second approach are called 'weight function *K*', or *numerical K* values. As mentioned before in Chapter 3, any discrepancy between these two sets, which is mathematically equivalent to a discrepancy between *a* vs. *N* data for the experimental and numerical simulations, would suggest that factors other than residual stresses are also affecting the crack growth. For reasons described in the following sections, where the numerical values for SIF is mentioned in this chapter, the specimen is assumed to be under pure tension and the value of SIF is taken from Gross-Brown [5.4]. However as discussed in the next sections, this does not undermine the general validity of the arguments.

It was mentioned in the previous sections that some authors use *Y* vs. $\frac{a}{T}$ data plots for analysis of experimental results. The geometry factor or *Y* is defined as:

$$Y = \frac{K}{\sigma_0 \sqrt{a}}$$

Where σ_0 is a characteristic stress and is representative of the loading on the specimen. However, in the case of the present tests, the stresses acting on the crack planes of the un-cracked specimens are not similar in form (they are the superposition of a residual stress field which is similar for the two specimens and a tensile load which is not equal for the two specimens, making the resultant stress fields dissimilar.). Since the stresses are not constant or uniform, no nominal stress value can characterise the stress field. Therefore it is deemed appropriate to avoid using these factors in the analysis of the results of these tests.

The comparison between the *experimental* and *numerical K* values for each specimen is shown in figures 5.4 and 5.5. Figure 5.6 shows the combined data from the two specimens; in this figure WF denotes values obtained using stress intensity factor

weight functions. Here a difference between the effective *C* and *m* (i.e. Paris law coefficients that fit the numerical results) and the experimental *C* and *m* (i.e. Paris law coefficients obtained from the CT tests) coefficients is evident.

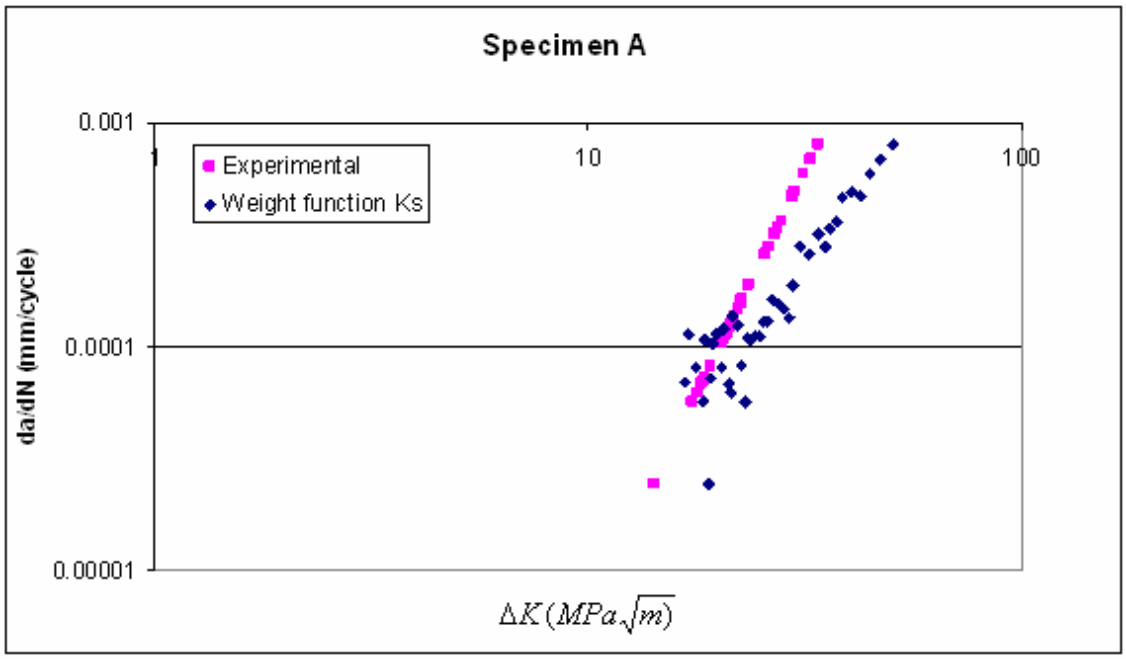

Figure 5.4- *Experimental* and *numerical* (*weight function*) SIFs for Specimen A

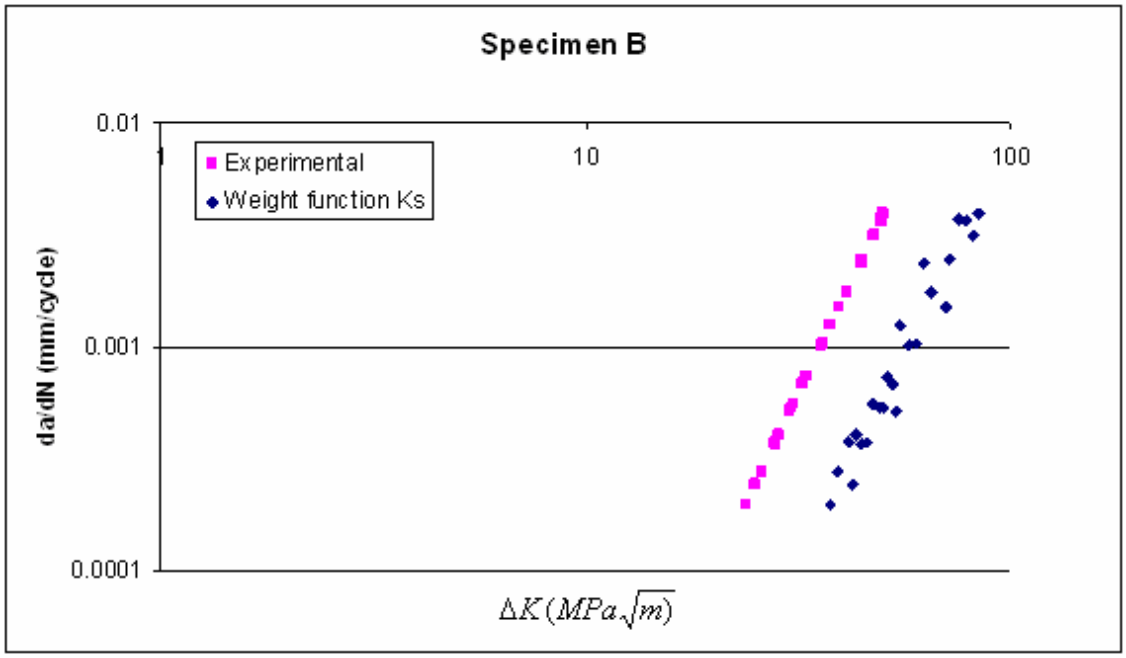

Figure 5.5- *Experimental* and *numerical* (*weight function*) SIFs for Specimen B

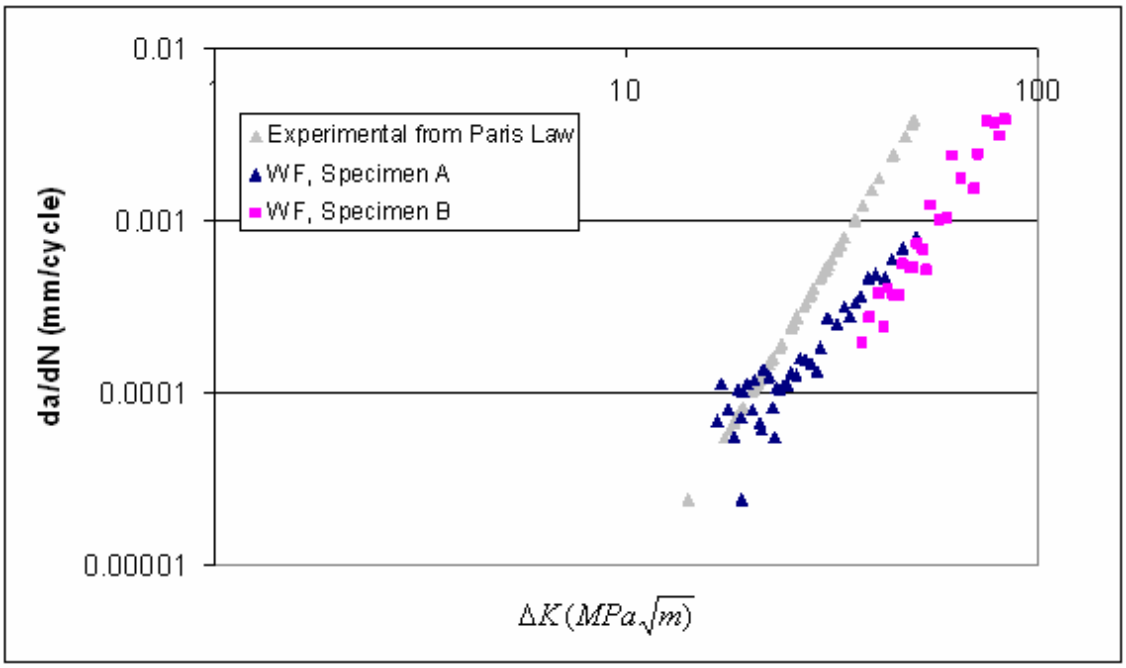

Figure 5.6- ***Experimental*** **and** ***numerical*** **(*weight function*) SIFs for Specimens A and B**

At this stage it can be argued that this shift in the Paris law coefficients may suggest that the Paris law coefficients are not transferable from CT tests to the current specimen geometry. If this is the case, then by a simple adjustment to the values of these coefficients they can be made suitable for the current geometry. However, the next sections will show that no adjustment can be made to the Paris law coefficients to model these tests and that the Paris law coefficients alone can not explain this discrepancy.

5.5) A Note on the Superposition of Applied and Residual Stresses

For the purpose of this new study, some assumptions have to be made. It will then be shown that these assumptions do not undermine the validity of the arguments resulted from this study.

An important decision at this stage is how to incorporate the residual stress values obtained from the neutron diffraction test in a one-dimensional analysis. In Chapter 4 the through-thickness distributions of residual stresses due to laser peening were

obtained from the neutron diffraction measurements. However, in a one-dimensional crack growth analysis the residual stress field can only be modelled using one stress value for each position along the potential path of the crack. The simplifying assumption introduced here is to average the stress at each profile and use this averaged value in the numerical model. From the findings of Chapter 4, this average stress value is $\sigma = -120.8MPa$. However, using this value as the residual stress value suggests that for both specimens A and B, in the peened region the material is *always* in compression and therefore no crack growth can occur. *One fundamental problem of this numerical methodology is that when the magnitude of the average compressive residual stress value is larger than the externally applied load, the model predicts no crack growth*. However, in reality both cracks did grow. If the total stress is taken as the superposition of the applied and the residual stress, negative values of total stress may be encountered. This suggests that if an averaged value of the residual stress is to be used for each section, then no Paris law coefficients can be used to predict the outcome of these tests. The crack growth in specimen A, despite the fact that the average compressive residual stress is -120MPa and the externally applied stress was 50MPa, signifies that the average compressive residual stress *does not* superimpose on the externally applied load. The fact that the crack grew indicates that K values are positive and non-zero. This will be discussed in detail in the next section.

5.6) The Concept of the Effective Fatigue Stress

In the previous section it was shown that an averaged value of the residual stress for each point can not be used for calculation of the stress intensity factor. Now the important question is which stress value should be used for the evaluation of stress intensity factors in laser peened specimens. This stress is here called the 'effective fatigue stress'.

In order to derive the effective fatigue stress, the following methodology is proposed. From the $\frac{da}{dN}$ values, experimental SIFs can be evaluated. These values depend on the

coefficients obtained from the CT test. Now, to find out what stress distribution gives the resulted $K_{\exp}$, one can write:

$$K = \int_0^a \sigma f(x,a)dx$$

Where f is the weight function and is known for each crack length for the current specimen geometry. For example, this can be derived using the MRS technique, as explained in a previous section in this chapter.

For the n discrete points of crack length measurement

$$a = [a_1, a_2, ..., a_n]$$

$K_{\exp}$ can be calculated as $K_{\exp_i} = \sqrt[m]{\frac{1}{C} \times (\frac{da}{dN})_i}$. Now, by assuming $\sigma = \sigma_{tensile}$ (derived from the analysis in Chapter 4) for $a = 0$ to $a = a_1$,

$$K_{\exp_1} = \int_0^{a_1} \sigma_{tensile} f(x,a_1)dx \quad (10)$$

and

$$K_{\exp_2} = \int_0^{a_1} \sigma_{tensile} f(x,a_2)dx + \int_{a_1}^{a_2} \sigma_{12} f(x,a_2)dx \quad (11)$$

Where σ_{12} denotes the stress acting on the section from $a = a_1$ to $a = a_2$. Similarly,

$$K_{\exp_3} = \int_0^{a_1} \sigma_{tensile} f(x,a_3)dx + \int_{a_1}^{a_2} \sigma_{12} f(x,a_3)dx + \int_{a_2}^{a_3} \sigma_{23} f(x,a_3)dx \quad (12)$$

From these equations, the stress values can be evaluated as:

$$\sigma_{tensile} = \frac{K_{\exp 1}}{\int_0^{a_1} f(x, a_1)dx}$$

$$\sigma_{12} = \frac{K_{\exp 2} - \int_0^{a_1} \sigma_{tensile} f(x, a_2)dx}{\int_{a_1}^{a_2} f(x, a_2)dx}$$

$$\sigma_{23} = \frac{K_{\exp 3} - \int_0^{a_1} \sigma_{tensile} f(x, a_3)dx - \int_{a_1}^{a_2} \sigma_{12} f(x, a_3)dx}{\int_{a_2}^{a_3} f(x, a_3)dx}$$

And by induction:

$$\sigma_{i-1,i} = \frac{K_{\exp_i} - \int_0^{a_1} \sigma_{tensile} f(x, a_i)dx - \sum_{k=1}^{i-3} \left[\int_{a_k}^{a_{k+1}} \sigma_{k,k+1} f(x, a_i)dx \right]}{\int_{a_{i-1}}^{a_i} f(x, a_i)dx}$$

Where $f(x, a_i)$ is the weight function for a crack length of a_i. This was modelled in a MATLAB® code and was used to evaluate the effective fatigue stress for specimens A and B.

Figure 5.7 shows the values of the effective fatigue stresses as obtained from the proposed technique. These values have been obtained by using the Paris law coefficients of $C = 6 \times 10^{-13}$ and $m = 4$ from the CT tests.

Specimen A was subjected to a cyclic tensile stress with a range of 90MPa and specimen B was under an applied cyclic stress range of 50MPa. To show the dependence of this stress on the Paris law coefficient *m*, the same analysis was carried out using a different *m* value (this time *m*=3.6). The result of this analysis is also shown in figure 5.8. In order to ensure the accuracy of these values, in a separate numerical simulation these stress values were applied to a computer code (developed in

MATLAB®) and the resulting crack growth behaviours were identical to the ones observed in the experiments.

It has been shown [5.13] that for a specific cracked sample geometry, the weight function is unique. This also directly proves the rather trivial point that for a certain crack geometry under a certain stress distribution, the stress intensity factor value is unique. Now if the crack length increments are infinitesimal, the incremental nature of the above analysis proves that for a certain *crack growth behaviour*, the stress distribution is unique.

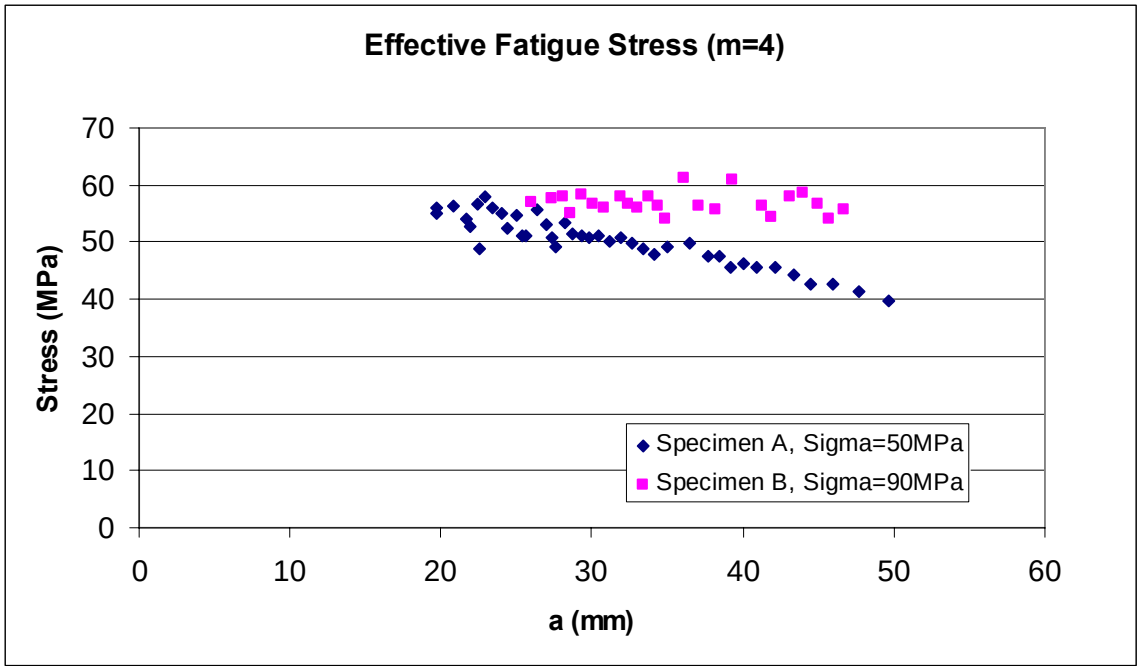

Figure 5.7- Effective fatigue stress distribution for specimens A and B (*m*=4.00). Here 'Sigma' denotes the applied stress range.

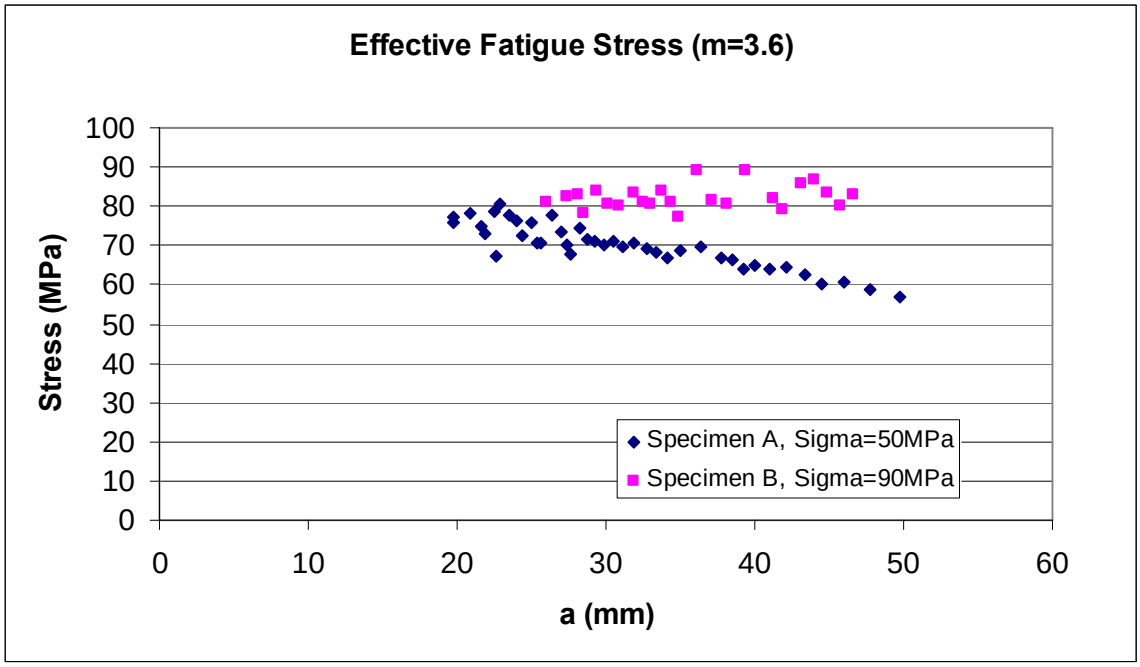

Figure 5.8- Effective fatigue stress distribution for specimens A and B (*m*=3.6). Here 'Sigma' denotes the applied stress range.

It can be seen that although the magnitude of these stresses depends on the choice of *m* value, but if instead of using CT specimens, the Paris law coefficients were obtained from a specimen identical to specimens A and B, then this dependence would not have been a point of doubt. Indeed the two figures (and various others obtained for different *m* values) show the same trends which is indicative of the independence of these trends to the Paris law coefficients. The important conclusion from these figures is that the effective fatigue stresses are not the algebraic sum of the externally applied residual stresses and the residual stresses due to laser peening. However, if the material were fully elastic and if the compressive residual stresses were the only effect of the laser peening process, then linear elasticity mandated that the effective stress should be the superposition of these two stresses.

5.7) Summary

In this chapter the results of the fatigue crack growth tests were analysed. Before undertaking the tests it was expected that laser peening would severely affect crack growth. Previous studies on shot peening (see Chapter 1) have indicated that peening can cause crack retardation in edge cracks and surface cracks. Since laser peening can penetrate deeper than shot peening, this method was expected to have an even more profound effect in the form of retarding or even completely stopping the cracks. Preliminary numerical analyses confirmed this view.

However, the results of the tests were not as expected: the crack growth retardation caused by the laser peening, if any, was not obvious from the crack growth data. An attempt to model the crack growth behaviour under the influence of the residual stresses failed, due to an apparent anomaly, namely that the crack grew when the stress intensity factors from traditional numerical analyses indicated no growth.

It was argued that the superposition of residual stresses and the externally applied stress does not yield the stress intensity factors which were observed in the experiments. This is assumed to be due to the effect of laser peening on the material and is further discussed in the next chapter. The concept of effective fatigue stresses was introduced and was derived computationally for the two specimens tested in Chapter 3, and it was shown that this stress does not comprise the residual stress and external loads. The results further confirmed the belief that the elastic residual stresses and the externally applied load do not exclusively determine the crack growth behaviour. This will be studied in the next chapter.

References

[5.1] R P Ojdrovic and H J Petroski, Weight functions from multiple reference states and crack profile derivatives, *Engineering Fracture Mechanics,* Vol. 39(1), pp. 105-111 (1991).

[5.2] F P Brennan, Evaluation of stress intensity factors by multiple reference state weight function approach, *Theoretical and Applied Fracture Mechanics,* Vol. 20, pp. 249-256 (1994).

[5.3] B Gross, J E Srawley and W E Brown Jr, Stress-intensity factors for a single-edge-notch tension specimen by boundary collocation of a stress function, NASA Technical Note, NASA TN D-2395, Lewis Research Center, Cleveland, Ohio (Aug 1964).

[5.4] B Gross and J E Srawley, Stress-intensity factors for single-edge notch specimens in bending or combined bending and tension by boundary collocation of a stress function, NASA Technical Note, NATA TN D-2603, Lewis Research Center, Cleveland, Ohio (Jan 1965).

[5.5] X R Wu. Approximate weight functions for centre and edge cracks, *Engineering Fracture Mechanics*, Vol. 20, No.11, pp. 35-49 (1984).

[5.6] X R Wu, Closed form weight function for edge crack problems, *Acta Mechanica Sinica*, Vol. 6, No. 2 (1990).

[5.7] W F Brown and J E Srawley, Plane Strain Crack Toughness Testing of High Strength Metallic Materials, ASTM STP 381 (1966).

[5.8] H F Bueckner, A novel principle for the computation of stress intensity factors, *Zeitschrift für Angewandte Mathemetik und Mechanik.* Vol. 50(9), pp. 529-546 (1970).

[5.9] P A Stark, Introduction to Numerical Methods, The Macmillan Company, Collier-Macmillan Limited (1970).

[5.10] E L Stiefel, An Introduction to Numerical Mathematics, translated by W C Rheinboldt, Academic Press Inc. (1963).

[5.11] Standard Test Method for Measurement of Fatigue Crack Growth Rates, ASTM International Standard E 647 - 05, American Society for Testing and Materials (2005).

[5.12] P C Paris and F Erdogan, A critical analysis of crack propagation laws, *Journal of Basic Engineering*, Vol. 85, pp. 528-534 (1963).

[5.13] J R Rice, Some remarks on the elastic crack-tip stress fields, *International Journal of Solids and Structures,* Vol. 8, pp. 751-758 (1972).

CHAPTER 6

6.0 Conclusions and Recommendations

6.1 Introduction

The previous five chapters outlined the full scope of the research. This chapter summarises the contents of these chapters, emphasising the salient points. It will also draw conclusions from the results of the research and further discuss the significance of some of these findings. This chapter also includes recommendations for future research to improve upon the current work.

6.2 Summary of the Thesis and Conclusions

An introduction to the state-of-the-art in stress intensity evaluation and also the residual stresses and their measurement was included in Chapter 1. The significance of cracks, including surface cracks, and the relation between crack growth and LEFM was emphasised. It was pointed that for uniform loading situations, reliable solutions exist both for the one-dimensional and the semi-elliptical surface cracks. The discussions led to the fact that for non-uniform stress fields, there are no robust and reliable weight functions for the surface crack stress intensity factors. Also the simplicity of the MRS approach for the calculation of SIF was highlighted.

In Chapter 2, a thorough background to the problem of surface cracks SIF weight functions was given. As a result of these studies, a new weight function was proposed for the surface crack which is based on the MRS methodology [6.1]. This WF would enable calculation of crack driving forces (SIFs) for non-uniform stress distribution loading situations. This is the main advantage of RMS SIF values over point SIF values that as discussed in detail in Chapter 1, would allow the Paris law to be used for growth predictions in surface cracks. The results obtained from this WF were then verified

against FE results for various loadings and crack geometries, and the WF results proved to be accurate for all these parameters.

However, there still remains the question of the applicability of this weight function. It was shown that these weight functions give reliable and accurate results for situations where the stress state is non-uniform. As mentioned in Chapter 1, residual stresses found in components and structures are one category of stress fields which are usually highly non-uniform. Also it was noted that through certain surface treatments generally known as peening, beneficial residual stresses are introduced into the material which are believed to improve fatigue resistance of the components.

It was discussed in Chapter 3 that in situations where a residual stress field is generated due to the peening process, it is customary to assume that the effect of the peening process on the crack growth rate is due to the residual stresses. These stresses, when superimposed on the externally applied stresses, alter the SIF and therefore affect the crack growth.

To examine this hypothesis, a set of experiments was proposed where fatigue crack growth in highly non-uniform stress fields was to be analysed. It was mentioned in Chapter 1 that being able to assess SIFs for a 'step' increase or decrease in the stress field along the crack front is the ultimate test for WFs. To avoid any other complications, thin specimens were chosen where it was initially believed that by using laser shock peening, a through-thickness compressive residual stress at the potential crack plane was achievable. This method was chosen on the basis of a number of reasons; being able to penetrate deeper than shot peening and leaving the specimen with less surface roughness compared to shot peened specimens were among these reasons.

The results of the tests were not as expected. Based on the assumptions by previous authors [6.2, 6.3], it was predicted that the crack would either stop or show a drastic decrease in growth rate. It was also predicted that should the crack stop, the residual stresses due to peening would, under the action of cyclic loading, eventually relax and

allow crack propagation to continue at a lower rate. However, the test results showed no apparent retardation in the crack growth.

The residual stress field in the laser peened specimens was then evaluated using the neutron diffraction technique (Chapter 4). The through-thickness distribution of the residual stresses in the laser peened region was found to be non-uniform, ranging from a highly compressive stress at the surfaces to tensile in the mid-section of the plate. However, the depth of the compressive region was much more than what could be achieved by shot peening. Analysis showed that the specimens included a tensile core which extended further than the actual peened boundaries.

Another point worth noting is that during the neutron diffraction measurements no residual stress relaxation was observed as a result of cyclic loading.

Before undertaking the tests, the plan was to establish the applicability of the weight function theory to stress fields that arise from surface peening techniques. It was assumed that any discrepancy between the predicted growth behaviour and the growth rate observed in the experiments was not due to the residual stresses and was likely to be caused by other factors such as plasticity, which would inevitably result from the peening process. It was further assumed that for the peened region of the specimen, defining new material constants (Paris law coefficients) would encompass these discrepancies and would enable one to separate these effects from the residual stress effects.

However, the analysis in Chapter 5 showed that if the residual stresses were to be superimposed on the externally applied load stresses, then no Paris law coefficient and exponent could be defined to predict the growth of the crack in the specimens. This led to the definition of the 'effective fatigue stress', i.e. a stress distribution which when used in conjunction with the Paris law, would give the crack growth behaviour that was observed in the test. This stress was not the algebraic sum of the residual stresses and the loading.

In Chapter 2, the RMS SIF was argued to even out the effects of surface and larger plastic zones in surface cracks by averaging the stress intensity using an RMS weighting filter. The reason for the introduction of this concept was to enable derivation of crack driving forces for different directions in cases where a point-by-point value of the SIF is not known. Also, it was argued that the Paris law coefficient C is not constant along the crack front and knowing the point-by-point SIF values would not suffice for crack growth prediction. The same argument can be made regarding the 'effective fatigue stress'. The depth-distribution of the residual stress along the crack front in the test specimens was not uniform, and therefore resort had to be made to an 'averaged' value for demonstration purposes. Whereas it was argued that the actual value of this averaged stress would not disturb the generality of the argument in Chapter 5, this averaging process could be investigated in more detail.

By drawing an analogy with the surface crack stress intensity factors, it could be said that by a certain averaging (or weighting) of the residual and applied stresses at the crack profile, the effective fatigue stress may be obtained.

However, there still remain the possible effects of the peening process apart from the residual stresses that may alter the crack growth. An experiment to facilitate the understanding of this 'averaging' process is explained in the next section.

6.3 Primary PhD Achievements

The previous section presented the observations and conclusions achieved from the work carried out in for this research. A list of the main conclusions and findings is given here:

- The role of the RMS SIF values in fatigue growth of surface cracks under non-uniform stress fields, such as the stresses arisen from peening surface treatments, was demonstrated and their advantages over the traditional point-by-point SIF life prediction approach were illustrated. It was shown that for non-uniform

loadings, the traditional approach may lead to errors that are not easily estimated and may result in non-conservative predictions.

- A weight function was developed for the calculation of the RMS SIF values in surface cracks under arbitrary loadings, and its accuracy and wide range of application were established by comparison against Finite Elements results.

- As an example of the non-uniform residual stress fields, the effect of laser shock peening on the stress state in steel specimens was studied using neutron diffraction technique. The stress field in the peened regions and the transition from compressive to tensile near the peened boundaries were analysed and a full picture of the stress distribution in simple, partially laser peened specimens was developed.

- Fatigue crack growth in laser peened specimens was experimentally studied, and it was observed that contrary to the current belief, the laser peened section of the material did not show a lower crack growth rate. Further analysis contributed this to the tensile core of the material. However, numerical attempts to predict the crack growth using SIF weight functions failed and it was concluded that apart from the residual stresses, laser peening also introduces other effects such as surface plasticity, which alter the material's fatigue behaviour.

- The discrepancy between the experimental observations and numerical predictions was successfully quantified by introduction of the 'effective fatigue stress'. It was shown that contrary to the common belief this stress, which quantifies fatigue crack growth behaviour of the specimen, is not the superposition of the applied and residual stresses.

6.4 Recommendations for Future Work

1. Appendix B outlined the work undertaken to derive a weight function for the embedded elliptical crack, based on the MRS technique. The results were not accurate and it was argued that choosing an appropriate functional form for the derivative of the crack face displacement would result in more accurate SIF results. The crack face displacement under remote tension is known for the embedded crack from the solution given by Kassir and Sih [6.4], and the SIF distribution from Green and Sneddon [6.5]. The importance of the embedded crack SIF WF is that if the WF is known, then by addition of some correction terms to the solution for the embedded crack, the SIF values for the semi-elliptical surface crack for each point along the crack front may be evaluated. These 'correction terms' should allow for the effect of the free surface on the SIF values.

2. Accurate measurement of the residual stresses arising from peening, particularly the out-of-peen region and the transience from compressive to tensile at the surface in the peened boundary would help to better understand the full effect of peening on the residual stress fields in the component and can complement the current measurements.

3. In the previous section, it was argued that an analogy may be drawn between the effective fatigue stress as calculated in the test specimens, and the concept of the RMS SIF is surface cracks. For a crack front where the stress intensity factor varies along the crack, an 'effective stress intensity factor' can be defined as the stress intensity factor that can be predicted from the Paris law. Now, the effective fatigue stress can be seen as the stress that causes the effective SIF. It was shown in Chapter 5 that the effective fatigue stress can not be taken simply as the superposition of the externally applied and the residual stresses. Therefore in order to quantify the effective fatigue stress in terms of the residual and applied stresses, and other possible parameters arising from the peening process (such as surface plasticity), an experimental study is proposed.

As a first step, to eliminate the effects of peening, an experiment is proposed in which a fatigue specimen is loaded under cyclic loading and the crack growth rate is recorded.

The state of stress at the crack plane is to linearly vary along the thickness of the specimen. This is to be achieved by out of plane bending of the specimen. The stress profile in the un-cracked body would then look like the one shown in figure 6.1. To keep the crack front relatively straight, excessive variation of stress through the thickness should be avoided.

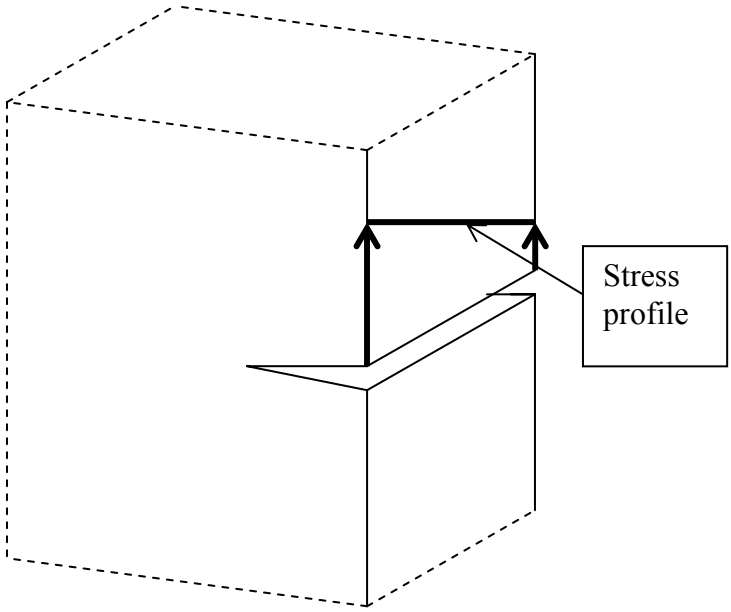

Figure 6.1- Proposed stress distribution for fatigue test

The SIF values obtained from the crack growth rate of the test would yield a value for the effective fatigue stress. Since no variations in stress along the crack length exists, this effective fatigue stress should be constant. Comparison between this value and the stress values at either surfaces of the specimen would disclose the weighting tactic for a linear stress distribution.

For a non-linear stress profile, the stress profile can be discretised into infinitesimal linear sections and for each section the average stress may be obtained from the test above, acting at the mid-point of the linear section. The procedure may be repeated until a single value of stress is obtained for as the overall average stress.

References

[6.1] R P Ojdrovic and H J Petroski, Weight functions from multiple reference states and crack profile derivatives, *Engineering Fracture Mechanics,* Vol. 39(1), pp. 105-111 (1991).

[6.2] L A Hackel and H L Chen, Laser Peenig – A Processing Tool to Strengthen Metals or Alloys to Imrpove Fatigue Lifetime and Retard Stress-Induced Corrosion Cracking, *Laser Science and Technology*, Sep 2003.

[6.3] H Berns and L Weber, Influence of Residual Stresses on Crack Growth, in Impact Surface Treatment, Edited by S A Meguid, Elsevier, pp. 33-44 (1984).

[6.4] M K Kassir and G C Sih, Three-dimensional stresses around elliptical crack in transversely isotropic solids, *Engineering Fracture Mechanics*, Vol. 1, pp. 327-345 (1968).

[6.5] Green and Sneddon: The distribution of stress in the neighbourhood of a flat elliptical crack in an elastic solid, Proceedings of the Cambridge Philosophical Society, Vol. 46(1) pp. 159-163 (1950).

Appendix A

Determination of *K* and *J* in ABAQUS

ABAQUS/Standard automatically finds the elements that form each contour from the regions given as the crack-tip or crack-line definition. Each contour is a ring of elements completely surrounding the crack tip or the nodes along the crack line from one crack face to the opposite crack face. New rings of elements are defined recursively to surround all previous contours. Since the number of evaluations possible is the number of such ring elements, the number of contours to be used in calculating contour integrals must be specified by the user.

ABAQUS/Standard evaluates the stress intensity factors by evaluating the energy release rate (the *J*-integral). The relation between the stress intensity factors and the *J*-integral is given by

$$J = \frac{1}{8\pi} K^T . B^{-1} . K$$

where $K = \left[K_I, K_{II}, K_{III}\right]^T$ and B is called the pre-logarithmic energy factor matrix [A.1]. For homogeneous, isotropic materials B is diagonal and the above equation simplifies to

$$J = \frac{1}{\overline{E}}\left(K_I{}^2 + K_{II}{}^2\right) + \frac{1}{2G} K_{III}{}^2$$

where $\overline{E} = E$ for plane stress and $\overline{E} = E/\left(1-\nu^2\right)$ for plane strain. For anisotropic materials, see the work of Barnett and Asaro [A.2].

Shih and Asaro [A.1] have proposed an interaction integral method to extract the individual stress intensity factors for a crack under mixed-mode loading, which is applicable to cracks in isotropic and anisotropic linear materials.

Interaction Integral Method

For a given problem, the *J*-integral can be written as

$$J = \frac{1}{8\pi}\left[K_I B_{11}^{-1} K_I + 2K_I B_{12}^{-1} K_{II} + 2K_I B_{13}^{-1} K_{III} + P_1\right]$$

where *P* represents terms not involving K_I.

For an auxiliary, pure mode *I* crack-tip field with stress intensity factor k_I, the *J*-integral is defined as

$$J_{aux}^{I} = \frac{1}{8\pi} k_I . B_{11}^{-1} . k_I$$

Now by superimposing the auxiliary field onto the actual field

$$J_{tot}^{I} = \frac{1}{8\pi}\left[(K_I + k_I) B_{11}^{-1} (K_I + k_1) + 2(K_I + k_1) B_{12}^{-1} K_{II} + 2(K_I + k_I) B_{13}^{-1} K_{III} + P_2\right]$$

Here *P* represents terms not involving K_I or k_I. Since $P_1 = P_2$, the interaction integral can be defined as

$$J_{\text{int}}^{\alpha} = \frac{k_\alpha}{4\pi} B_{\alpha\beta}^{-1} K_\beta \qquad \text{(no sum on } \alpha\text{=}I,II,III\text{)}$$

Now if k_α are assigned unit values, the above equations yield

$$K = 4\pi B.J_{\text{int}}$$

$$J_{\text{int}} = \left[J_{\text{int}}^{I}, J_{\text{int}}^{II}, J_{\text{int}}^{III}\right]^{T}$$

In order to evaluate this integral, based on the definition of the *J*-integral, the interaction integrals J_{int}^{α} can be expressed as

$$J_{\text{int}}^{\alpha} = \lim_{\Gamma \to 0} \int_{\Gamma} n.M^{\alpha}.qd\Gamma$$

With M^{α} given as

$$M^{\alpha} = \sigma : \varepsilon_{aux}^{\alpha} I - \sigma.\left(\frac{\partial u}{\partial x}\right)_{aux}^{\alpha} - \sigma_{aux}^{\alpha}.\frac{\partial u}{\partial x}$$

Γ is a contour that lies in the normal plane position *s* along the crack front, beginning on the bottom crack surface and ending on the top surface (see figure A.1). The limit $\Gamma \to 0$ indicates that Γ shrinks onto the crack tip.

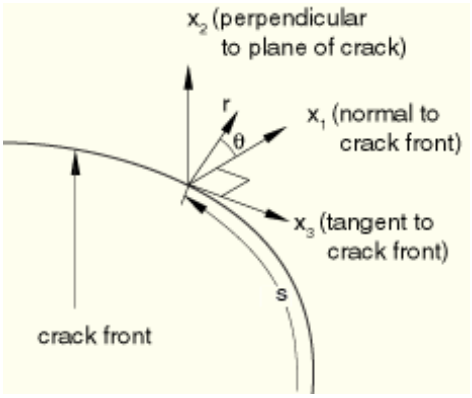

Figure A.1- Definition of local orthogonal Cartesian coordinates at the crack front (taken from ABAQUS Theory Manual)

In ABAQUS/Standard, an interaction integral for a virtual crack advance $\lambda(s)$ is defined

$$\bar{J}^{\alpha}_{\text{int}} = \int_L J^{\alpha}_{\text{int}}(s)\lambda(s)ds = \int_A \lambda(s) n.M^{\alpha}.qdA$$

Where L denotes the crack front under consideration; dA is a surface element on a vanishingly small tubular surface enclosing the crack tip (*i.e.*, $dA=dsd\Gamma$). n is the outward normal to dA, and q is the local direction of virtual crack propagation. To obtain J^{α}_{int} at each node set P along the crack front line, λ is discretised with the same interpolation functions as those used in the finite elements along the crack front:

$$\lambda(s) = N^{Q}(s)\lambda^{Q}$$

Where λ^{Q}=1 at the node set P and all other λ^{Q} are zero. The result is substituted into the expression for $\bar{J}^{\alpha}_{\text{int}}$. Finally the interaction integral value at each node set P along the crack front can be calculated as

$$J^{\alpha\ P}_{\text{int}} = \bar{J}^{\alpha\ P}_{\text{int}} / \int_L N^{P} ds$$

Note on Domain Dependence of the Contour Integral

Since stress intensity factors are determined from the J-integral, the stress intensity factors have the same domain dependence features as the J-integral.

The J-integral should be independent of the domain used provided that the crack faces are parallel to each other; a strong variation in estimates from different rings suggests an error in the contour integral definition, whereas gradual variation in these estimates may indicate that a finer mesh is needed. If the first contour integral is defined by specifying the nodes at the crack tip, the first few contours may be inaccurate. In linear elastic problems the first and second contours typically should be ignored as inaccurate [A.3].

References

[A.1] C F Shih and R J Asaro, Elastic-plastic analysis of cracks on biomaterial interfaces: Part I- Small scale yielding, *Journal of Applied Mechanics*, 1988, pp.299-316.

[A.2] D M Barnett and R J Asaro, The fracture mechanics of slit-like cracks in anisotropic elastic media, *Journal of Mechanics and Physics of Solids*, Vol.20, pp.353-366 (1972).

[A.3] ABAQUS Analysis User's Guide, Volume III: Analysis, Version 6.5, ABAQUS, Inc. 2004.

Appendix B

The Embedded Elliptical Crack

The problem of the stress intensity factor distribution in embedded penny-shaped cracks in an infinite elastic solid, like the one shown in figure (B.1), under the action of a tensile crack-face loading was solved by Tada et al. [B.1] as $K_I = \frac{2}{\pi}\sigma\sqrt{\pi a}$; it is clear that the value of K is constant along the crack front.

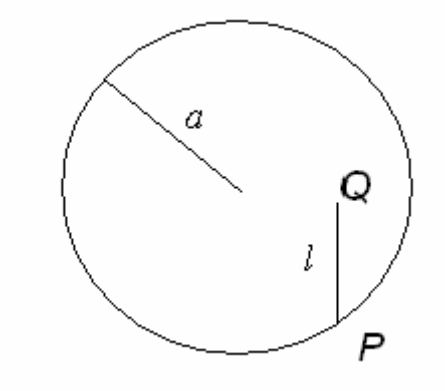

Figure B.1- A penny-shaped crack

Guidera and Lardner [B.2] have determined the stress intensity factor weight function for the penny-shaped crack situated in an infinite isotropic elastic medium as:

$$WF_{QP} = \frac{\sqrt{a^2 - r^2}}{\pi\sqrt{\pi a}}\frac{1}{l^2} \qquad \text{(B-1)}$$

Where Q is a point on the crack face where force is applied and P is a point on the crack front where the stress intensity factor is to be evaluated; l is the distance between these two points, as shown in figure B.1. a is the radius of the crack.

For an embedded elliptical crack such as the one shown in figure B.2, Irwin [B.3] has obtained the stress intensity factor variation along the crack for tensile loading as

$$K = \frac{\sigma\sqrt{\pi a}}{E(k)}\left(\sin^2\theta + \frac{a^2}{b^2}\cos^2\theta\right)^{1/4} \qquad \text{(B-2)}$$

where

$k^2 = 1 - \frac{a^2}{b^2}$ and *E(k)* is the complete elliptic integral of the second kind, defined as

$$E(k) = \int_0^{\frac{\pi}{2}} \sqrt{1 - k^2\sin^2\phi}\, d\phi$$

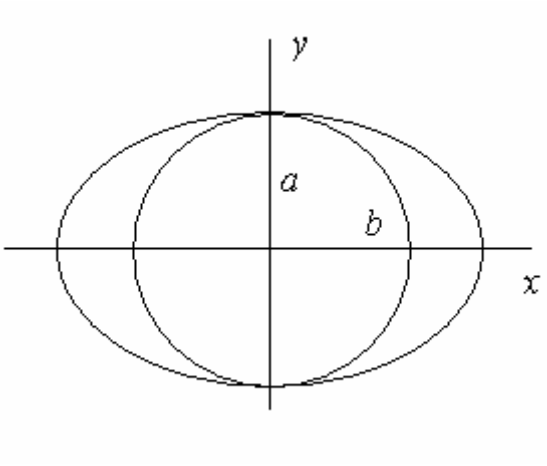

Figure B.2- An embedded elliptical crack

Kassir and Sih [B.4] evaluated the *K* distribution for an embedded crack under a linear stress distribution of $\sigma = \sigma_0\left(\frac{1}{2} + \frac{y}{2a}\right)$ as:

$$K = \frac{\sigma\sqrt{\pi a}}{E(k)}\left(\sin^2\theta + \frac{a^2}{b^2}\cos^2\theta\right)^{1/4}\left[1 + \frac{k^2 E(k)\sin\theta}{(1+k^2)E(k) - k'^2 K(k)}\right] \qquad \text{(B-3)}$$

where *K(k)* is the complete elliptic integral of the first kind, defined as:

$$K(k) = \int_0^{\frac{\pi}{2}} \frac{d\phi}{\sqrt{1 - k^2 \sin^2 \phi}}$$

Shah and Kobayashi [B.5] derived the stress intensity factors for an elliptical crack under the action of the following general stress distribution:

$$\sigma(x, y) = A_{00} + A_{10}x + A_{01}y + A_{20}x^2 + A_{11}xy + A_{02}y^2 + A_{30}x^3 + A_{21}x^2 y + A_{12}xy^2 + A_{03}y^3$$

which gives the Irwin's solution [B.3] when all coefficients except A_{00} are zero, and Kassir and Sih's solution [B.4] for the case where all coefficients expect A_{10} are zero.

B.1) MRS WF for the Embedded Crack

Shah-Kobayashi's solutions for stress intensity factors in embedded cracks [B.5] are used here as reference solutions in order to construct an approximate weight function for the embedded crack. This approach is based on using the weight function for the penny-shaped crack as a starting point, and correcting it for the embedded crack through calibrating unknown coefficient using reference solutions. The approximate weight function has been taken as

$$WF = C_0 m + C_1 f_1 + C_2 f_2 \qquad \text{(B-4)}$$

where *m* is the weight function for a penny-shaped crack (figure B.1) whose radius is equal to the larger of the ellipse's two semi axes (*i.e.* semi-major axis). f_1 and f_2 are correction functions, arbitrarily chosen as

$$f_1^2 = \left(1 - \frac{x}{c}\right)^3 \left(1 - \frac{y}{a}\right)\left(1 + \frac{x}{c}\right)\left(1 + \frac{y}{a}\right)$$

and

$$f_2{}^2 = \left(1-\frac{x}{c}\right)\left(1-\frac{y}{a}\right)^3\left(1+\frac{x}{c}\right)\left(1+\frac{y}{a}\right)$$

The penny-shaped weight function is an axi-symmetrical function in the sense that the crack is not directional in the *x*-*y* plane. The idea behind the use of functions f_1 and f_2 is to correct the penny-shaped weight function for the difference in the weight function behaviour in different directions.

The reference solutions were taken from Shah-Kobayashi [B.5] for the following three loading cases: $\sigma = \sigma_0$, $\sigma = \sigma_0\left(1+\frac{y}{a}\right)$ and $\sigma = \sigma_0\left(1+\frac{x}{c}\right)$.

The following set of three simultaneous equations results from substituting the reference values, here denoted by numeric subscripts *i*=1, 2 and 3:

$$K_i = \iint_A WF\sigma_i dA = C_0 \iint_A m\sigma_i dA + C_1 W_{1i} + C_2 W_{2i} \quad (i=1,2,3) \tag{B-5}$$

Where

$$W_{ji} = \iint_A f_j \sigma_i dA \quad (i=1,2,3 \text{ and } j=1,2)$$

The values of the coefficients were calculated for two different cracks with aspects ratios of 0.6 and 0.2. Figures (B.3a-e) show a comparison between the *Y* values for different types of loading, *i.e.* $\sigma = \sigma_0\left(\frac{x}{c}\right)^2$, $\sigma = \sigma_0\left(\frac{x}{c}\right)^3$ and $\sigma = \sigma_0\left(\frac{x}{c}\right)\left(\frac{y}{a}\right)$ for a/c=0.6 and $\sigma = \sigma_0\left(\frac{x}{c}\right)^2$ and $\sigma = \sigma_0\left(\frac{x}{c}\right)\left(\frac{y}{a}\right)$ for a/c=0.2, obtained from the weight function, with the exact values given by the method suggested by Shah-Kobayashi [B.5]. The only reason for choosing these loadings is the fact that exact solutions for these cases are given by Shah-Kobayashi [B.5]. For simplicity, the weight functions

have only been integrated on a quarter ellipse from 0 to $\frac{\pi}{2}$. 'WF' denotes that the values were calculated from the weight functions, and are therefore discrete values. The connecting lines are only for visual clarification and do not show the intermediate values of SIF. 'SK' curves are the exact continuous values obtained from Shah-Kobayashi formulae.

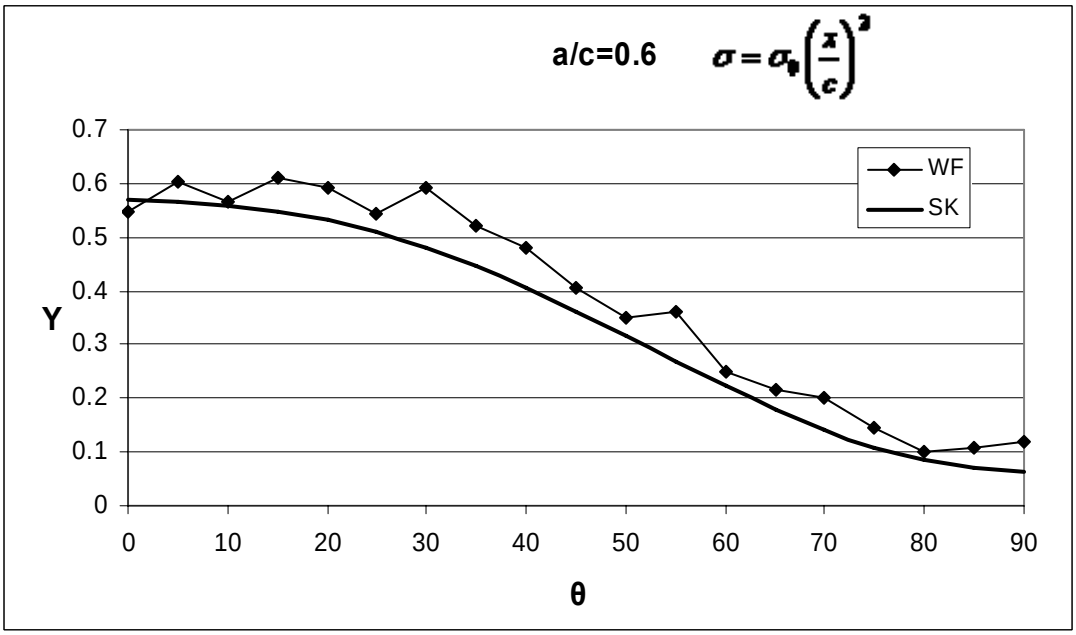

Figure B.3a- ***Y*** **distribution under the loading of** $\sigma = \sigma_0\left(\frac{x}{c}\right)^2$

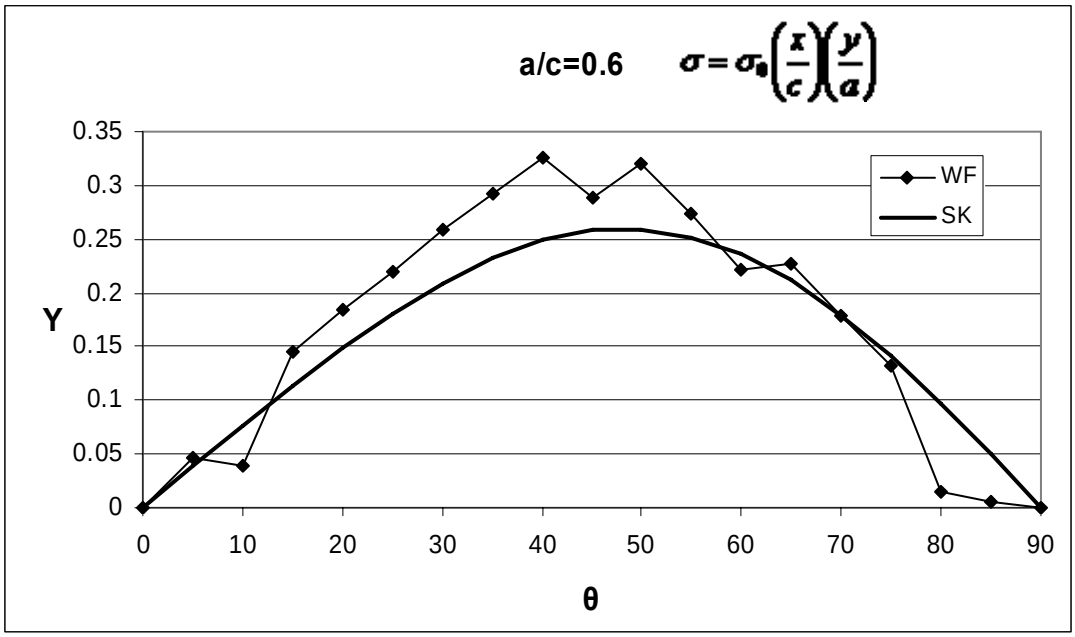

Figure B.3b- ***Y*** **distribution under the loading of** $\sigma = \sigma_0\left(\frac{x}{c}\right)\left(\frac{y}{a}\right)$

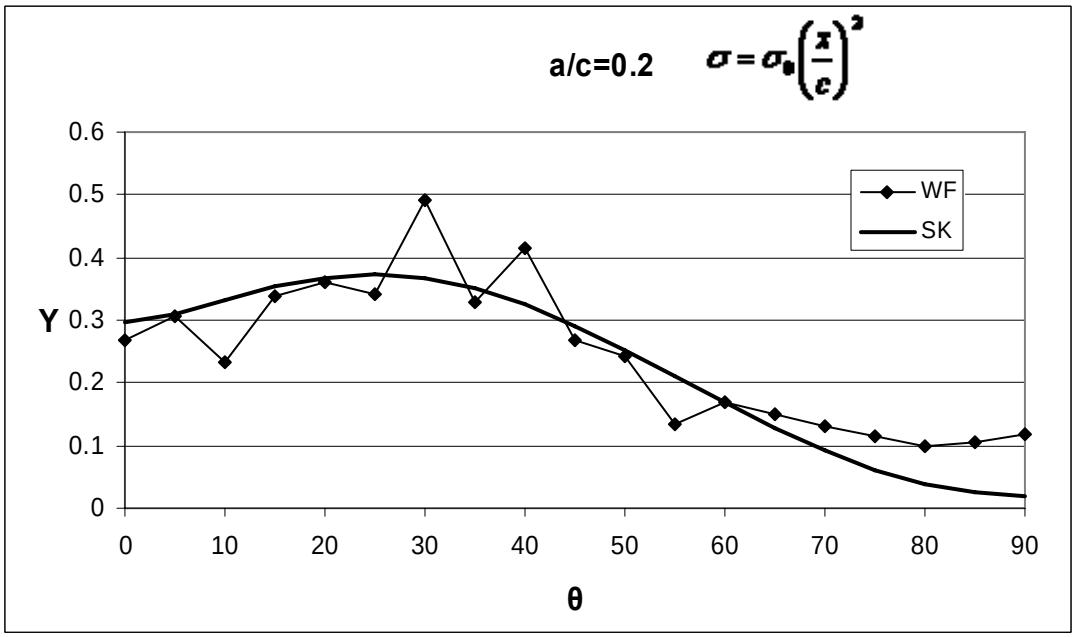

Figure B.3c- ***Y*** **distribution under the loading of** $\sigma = \sigma_0\left(\frac{x}{c}\right)^2$

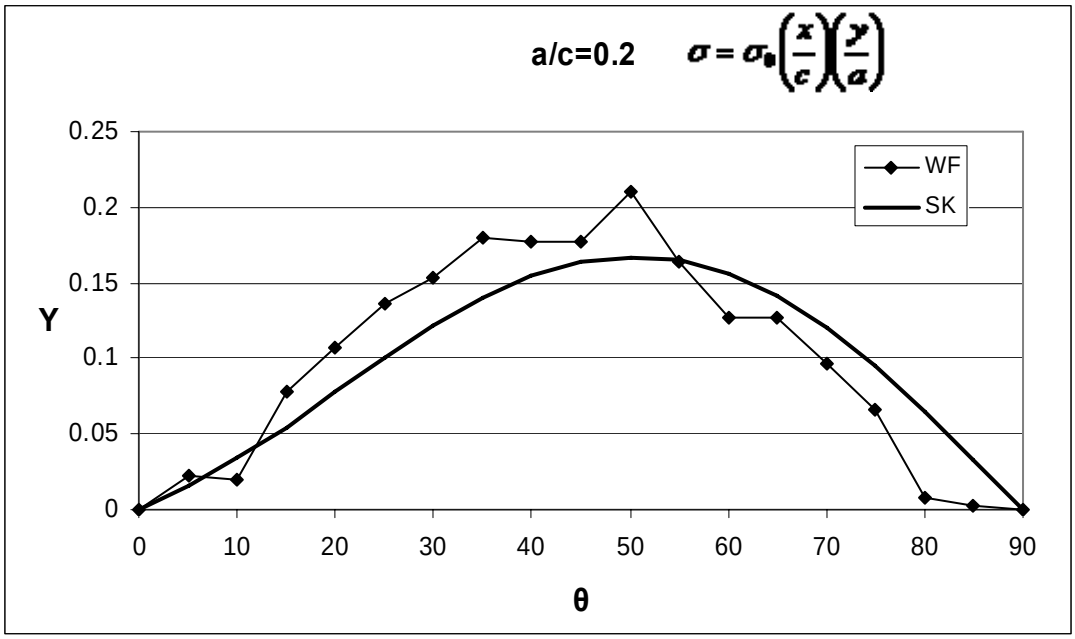

Figure B.3d- ***Y*** **distribution under the loading of** $\sigma = \sigma_0\left(\frac{x}{c}\right)\left(\frac{y}{a}\right)$

B.2) Discussion

It is observed from the figures above that the approximate weight function gives more accurate results for cracks with larger aspect ratios, *i.e.* cracks that are closer to the penny-shaped crack. This could be attributed to the fact that the leading term of the weight function is chosen as the weight function for a circular crack. A study of the variation of the coefficients for these different cases is also helpful in understanding the behaviour of the weight function. Figure A.4 shows the variations of three coefficients for the crack with an aspect ratio of $a/c = 0.6$, and figure A.5 shows that of the crack with an aspect ratio of $a/c = 0.2$.

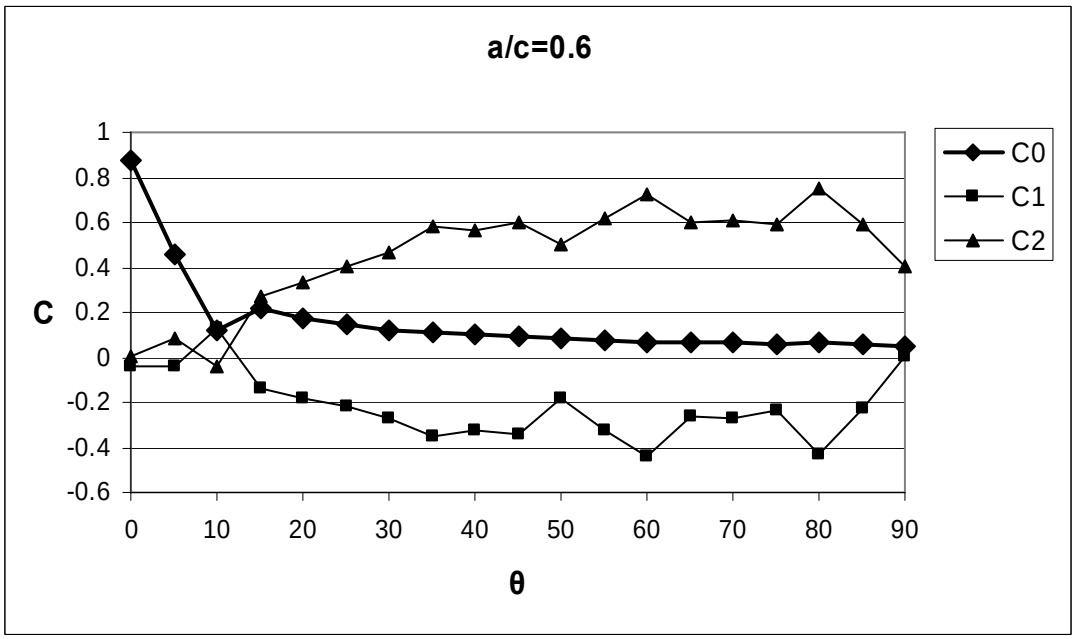

Figure B.4

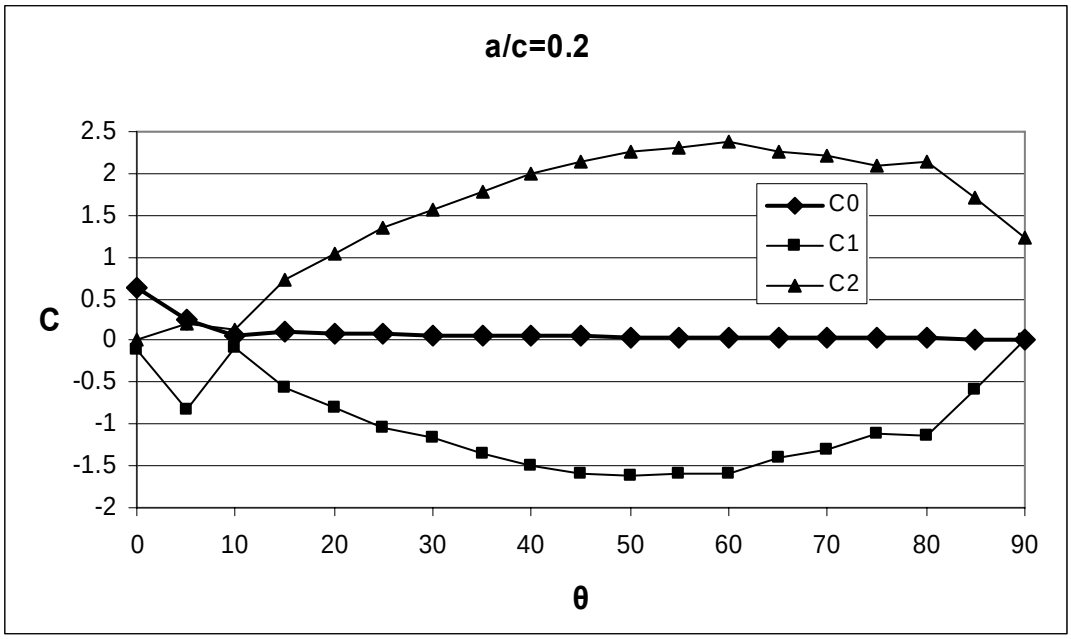

Figure B.5

From these two figures, it can be observed that the first coefficient (C_0) is maximum for $\theta = 0$. It can be reasoned that this is because at $\theta = 0$, though the local radius of curvature and that radius of the penny-shaped crack whose weight function is *m*, do not coincide, but the two cracks actually share this point on the *x* axis. A larger value of C_0 means smaller values for C_1 and C_2, *i.e.* the crack's behaviour closely resembles that of a penny-shaped crack. Another interesting feature is that the values of C_1 and C_2 seem to roughly mirror each other.

References

[B.1] H Tada, P C Paris and G R Irwin, The Stress Analysis of Cracks Handbook, 2nd ed., Paris Production Inc. (1985).

[B.2] J T Guidera and R W Lardner, Penny-shaped cracks, *Journal of Elasticity*, Vol. 5(1), pp. 59-73 (1975).

[B.3] G R Irwin, Crack-Extension Force for a Part-Through Crack in a Plate, *ASME Journal of Applied Mechanics*, Vol. 29, pp. 651-654 (1962).

[B.4] M K Kassir and G C Sih, Three-dimensional stresses around elliptical crack in transversely isotropic solids, *Engineering Fracture Mechanics*, Vol. 1, pp. 327-345 (1968).

[B.5] R C Shah and S Kobayashi, Stress intensity factor for an elliptical crack under arbitrary normal loading, *Engineering Fracture Mechanics*, Vol. 3, pp. 71-96 (1971).

Appendix C

Wu's Weight Function for Edge Cracks

For an edge crack in a plate, the stress intensity factor can be expressed as:

$$K = f\sigma\sqrt{\pi a W} \tag{1}$$

By assuming the crack face displacement to be in the following form [C.1]:

$$u_r(a,x) = \frac{\sigma a}{E'}\sum_{j=1}^{J} F_j(a)\left[1-\left(\frac{x}{a}\right)^2\right]^{j-\frac{1}{2}} \tag{2}$$

Wu [C.1, C.2] derived the following weight function for the stress intensity factor:

$$m(a,x) = \frac{1}{\sqrt{2\pi a}}\sum_{i=1}^{5}\beta_i(a)\left(1-\frac{x}{a}\right)^{i-\frac{3}{2}} \tag{3}$$

Where f can be evaluated as:

$$f = \int_0^a \frac{\sigma(x)}{\sigma}\frac{m(a,x)}{\sqrt{\pi a}}dx = \frac{1}{\sqrt{2\pi a}}\int_0^a \frac{\sigma(x)}{\sigma}\sum_{i=1}^{5}\beta_i(a)\left(1-\frac{x}{a}\right)^{i-\frac{3}{2}}dx \tag{4}$$

Values of $\beta_i(a)$ are derived as follows [C.3] (here a is the normalised crack length which can vary in the range of 0 to 1):

$$\beta_1(a) = 2.0$$

$$\beta_2(a) = \left[4af_r'(a) + 2f_r(a) + \frac{3}{2}F_2(a)\right] / f_r(a)$$

$$\beta_3(a) = \left\{ aF_2'(a) + \frac{1}{2}\left[5F_3(a) - F_2(a)\right] \right\} / f_r(a)$$

$$\beta_4(a) = \left\{ aF_3'(a) + \frac{1}{2}\left[7F_4(a) - 3F_3(a)\right] \right\} / f_r(a)$$

$$\beta_5(a) = \left[aF_4'(a) - \frac{5}{2}F_4(a) \right] / f_r(a)$$

In which

$$f_r(a) = \left(\sum_{i=0}^{7} \alpha_i a^i \right) / (1-a)^{\frac{3}{2}}$$

α_i = 1.1214, -1.6349, 7.3168, -18.7746, 31.8028, -33.2295, 19.1286, -4.6091.

$$F_1(a) = 4 f_r(a)$$

$$F_2(a) = \frac{1}{12\sqrt{2}}\left[315\pi\phi(a) - 105V_r(a) - 208\sqrt{2} f_r(a)\right]$$

$$F_3(a) = \frac{1}{30\sqrt{2}}\left[-1260\pi\phi(a) + 525V_r(a) + 616208\sqrt{2} f_r(a)\right]$$

$$F_4(a) = \sqrt{2}V_r(a) - \left[F_1(a) + F_2(a) + F_3(a)\right]$$

$$\phi(a) = \frac{1}{a^2}\int_0^a s.\left[f_r(s)\right]^2 ds$$

$$V_r = \left(\sum_{i=0}^{7} \gamma_i a^i \right) / (1-a)^2$$

γ_i = 2.9086, -5.5749, 19.572, -39.0199, 58.2697, -54.7124, 29.4039, -6.8949.

Preparation of the above formulae for numerical computation

The formulae for calculation of $\beta_i(a)$ values require derivatives of some of the above functions. To avoid any errors resulting from numerical differentiation, derivatives of these functions should be derived analytically where possible. For $f_r(a)$,

$$f_r'(a) = \frac{d}{da}\left[\frac{\sum_{i=0}^{7}\alpha_i a^i}{(1-a)^{3/2}}\right]$$

$$\boxed{f_r'(a) = \frac{\left(\sum_{i=0}^{7} i.\alpha_i.a^{i-1}\right)(1-a)^{3/2} + \frac{3}{2}(1-a)^{\frac{1}{2}}\left(\sum_{i=0}^{7}\alpha_i.a^i\right)}{(1-a)^3}}$$

And for $\phi(a)$:

$$\phi(a) = \frac{1}{a^2}\int_0^a s.[f_r(s)]^2\,ds$$

Bearing in mind that

$$[f_r(s)]^2 = \frac{\left(\sum_{i=0}^{7}\alpha_i s^i\right)^2}{(1-s)^3}$$

Then

$$\phi(a) = \frac{1}{a^2}\int_0^a s.\frac{\left(\sum_{i=0}^{7}\alpha_i s^i\right)^2}{(1-s)^3}\,ds = \frac{1}{a^2}I(a)$$

Now, by applying Leibniz Integral Rule:

$$\frac{\partial}{\partial z}\int_{a(z)}^{b(z)} f(x,z)dx = \int_{a(z)}^{b(z)}\frac{\partial f}{\partial z}dx + f(b(z),z)\frac{\partial b(z)}{\partial z} - f(a(z),z)\frac{\partial a(z)}{\partial z}$$

$$\boxed{\phi'(a) = \frac{1}{a}\left\{[f_r(a)]^2 - 2\phi(a)\right\}}$$

And for $V_r(a)$,

$$V_r = \left(\sum_{i=0}^{7} \gamma_i a^i \right) / (1-a)^2$$

$$\boxed{V_r' = \frac{2}{(1-a)^3} \sum_{i=0}^{7} \gamma_i a^i + \frac{1}{(1-a)^2} \sum_{i=1}^{7} i.\gamma_i a^{i-1}}$$

Which are all now is a form suitable for numerical computer-aided analysis.

References

[C.1] X R Wu. Approximate weight functions for centre and edge cracks, *Engineering Fracture Mechanics*, Vol. 20, No.11, pp. 35-49 (1984).

[C.2] X R Wu, Closed form weight function for edge crack problems, *Acta Mechanica Sinica*, Vol. 6, No. 2 (1990).

[C.2] X R Wu and A J Carlsson, Weight Functions and Stress Intensity Factor Solutions, Pergamon Press, ISBN 0-08-041702-7 (1991).